

CHEMICAL MODIFICATIONS OF α -MANGOSTIN FOR CYTOTOXIC STUDY ON LUNG
CANCER CELL LINES



A Thesis Submitted in Partial Fulfillment of the Requirements
for the Degree of Master of Science in Pharmaceutical Sciences and Technology

Common Course

FACULTY OF PHARMACEUTICAL SCIENCES

Chulalongkorn University

Academic Year 2019

Copyright of Chulalongkorn University

การดัดแปลงทางเคมีของ แอลฟา-แมงโกสตินเพื่อศึกษาความเป็นพิษต่อเซลล์มะเร็งปอด



วิทยานิพนธ์นี้เป็นส่วนหนึ่งของการศึกษาตามหลักสูตรปริญญาวิทยาศาสตรมหาบัณฑิต

สาขาวิชาเภสัชศาสตร์และเทคโนโลยี ไม่สังกัดภาควิชา/เทียบเท่า

คณะเภสัชศาสตร์ จุฬาลงกรณ์มหาวิทยาลัย

ปีการศึกษา 2562

ลิขสิทธิ์ของจุฬาลงกรณ์มหาวิทยาลัย

Thesis Title	CHEMICAL MODIFICATIONS OF α -MANGOSTIN FOR CYTOTOXIC STUDY ON LUNG CANCER CELL LINES
By	Miss Nan Yadanar Lin Pyae
Field of Study	Pharmaceutical Sciences and Technology
Thesis Advisor	Assistant Professor SUPAKARN CHAMNI, Ph.D.
Thesis Co Advisor	PREEDAKORN CHUNHACHA, Ph.D.

Accepted by the FACULTY OF PHARMACEUTICAL SCIENCES, Chulalongkorn
University in Partial Fulfillment of the Requirement for the Master of Science

..... Dean of the FACULTY OF
PHARMACEUTICAL SCIENCES
(Assistant Professor RUNGPETCH SAKULBUMRUNGSIL,
Ph.D.)

THESIS COMMITTEE

..... Chairman
(Professor WANCHAI DE-EKNAMKUL, Ph.D.)

..... Thesis Advisor
(Assistant Professor SUPAKARN CHAMNI, Ph.D.)

..... Thesis Co-Advisor
(PREEDAKORN CHUNHACHA, Ph.D.)

..... Examiner
(Associate Professor BOONCHOO SRITULARAK, Ph.D.)

..... Examiner
(Assistant Professor CHAISAK CHANSRINIYOM, Ph.D.)

..... External Examiner
(Associate Professor Surattana Amnuoypol, Ph.D.)

นาน ยาดานาร์ ลิน พย : การดัดแปลงทางเคมีของ แอลฟา-แมงโกสตินเพื่อศึกษาความเป็นพิษต่อเซลล์มะเร็งปอด. (CHEMICAL MODIFICATIONS OF α -MANGOSTIN FOR CYTOTOXIC STUDY ON LUNG CANCER CELL LINES) อ.ที่ปรึกษาหลัก : ผศ. ดร.ศุภกา ญาญ์ ชำนิ, อ.ที่ปรึกษาร่วม : อ. ภก. ดร.ปริดากร ชุมหะชา

แอลฟา-แมงโกสติน คือ สารผลิตภัณฑ์ธรรมชาติในกลุ่มแซนโทนที่มีออกซิเจนและฟีนอลเป็นองค์ประกอบในโครงสร้าง ซึ่งส่วนใหญ่แยกได้จากเปลือกของผลมังคุด โดยแอลฟา-แมงโกสตินมีคุณสมบัติทางเภสัชวิทยามากมายและมีแนวโน้มในการพัฒนาเป็นยา อย่างไรก็ตามพบว่าแอลฟา-แมงโกสตินที่มีการละลายน้ำต่ำและมีการดูดซึมที่ไม่ดีจึงทำให้เกิดข้อจำกัดต่อการพัฒนาเพื่อใช้ในการรักษาโรค ดังนั้น การปรับเปลี่ยนโครงสร้างทางเคมีเพื่อค้นหาสารอนุพันธ์จึงเป็นแนวทางหนึ่งในการปรับปรุงข้อจำกัดและพัฒนาสารกลุ่มนี้ ในการศึกษานี้ได้พัฒนากระบวนการทางเคมีเพื่อสังเคราะห์อนุพันธ์ของแอลฟา-แมงโกสตินขึ้น 2 กระบวนการ โดยการปรับเปลี่ยนกลุ่มฟีนอลิกไฮดรอกซีที่คาร์บอนตำแหน่งที่ 3 และตำแหน่งที่ 6 ด้วยปฏิกิริยาการจัดเรียงใหม่ของสโมลล์เพื่อสร้างหมู่เอมีนและปฏิกิริยาการเติมของไอโซไซยานตเพื่อสร้างหมู่คาร์บาเมต ซึ่งเป็นกระบวนการไม่เคยถูกรายงานมาก่อนการศึกษาระบบการกึ่งสังเคราะห์ในการสร้างอนุพันธ์ของแอลฟา-แมงโกสตินนี้ เน้นการศึกษาสถานะของกระบวนการเคมีประกอบด้วยตัวทำละลาย ตัวเร่งปฏิกิริยา และเวลาในการทำปฏิกิริยา นอกจากนี้ คุณสมบัติทางเคมีฟิสิกส์ของสารอนุพันธ์โดยถูกทำนายจากการคำนวณด้วยโปรแกรม SwissADME จากผลการคำนวณด้วยเทคนิค ESOL สารอนุพันธ์ **4a** และ **4c** ที่มีโนโตรเจนเชื่อมต่อที่คาร์บอนตำแหน่งที่ 3 และตำแหน่งที่ 6 มีแนวโน้มแสดงความสามารถในการละลายน้ำในระดับปานกลางซึ่งดีขึ้นกว่าแอลฟา-แมงโกสติน นอกจากนี้ได้ทำการศึกษาความเป็นพิษต่อเซลล์มะเร็งปอดชนิดไม่ใช้เซลล์ขนาดเล็กของมนุษย์ประเภท H460 และ H292 เซลล์ ผลการวิจัยแสดงให้เห็นว่าสารอนุพันธ์ **5b** (IC_{50} $11.52 \pm 1.32 \mu M$) แสดงความเป็นพิษต่อเซลล์สูงสุดเมื่อเปรียบเทียบกับอนุพันธ์อื่น ๆ ในงานวิจัยนี้ โดยแสดงความเป็นพิษต่อเซลล์ H460 สูงกว่าแอลฟา-แมงโกสตินสามเท่า (IC_{50} $38.04 \pm 2.44 \mu M$) อย่างไรก็ตามอนุพันธ์ของแอลฟา-แมงโกสตินที่มีหมู่คาร์บาเมตนั้นไม่เสถียรและเกิดการสลายตัวเนื่องจากน้ำหรือหมู่ไฮดรอกซิลที่มีอยู่ในโครงสร้างสาร โดยสรุปกระบวนการทางเคมีในการปรับปรุงโครงสร้างของแอลฟา-แมงโกสตินได้ถูกพัฒนาขึ้นเพื่อเปลี่ยนกลุ่มฟีนอลิกไฮดรอกซีที่คาร์บอนตำแหน่งที่ 3 และตำแหน่งที่ 6 เป็นหมู่ที่มีโนโตรเจนเป็นองค์ประกอบ ได้แก่ เอมี เอไมด์ และคาบาเมต

สาขาวิชา เกษษศาสตร์และเทคโนโลยี
ปีการศึกษา 2562

ลายมือชื่อนิสิต

ลายมือชื่อ อ.ที่ปรึกษาหลัก

ลายมือชื่อ อ.ที่ปรึกษาร่วม

6176126833 : MAJOR PHARMACEUTICAL SCIENCES AND TECHNOLOGY

KEYWORD: **α**-MANGOSTIN / SEMI-SYNTHESIS / SMILES REARRANGEMENT / **α**-MANGOSTIN-CARBAMATE PRODRUG / NON-SMALL CELL LUNG CANCER CELL LINE/ CYTOTOXICITY

Nan Yadanar Lin Pyae : CHEMICAL MODIFICATIONS OF **α**-MANGOSTIN FOR CYTOTOXIC STUDY ON LUNG CANCER CELL LINES. Advisor: Asst. Prof. SUPAKARN CHAMNI, Ph.D. Co-advisor: PREEDAKORN CHUNHACHA, Ph.D.

α-Mangostin is a natural oxygenated and prenylated xanthone, which is mainly isolated from the pericarps of *Garcinia mangostana*. It possesses numerous pharmacological properties and promising therapeutic effects. However, the limitations of **α**-mangostin such as highly hydrophobicity and poor bioavailability hinder its therapeutic applications. To overcome these drawbacks of **α**-mangostin, chemical modifications have been performed to discover the improved analogs. Herein, two semi-synthetic approaches to obtain new **α**-mangostin derivatives were investigated by the modifications of the phenolic hydroxy groups at C-3 and C-6 positions involving Smiles rearrangement to install amine functional groups and the addition reaction of isocyanate to form the carbamate motif, which have never been reported. In this study, semi-syntheses of **α**-mangostin derivatives were focused on the reaction optimizations by controlling solvent, base, catalyst, and reaction time. In addition, the physicochemical property prediction was performed by *in silico* modeling using SwissADME. Based on ESOL model, compounds **4a** and **4c** having nitrogen bound to C-3 and C-6 positions potentially improved water solubility better than **α**-mangostin showing moderate solubility, respectively. Furthermore, the cytotoxicity was evaluated against H460 and H292 human non-small lung cancer cell lines along with nuclear staining assay. The results suggested that compound **5b** exhibited the most potent cytotoxicity among all derivatives in this study, displaying 3-fold (IC_{50} $11.52 \pm 1.32 \mu M$) more potent than **α**-mangostin (IC_{50} $38.04 \pm 2.44 \mu M$) against H460 cell lines. Although, the carbamate derivatives of **α**-mangostin **5a-e** were unstable and prone to decompose by hydrolysis from either water or the free hydroxyl group in its structure. In summary, new chemical modifications of **α**-mangostin were developed to transform phenolic hydroxy groups at C-3 and C-6 positions to the nitrogen-containing functionalities such as amine, amide, and carbamate.

Field of Study:	Pharmaceutical Sciences and Technology	Student's Signature
Academic Year:	2019	Advisor's Signature
		Co-advisor's Signature

ACKNOWLEDGEMENTS

First of all, I would like to disclose my sincere appreciation to my advisor, Assistant Professor Supakarn Chamni, the Department of Pharmacognosy and Pharmaceutical Botany, Faculty of Pharmaceutical Sciences, Chulalongkorn University, for her invaluable mentorship, encouragement, guidance, advice, and support throughout the process of this thesis. Also, I would like to deeply thank my co-advisor, Dr. Preedakorn Chunhacha, the Department of Biochemistry and Microbiology, Faculty of Pharmaceutical Sciences, Chulalongkorn University, for his support, advice, and help in the completion of this study.

I would like to extend my sincere gratitude to all my thesis committee members for their insightful comments, discussions, and suggestions.

Moreover, I am very thankful to Chulalongkorn University for the graduate scholarship program for ASEAN countries, which has been the essential support along with the Chulalongkorn Academic Advancement into Its 2nd Century (CUAASC) Project and Natural Products and Nanoparticles Research Unit for research funding.

I would like to express my special thanks to all teachers, staff members, graduate students, and lab members of the Pharmaceutical Sciences and Technology Graduate Program and the Department of Pharmacognosy and Pharmaceutical Botany, along with the Department of Biochemistry and Microbiology, Faculty of Pharmaceutical Sciences, Chulalongkorn University, for their helpful advice and kind friendships. Besides, I especially thank Miss Latcha Chunwijitra, International Student Assistant, for her help during the COVID-19 pandemic.

Finally, my highest acknowledge to my beloved family for their eternal love, unconditional care, warm encouragement, and constant support.

Nan Yadanar Lin Pyae

TABLE OF CONTENTS

	Page
ABSTRACT (THAI).....	iii
ABSTRACT (ENGLISH).....	iv
ACKNOWLEDGEMENTS	v
TABLE OF CONTENTS	vi
LIST OF FIGURES	1
LIST OF TABLES	4
LIST OF SCHEMES	6
LIST OF ABBREVIATIONS	7
CHAPTER I INTRODUCTION.....	12
CHAPTER II LITERATURE REVIEW	16
2.1 Taxonomy and classification of <i>Garcinia mangostana</i>	17
2.2 Chemical constituents of <i>Garcinia mangostana</i>	18
2.3 Biological activities of α -mangostin	25
2.4 Syntheses of α -mangostin derivatives	27
2.4.1 Modification of hydroxy groups at the positions of C-1, C-3, and C-6.....	28
2.4.2. Modification of prenyl groups at the positions of C-2 and C-8.....	29
2.4.3 Substitution reaction at the positions of C-4 and C-5	31
2.4.4 Modification of methoxy group at the position of C-7	33
CHAPTER III RESEARCH METHODOLOGY	38
3.1 Plant materials.....	40
3.2 General experimental procedures.....	40

3.2.1 Thin-layer chromatography (TLC)	40
3.2.2 Quick column chromatography (QCC).....	40
3.2.3 Flash column chromatography (FCC)	41
3.2.4 Nuclear magnetic resonance spectroscopy (NMR).....	42
3.2.5 Mass spectrometry (MS)	42
3.2.6 Ultraviolet-visible spectrophotometer (UV-vis)	42
3.2.7 Chemicals and solvents.....	42
3.2.8 SwissADME web tool.....	43
3.2.9 Cell culture	43
3.2.10 Statistical analysis.....	43
3.3 Extraction, isolation, and purification of mangosteen pericarp.....	44
3.4 Chemical and biological study of α -mangostin derivatives from Smiles rearrangement	45
3.4.1 Semi-synthesis of α -mangostin derivatives via Smiles rearrangement.....	45
3.4.1.1 General procedure	45
3.4.1.2 Reaction condition optimization	46
3.4.2 Estimation of aqueous solubility and drug-likeness of α -mangostin derivatives from Smiles rearrangement	47
3.4.3 Cytotoxicity assay against the non-small-cell lung cancer cell lines (H460 and H292).....	47
3.4.4 DNA staining assay on against the non-small-cell lung cancer cell lines (H460 and H292)	48
3.5 Chemical and biological study of α -mangostin-carbamate prodrugs	49
3.5.1 Semi-synthesis of α -mangostin derivatives containing carbamate moiety	49

3.5.1.1 Reaction condition optimization	49
3.5.1.2 Semi-synthesis of α -mangostin derivatives containing carbamate motif	50
3.5.1.3 General procedure	52
3.5.2 Estimation of aqueous solubility and drug-likeness of α -mangostin derivatives containing carbamate moiety	52
3.5.3 Detection of stability of α -mangostin derivatives by UV-vis spectrophotometer.....	52
3.5.4 Cytotoxicity assay against the non-small-cell lung cancer cell line (H460)	53
CHAPTER IV RESULTS AND DISCUSSION	54
4.1 Extraction, purification, and structure determination of isolated compounds from mangosteen pericarp	56
4.2 Chemical and biological study of α -mangostin derivatives from Smiles rearrangement	66
4.2.1 Chemical synthesis.....	66
4.2.2 Structural determination of α -mangostin derivatives from Smiles rearrangement.....	70
4.2.2.1 Structural determination of compound 4a.....	70
4.2.2.2 Structural determination of compound 4b	72
4.2.2.3 Structural determination of compound 4c.....	74
4.2.3 Aqueous solubility and drug-likeness of α -mangostin derivatives from Smiles rearrangement.....	76
4.2.4 Cytotoxic activity against H460 and H292 cell lines.....	80
4.2.5 Quantification of apoptotic cells.....	82

4.3 Chemical and biological study of α -mangostin-carbamate prodrugs	88
4.3.1 Chemical synthesis	88
4.3.2 Structural determination of α -mangostin-carbamate derivatives	91
4.3.2.1 Structural determination of compound 5a.....	91
4.3.2.2 Structural determination of compound 5b	94
4.3.2.3 Structural determination of compound 5c.....	95
4.3.2.4 Structural determination of compound 5d	96
4.3.2.5 Structural determination of compound 5e.....	97
4.3.3 Aqueous solubility and drug-likeness of α -mangostin-carbamate derivatives	101
4.3.4 Stability of α -mangostin-carbamate derivatives evaluated by UV-vis spectroscopy	105
4.3.5 Cytotoxic activity against H460 cell line	109
CHAPTER V CONCLUSION.....	110
REFERENCES	112
APPENDIX.....	122
VITA.....	133

LIST OF FIGURES

Figure 1	Chemical structure of α -mangostin.....	12
Figure 2	α -Mangostin derivatives having carbamate moiety.....	14
Figure 3	Chemical structure of irinotecan	14
Figure 4	Structures of xanthenes from <i>G. mangostana</i>	22
Figure 5	α -Mangostin derivatives (AD) with modification of hydroxy groups of α -mangostin at C-3 and C-6 positions.....	34
Figure 6	α -Mangostin derivatives (AD) with modification of prenyl groups of α -mangostin at C-2 and C-8 positions.....	35
Figure 7	α -Mangostin derivatives (AD) with substitution of aromatic sites of α -mangostin at C-4 and C-5 positions.....	36
Figure 8	α -Mangostin derivatives (AD) with modification of C-2 and C-6 positions....	37
Figure 9	General reaction for Smiles rearrangement.....	45
Figure 10	General reaction for the synthesis of carbamate from 3-chlorophenyl isocyanate	49
Figure 11	Carbamate formation.....	52
Figure 12	^1H NMR (300 MHz) spectrum of compound 1 in $(\text{CD}_3)_2\text{CO}$	61
Figure 13	^1H NMR (300 MHz) spectrum of compound from fraction X-1 in $(\text{CD}_3)_2\text{CO}$.	63
Figure 14	^1H NMR (300 MHz) spectrum of compound from fraction X-2 in $(\text{CD}_3)_2\text{CO}$.	63
Figure 15	Smiles rearrangement mechanism.....	66
Figure 16	Semi-synthesis and proposed mechanism of 4a , 4b , and 4c via Smiles rearrangement of α -mangostin	67

Figure 17 Morphological changes in the H460 cell nuclei detected with costaining of Hoechst33342/PI under the fluorescence microscope (a) α-mangostin , (b) 4a , (c) 4b , and (d) 4c	83
Figure 18 Morphological changes in the H292 cell nuclei detected with costaining of Hoechst33342/PI under the fluorescence microscope (a) α-mangostin , (b) 4a , (c) 4b , and (d) 4c	84
Figure 19 Percentage of apoptotic cells death in H460 cells	86
Figure 20 Percentage of apoptotic cells death in H292 cells	87
Figure 21 Comparison of ^1H NMR (300 MHz) spectrum of compounds 1 and 5a	93
Figure 22 Comparison of ^1H NMR (300 MHz) spectrum of compounds 1 and 5b	95
Figure 23 Comparison of ^1H NMR (300 MHz) spectrum of compounds 1 and 5c	96
Figure 24 Comparison of ^1H NMR (300 MHz) spectrum of compounds 1 and 5d	97
Figure 25 Comparison of ^1H NMR (300 MHz) spectrum of compounds 1 and 5e	98
Figure 26 ^1H NMR (300 MHz) spectrum of compound 1 in $(\text{CD}_3)_2\text{CO}$	122
Figure 27 ^1H NMR (300 MHz) spectrum of compound from fraction X-1 in $(\text{CD}_3)_2\text{CO}$	122
Figure 28 ^1H NMR (300 MHz) spectrum of compound from fraction X-2 in $(\text{CD}_3)_2\text{CO}$	123
Figure 29 Mass spectrum of 4a	124
Figure 30 ^1H NMR (300 MHz) spectrum of compound 4a in $(\text{CD}_3)_2\text{CO}$	125
Figure 31 ^{13}C NMR (300 MHz) spectrum of compound 4a in $(\text{CD}_3)_2\text{CO}$	125
Figure 32 Mass spectrum of 4b	126
Figure 33 ^1H NMR (300 MHz) spectrum of compound 4b in $(\text{CD}_3)_2\text{CO}$	127
Figure 34 ^{13}C NMR (300 MHz) spectrum of compound 4b in $(\text{CD}_3)_2\text{CO}$	127
Figure 35 Mass spectrum of 4c	128
Figure 36 ^1H NMR (300 MHz) spectrum of compound 4c in $(\text{CD}_3)_2\text{CO}$	129
Figure 37 ^{13}C NMR (300 MHz) spectrum of compound 4c in $(\text{CD}_3)_2\text{CO}$	129

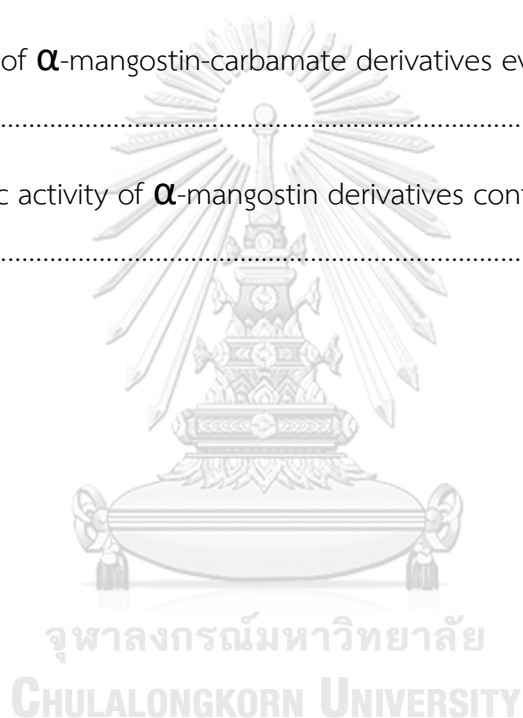
Figure 38	^1H NMR (300 MHz) spectrum of compound 5a in $(\text{CD}_3)_2\text{CO}$	130
Figure 39	^{13}C NMR (300 MHz) spectrum of compound 5a in $(\text{CD}_3)_2\text{CO}$	130
Figure 40	^1H NMR (300 MHz) spectrum of compound 5b in $(\text{CD}_3)_2\text{CO}$	131
Figure 41	^1H NMR (300 MHz) spectrum of compound 5c in $(\text{CD}_3)_2\text{CO}$	131
Figure 42	^1H NMR (300 MHz) spectrum of compound 5d in $(\text{CD}_3)_2\text{CO}$	132
Figure 43	^1H NMR (300 MHz) spectrum of compound 5e in $(\text{CD}_3)_2\text{CO}$	132



LIST OF TABLES

Table 1 Natural xanthenes from <i>G. mangostana</i> reported during 1958-2017	19
Table 2 Cytotoxicity of α -mangostin towards different cancer cell lines reported during 2003-2020	26
Table 3 Reaction optimization of Smiles rearrangement.....	46
Table 4 Optimization conditions for carbamate formation	50
Table 5 Structures of chlorinated isocyanate reagents and the corresponding α -mangostin derivatives containing carbamate moiety.....	51
Table 6 ^1H NMR spectral data of compound 1	62
Table 7 ^1H NMR spectral data of fraction X-1 in $(\text{CD}_3)_2\text{CO}$	64
Table 8 ^1H NMR spectral data of fraction X-2 in $(\text{CD}_3)_2\text{CO}$	65
Table 9 Percent yields of compounds 4a , 4b , and 4c	69
Table 10 NMR spectral data of compound 4a in $(\text{CD}_3)_2\text{CO}$	71
Table 11 NMR spectral data of compound 4b in $(\text{CD}_3)_2\text{CO}$	73
Table 12 NMR spectral data of compound 4c in $(\text{CD}_3)_2\text{CO}$	75
Table 13 General physicochemical properties and aqueous solubility of α -mangostin derivatives from Smiles rearrangement	77
Table 14 Drug-likeness parameters of α -mangostin derivatives from Smiles rearrangement.....	79
Table 15 Dose of precipitation and treatment of α -mangostin derivatives from Smiles rearrangement.....	80
Table 16 Cytotoxic activity of α -mangostin derivatives from Smiles rearrangement.	81
Table 17 Reaction optimization of carbamate formation by solvent	88
Table 18 Reaction optimization of carbamate formation by the base.....	89

Table 19 Formation of α -mangostin-carbamate derivatives	90
Table 20 NMR spectral data of compound 5a in $(\text{CD}_3)_2\text{CO}$	92
Table 21 ^1H NMR spectral data of compound 5b , 5c , 5d , and 5e in $(\text{CD}_3)_2\text{CO}$	99
Table 22 General physicochemical properties and aqueous solubility of α -mangostin derivatives containing carbamate moiety.....	102
Table 23 Drug-likeness parameters of α -mangostin derivatives containing carbamate moiety.....	104
Table 24 Stability of α -mangostin-carbamate derivatives evaluated by UV-vis spectroscopy	106
Table 25 Cytotoxic activity of α -mangostin derivatives containing carbamate moiety	109

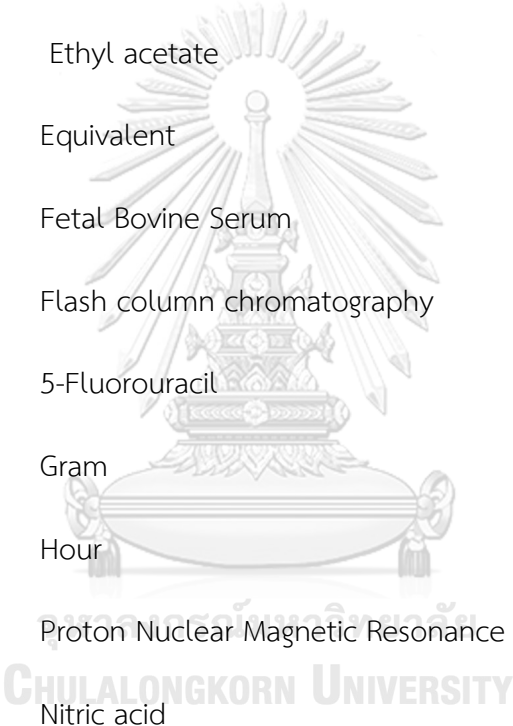


LIST OF SCHEMES

Scheme 1	Semi-synthesis of α -mangostin derivative <i>via</i> Smiles rearrangement.....	13
Scheme 2	Syntheses of α -mangostin derivatives 1a-1h	28
Scheme 3	Syntheses of α -mangostin derivatives 2a-2d	29
Scheme 4	Syntheses of α -mangostin derivatives 2e-2i	30
Scheme 5	Syntheses of α -mangostin derivatives 3a-3e	31
Scheme 6	Syntheses of α -mangostin derivatives 3f and 3g	32
Scheme 7	Syntheses of α -mangostin derivatives 4a-4c	33
Scheme 8	Extraction of <i>G. mangostana</i> pericarp.....	57
Scheme 9	Separation of hexane crude extract of <i>G. mangostana</i>	59
Scheme 10	Separation of EtOAc crude extract of <i>G. mangostana</i>	60
Scheme 11	Proposed mechanism of carbamate hydrolysis	93

LIST OF ABBREVIATIONS

Å	=	Angstrom
ACF	=	Aberrant crypt foci
Ac ₂ O	=	Acetic anhydride
AcOH	=	Acetic acid
AR	=	Analytical reagent
br	=	Broad (for NMR spectra)
°C	=	Degree Celsius
(CD ₃) ₂ CO	=	Deuterated acetone
CDCl ₃	=	Deuterated chloroform
CHCl ₃	=	Chloroform
CH ₃ I	=	Methyl iodide
cm	=	Centimeter
¹³ C NMR	=	Carbon Nuclear Magnetic Resonance
CO ₂	=	Carbon dioxide
Cs ₂ CO ₃	=	Cesium carbonate
CuSO ₄	=	Copper sulphate
d	=	Doublet (for NMR spectra)
dd	=	Doublet of doublet (for NMR spectra)
ddd	=	Doublet of doublet of doublet (for NMR spectra)



DCM (CH_2Cl_2)	=	Dichloromethane
DMAP	=	4-Dimethylaminopyridine
DMF	=	<i>N,N</i> -dimethylformamide
DMH	=	1,2-Dimethylhydrazine
DMSO	=	Dimethylsulfoxide
DNA	=	Deoxyribonucleic acid
EtOAc	=	Ethyl acetate
equiv	=	Equivalent
FBS	=	Fetal Bovine Serum
FCC	=	Flash column chromatography
5-FU	=	5-Fluorouracil
g	=	Gram
h	=	Hour
^1H NMR	=	Proton Nuclear Magnetic Resonance
HNO_3	=	Nitric acid
HPLC	=	High-performance liquid chromatography
HRESIMS	=	High-resolution Electrospray Ionization Mass Spectra
Hz	=	Hertz
IC_{50}	=	Concentration exhibiting 50% inhibition
J	=	Coupling constant
K_2CO_3	=	Potassium carbonate

kg	=	Kilogram
KI	=	Potassium iodide
KOH	=	Potassium hydroxide
L	=	Liter
m	=	Multiplet (for NMR spectra)
MeOH	=	Methanol
mg	=	Milligram
MgSO ₄	=	Magnesium sulphate
min	=	Minute
mL	=	Milliliter
mm	=	Millimeter
mM	=	Millimolar
mmol	=	Millimole
MS	=	Mass Spectrometry
MTT	=	3-(4,5-Dimethylthiazol-2-yl)-2,5-diphenyltetrazolium bromide
μL	=	Microliter
μM	=	Micromolar
<i>m/z</i>	=	Mass to charge ratio
NaH	=	Sodium hydride
NaIO ₄	=	Sodium periodate
NaN ₃	=	Sodium azide

NBS	=	<i>N</i> -bromosuccinimide
NCS	=	<i>N</i> -chlorosuccinimide
NH ₂	=	Amine
nm	=	Nanometer
NMO	=	4-Methylmorpholine
NMR	=	Nuclear Magnetic Resonance
OCH ₃	=	Methoxy
OH	=	Hydroxy
OsO ₄	=	Osmium tetroxide
PBS	=	Phosphate buffer solution
Pd/C	=	Palladium on carbon
PI	=	Propidium iodide
ppm	=	Part per million
q	=	Quartet (for NMR spectra)
QCC	=	Quick column chromatography
RPMI	=	Roswell Park Memorial Institute
r.t.	=	Room temperature
s	=	Singlet (for NMR spectra)
SCR	=	Structure-cytotoxicity relationship
S.D.	=	Standard deviation
t	=	Triplet (for NMR spectra)

TEA	=	Triethylamine
THF	=	Tetrahydrofuran
TLC	=	Thin layer chromatography
UV-vis	=	Ultraviolet-visible spectrophotometer
δ	=	Chemical shift



CHAPTER I INTRODUCTION

Cancer is ranked as one of the life-threatening diseases globally in the 21st century. Among them, lung cancer is one of the most common causes of death in both males and females [1]. The leading cause of lung cancer is smoking. However, there are several cases of lung cancer patients with non-smoking behavior that are related to lung disease, asbestos, silica, and air pollution [2]. Importantly, the poor prognosis of cancer symptoms in the early stage and resistance to chemotherapy have become a serious concern for lung cancer treatment [3]. Recently, the natural products play an important role in the discovery of new anti-lung cancer agents such as curcumin (*Curcuma longa*) [3], epigallocatechin gallate from green tea (*Camellia sinensis*) [4], isothiocyanates such as benzyl isothiocyanate, and phenethyl isothiocyanate from broccoli sprouts (*Brassica oleracea*) [5, 6], and genistein from soybean (*Glycine max*) [7].

The natural xanthenes from mangosteen pericarps, α -mangostin, and its derivatives have surprisingly exhibited anti-cancer activities [8]. However, its high hydrophobicity and poor oral bioavailability seem to be one of the major limitations. Modification of α -mangostin chemical structures could be the possible option to solve these limitations. Based upon the reported structure-cytotoxicity relationship (SCR) studies of α -mangostin, chemical modifications at C-1, C-2, C-3, C-4, C-5, C-6, C-7, and C-8 positions have been described [9] (**Figure 1**).

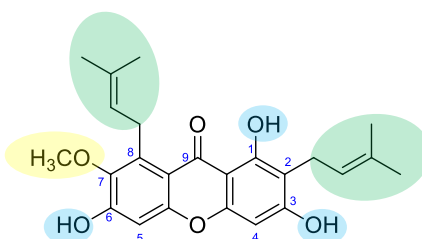
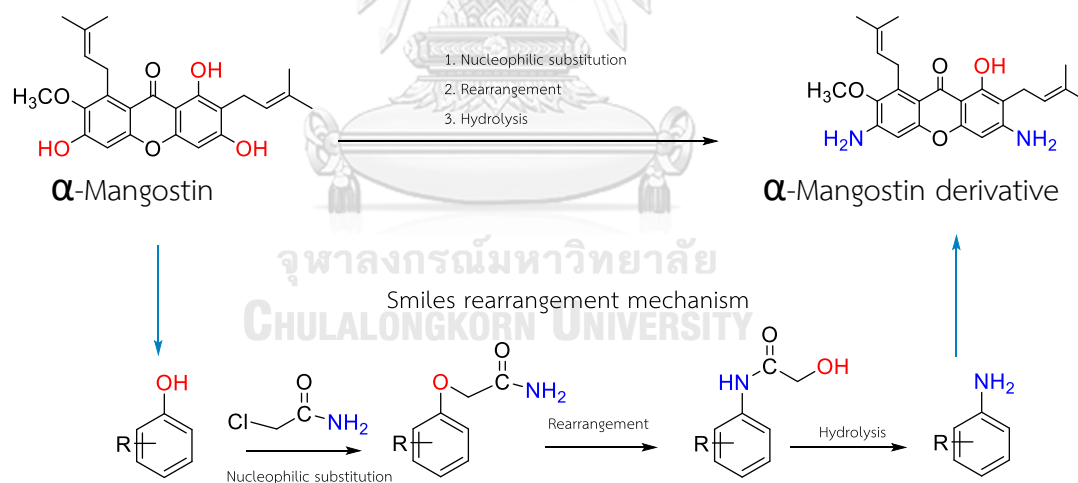


Figure 1 Chemical structure of α -mangostin

Regarding cytotoxicity, phenolic hydroxy groups at C-3 and C-6 positions are possible for chemical modifications. Importantly, converting the structure of prenyl at C-2 and C-8 showed a reduction of the cytotoxicity against human lung cancer cell lines A-549 and H460 [9, 10]. Moreover, keeping the original hydrogen atom on C-4 and C-5 and the methoxy group at C-7 potentially maintain cytotoxicity against A-549 and H460 [9, 10].

In this research, chemical modifications of α -mangostin were focused on C-3 and C-6 positions, including optimized reaction conditions and structural characterization. The phenolic hydroxy group is proposed to transform into amine group *via* Smiles rearrangement [11] with three steps of chemical mechanism involving nucleophilic substitution, rearrangement, and hydrolysis (**Scheme 1**). The new derivatives of α -mangostin having additional nitrogen motif were hypothesized to increase solubility.



Scheme 1 Semi-synthesis of α -mangostin derivative *via* Smiles rearrangement

Furthermore, α -mangostin was semi-synthesized by the addition reaction of isocyanate to form carbamate analogs as a prodrug to improve their physicochemical and biological properties (Figure 2). Carbamate motif plays a noteworthy role in medicinal chemistry not only because of its excellent permeability across the cell membranes but also its function as a prodrug [12]. A well-known anticancer drug is irinotecan (Figure 3), which contains a carbamate bond that improves the overall aqueous solubility [12]. Thus, the new α -mangostin derivatives containing carbamate moiety potentially possess the improvement in both solubility and anti-cancer activity.

In addition, the semi-synthesis of α -mangostin derivatives having amine and carbamate moiety were evaluated their cytotoxicities toward human lung cancer cell lines in this study.

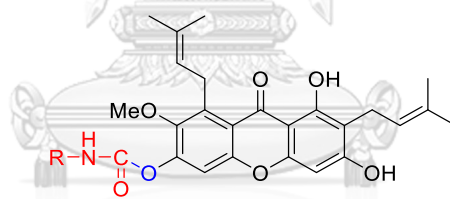


Figure 2 α -Mangostin derivatives having carbamate moiety

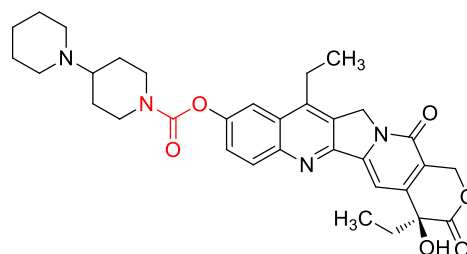


Figure 3 Chemical structure of irinotecan

The main purposes of this thesis are

1. To modify the structure of α -mangostin focusing on the transformation of the hydroxy group to the amine.
2. To semi-synthesize α -mangostin derivatives containing carbamate moiety.
3. To estimate the physicochemical properties by *in silico* technique and evaluate the cytotoxicity of α -mangostin analogs toward non-small-cell lung cancer cell lines.



CHAPTER II LITERATURE REVIEW

Contents

- 2.1. Taxonomy and classification of *Garcinia mangostana*
- 2.2. Chemical constituents of *Garcinia mangostana*
- 2.3. Biological activities of α -mangostin
- 2.4. Syntheses methods of α -mangostin derivatives
 - 2.4.1. Modification of hydroxy groups at the positions of C-1, C-3, and C-6
 - 2.4.2. Modification of prenyl groups at the positions of C-2 and C-8
 - 2.4.3. Substitution reaction at the positions of C-4 and C-5
 - 2.4.4. Modification of methoxy group at the position of C-7

2.1 Taxonomy and classification of *Garcinia mangostana*

Domain: Eukaryota

Kingdom: Plantae

Phylum: Spermatophyta

Class: Magnoliopsida

Order: Theales

Family: Clusiaceae

Genus: *Garcinia*

Species: *Garcinia mangostana*

Mangosteen (*Garcinia mangostana*) is a tropical evergreen tree belonging to the Clusiaceae family. It is native to Southeast Asia and is known as “queen of the fruits” regarding its pleasant taste and beautiful appearance. The tree can grow 6-25 m with brownish-black and flaky bark. The inner bark is full of yellow and bitter latex. The leaves are opposite, elliptic in shape, entire margin, acute apex, cuneate base, pinnately reticulate venation, leathery, thick, and dark-green color appearance. The upper surface of the leaf is glabrous but dull in the lower surface. The fruit is composed of three parts such as pericarp, pulp, and seed. The whole fruit is 3.4-7.5 cm in diameter attached with green calyx and has white and soft inner pulp, which is edible, while the inedible dark purple pericarp contains various biologically active compounds [13-15]. The pericarp is 0.6-1 cm thick, dark purple or reddish color, and consists of bitter yellow resin. The pulp portion contains four to eight white, juicy, and soft triangular segments. The seed is ovoid, normally 2.5 cm length and 1.6 cm in diameter.

The different parts of mangosteen including pericarp, leaves, and bark have been used as traditional herbal medicine for centuries [13]. The pericarp is used in

the treatment of skin infections, wounds, amoebic dysentery, abdominal pain, diarrhea, fever, and inflammation. The leaves are also used in diarrhea, dysentery, and fever. The bark is applied for urinary tract infection and oral disease. The medicinal properties of mangosteen have corresponded to the chemical constituents in the *G. mangostana*.

2.2 Chemical constituents of *Garcinia mangostana*

Regarding advancements in the field of phytochemistry, the biologically active compounds contained in the mangosteen are isolated and characterized as the secondary metabolites including xanthenes, anthocyanins, phenolic acids, tannins, flavonoids, and isoflavones [16, 17]. Interestingly, the important chemical constituent found in the mangosteen extract is xanthenes, which are the polyphenolic secondary metabolites having a unique chemical structure of tricyclic aromatic system bearing prenyl, methoxy, and hydroxy groups [17]. More than 60 xanthenes (**Figure 4** and **Table 1**) have been isolated from the mangosteen with various isolated solvents including oxygenated solvents such as methanol [18], ethanol [19], and ethyl acetate [20], and non-oxygenated solvents such as benzene [21], and hexane [22]. Based on reported data, the most studied xanthenes are α -mangostin, β -mangostin, gartanin, γ -mangostin, garcinone E, and 8-desoxygartanin [15] because of their wide range of pharmacological properties and potent anti-cancer activity [23]. Among them, α -mangostin is the major natural xanthone, which has an isolation yield around 121 mg/g of dry mangosteen pericarp [24]. Various chemical and biological studies of α -mangostin have been reported [22, 23].

Table 1 Natural xanthenes from *G. mangostana* reported during 1958-2017

Compounds	Plant parts	References
α -Mangostin (1)	Pericarp, bark	[25, 26]
β -Mangostin (2)	Pericarp, bark	[21, 26, 27]
8-Desoxygartanin (3)	Pericarp, bark	[28, 29]
γ -Mangostin (4)	Pericarp	[21]
2,8-Bis-(γ , γ -dimethylallyl)-1,3,7-trihydroxyxanthone (5)	Pericarp	[21]
1-Hydroxy-8-(2-hydroxy-3-methylbut-3-enyl)-3,6,7-trimethoxy-2-(3-methylbut-2-enyl)-xanthone (Methoxy- β -mangostin) (6)	Pericarp, bark	[13, 30, 31]
Cudraxanthone G (7)	Pericarp	[32]
8-Hydroxycudraxanthone G (8)	Pericarp	[32]
Gartanin (9)	Pericarp, bark, leaves	[21, 29, 33]
Garcinone A (10)	Pericarp	[34]
Mangostanol (11)	Pericarp, bark	[35, 36]
3-Isomangostin (12)	Pericarp, bark	[21, 29]
Calabaxanthone (13)	Pericarp	[21]
9-Hydroxycalabaxanthone (Garciniafuran, 5,9-Dihydroxy-8-methoxy-2,2-dimethyl-7-(3-methylbut-2-enyl)-2H,6H-pyrano-[3,2-b]xanthen-6-one) (14)	Pericarp, bark	[29, 35-37]
Demethylcalabaxanthone (15)	Pericarp	[21, 37]
Smeathxanthone A (16)	Pericarp	[32]
Mangostinone (17)	Pericarp	[37]
BR-xanthone B (18)	Pericarp	[38]
1,3,7-Trihydroxy-2-methoxyxanthone (19)	Bark	[39]
3',6'-Dihydroxy-2,4,4'-trimethoxybenzophenone (20)	Bark	[39]

Table 1 Natural xanthenes from *G. mangostana* reported during 1958-2017

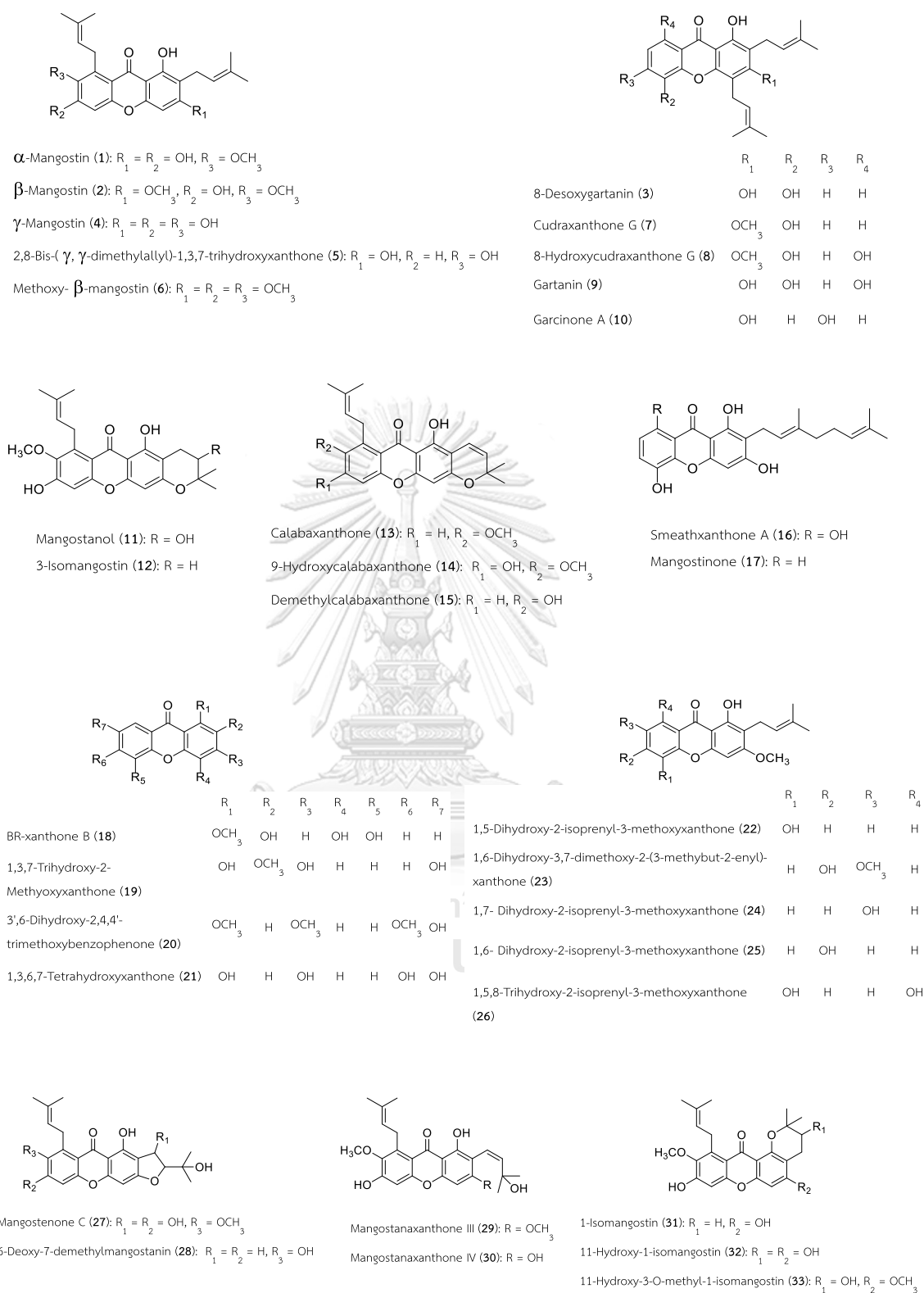
(continued)

Compounds	Plant parts	References
1,3,6,7-Tetrahydroxyxanthone (21)	Bark	[40]
1,5-Dihydroxy-2-isoprenyl-3-methoxyxanthone (22)	Pericarp	[41]
1,6-Dihydroxy-3,7-dimethoxy-2-(3-methylbut-2-enyl)-xanthone (23)	Bark	[30, 36]
1,7- Dihydroxy-2-isoprenyl-3-methoxyxanthone (24)	Pericarp	[41]
1,6- Dihydroxy-2-isoprenyl-3-methoxyxanthone (25)	Leaves	[33]
1,5,8-Trihydroxy-2-isoprenyl-3-methoxyxanthone (26)	Leaves	[33]
Mangostenone C (27)	Pericarp	[35]
6-Deoxy-7-demethylmangostanin (28)	Pericarp	[42]
Mangostanaxanthone III (29)	Pericarp	[43]
Mangostanaxanthone IV (30)	Pericarp	[43]
1-Isomangostin (31)	Pericarp	[21]
11-Hydroxy-1-isomangostin (32)	Pericarp, bark	[20, 29]
11-Hydroxy-3-O-methyl-1-isomangostin (33)	Bark	[29]
Mangostenone E (34)	Pericarp	[35]
Garcinone C (35)	Pericarp	[34]
Garcinone D (36)	Pericarp, bark	[22, 34]
Mangostenone D (37)	Pericarp	[35]
Garcimangosone C (38)	Pericarp	[44]
Mangostenol (39)	Pericarp	[18]
1-Isomangostin hydrate (40)	Pericarp	[21]
3-Isomangostin hydrate (41)	Pericarp	[21]
Trapezifolixanthone (42)	Pericarp	[18]
BR-xanthone A (43)	Pericarp	[38]
Mangostanin (44)	Pericarp	[37]
Mangostenone A (45)	Pericarp	[18]
Mangostenone B (46)	Pericarp	[18]

Table 1 Natural xanthenes from *G. mangostana* reported during 1958-2017

(continued)

Compounds	Plant parts	References
Garcinone B (47)	Pericarp	[34]
Garcinone E (48)	Pericarp	[45]
Garcimangosone A (49)	Pericarp	[44]
Garcimangosone B (50)	Pericarp	[44]
Tovophyllin A (51)	Pericarp	[32]
Tovophyllin B (52)	Pericarp	[36, 37]
Mangoxanthone (53)	Bark	[39]
Mangostingone (54)	Pericarp	[32]
1,3,5-trihydroxy-13,13-dimethyl-2H-pyran[6,7-b]xanthen-9-one (55)	Bark	[39]
7-O-demethyl mangostanin (56)	Pericarp	[19]
Mangosenone F (57)	Pericarp	[46]
Mangostanaxanthone I (58)	Pericarp	[47]
Mangostanaxanthone II (59)	Pericarp	[47]
Parvifolixanthone C (60)	Pericarp	[47]
Rubraxanthone (61)	Pericarp	[47]
Thwaitesixanthone (62)	Pericarp	[35]
Mangosharin (63)	Bark	[36]
Dulxanthone (64)	Bark	[39]
1,2-Dihydro-1,8,10-trihydroxy-2-(2-hydroxypropan-2-yl)-9-(3-methylbut-2-enyl)furo[3,2-a]xanthen-11-one (65)	Pericarp	[42]

Figure 4 Structures of xanthones from *G. mangostana*

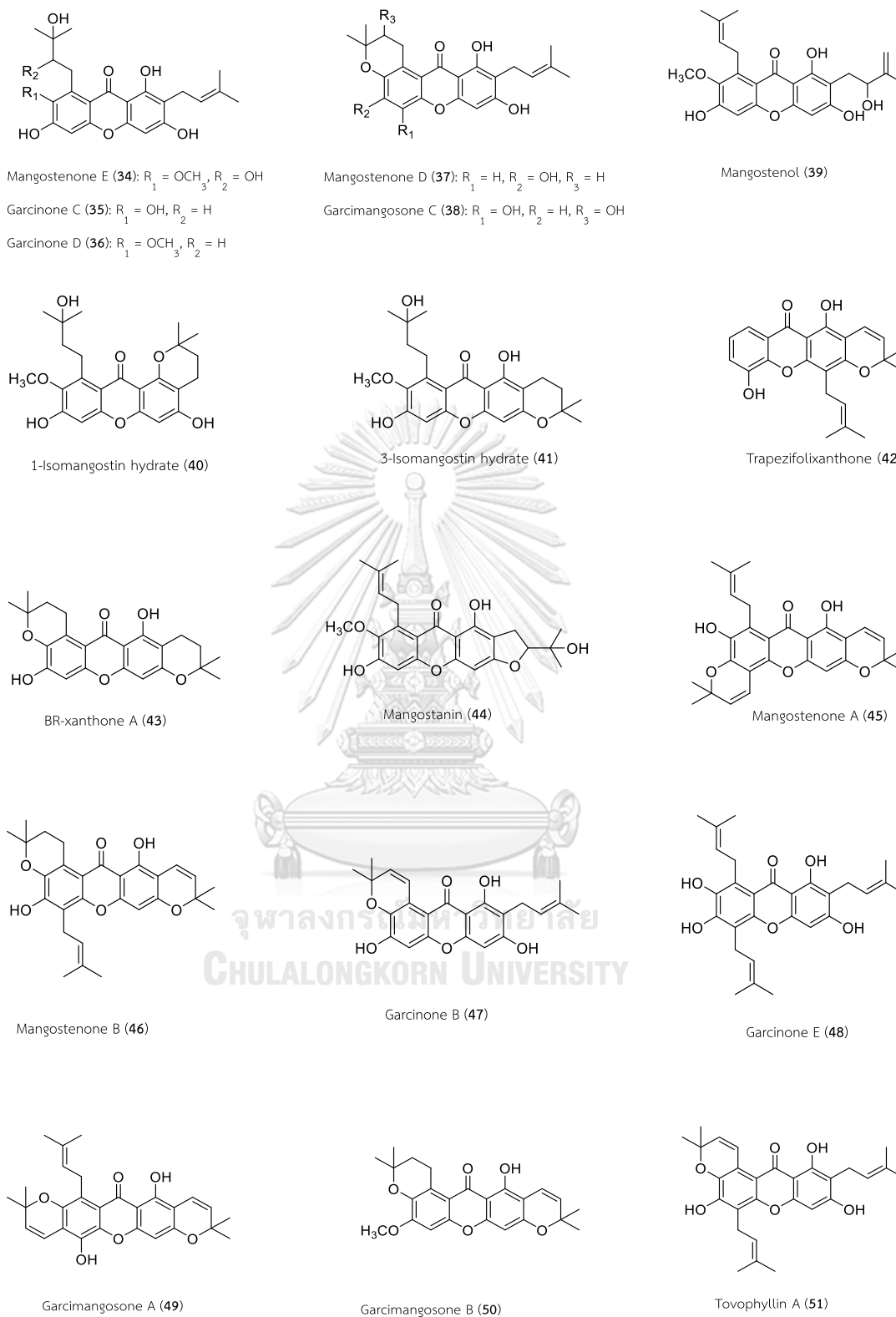


Figure 4 Structures of xanthones from *G. mangostana* (continued)

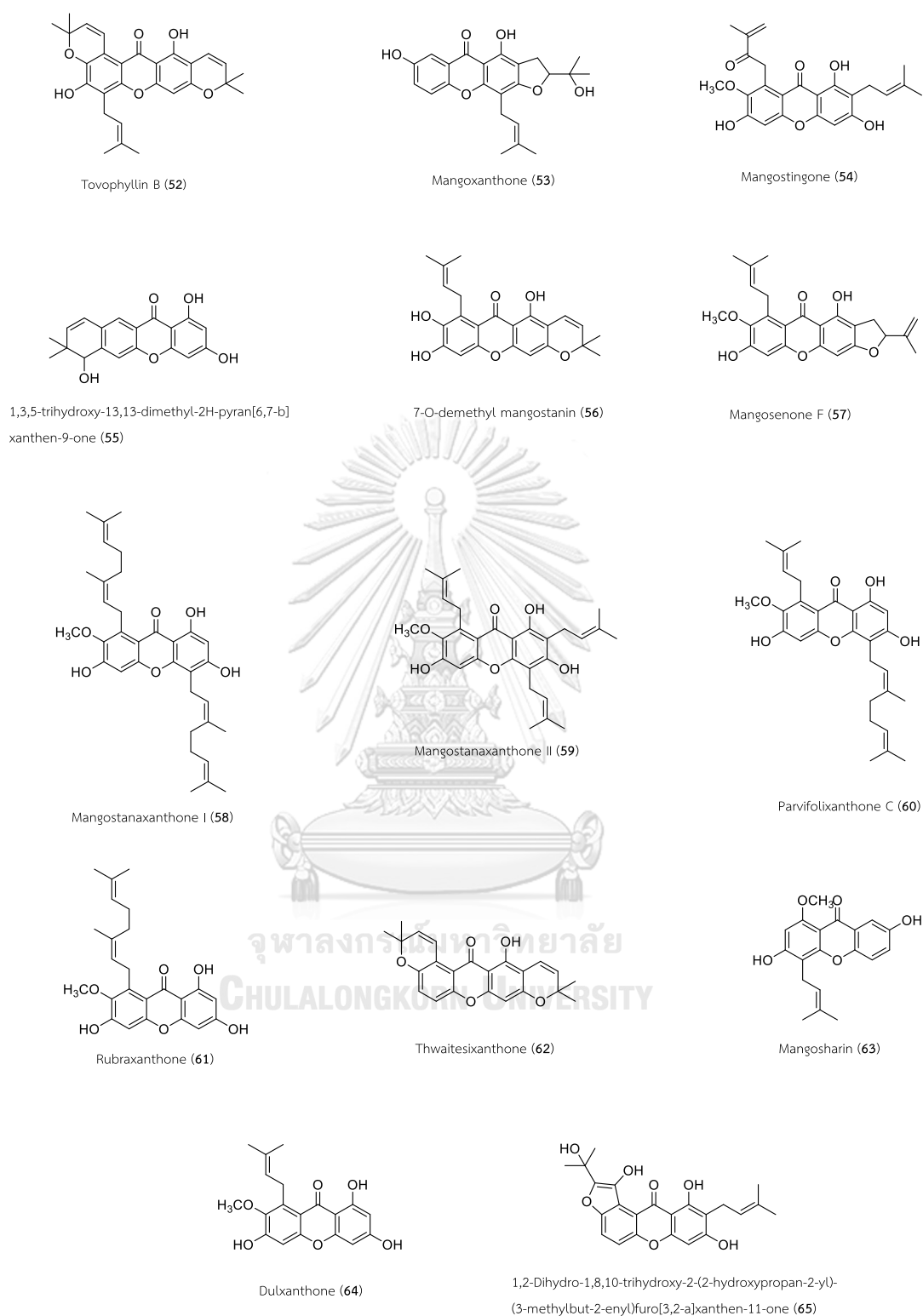


Figure 4 Structures of xanthones from *G. mangostana* (continued)

2.3 Biological activities of α -mangostin

Mangosteen pericarps have been used extensively as folk medicine in Southeast Asia for long times to treat a skin infection, wound, amoebic dysentery, inflammation, diarrhea, and cholera [15]. The major active compound is xanthenes wherein α -mangostin has remarkable pharmacological functions. Numerous *in vitro* and *in vivo* studies had demonstrated that α -mangostin exhibits a wide range of pharmacological properties including antioxidant, anti-inflammatory, anti-bacterial, anti-malarial, anti-obesity, neuroprotective, hepatoprotective, cardioprotective, anti-viral, and anti-cancer effects [8]. Besides, anti-cancer mechanisms of α -mangostin have been described involving cell proliferation, angiogenesis, apoptosis, and cell cycle arrest [8]. To date, α -mangostin has been well-recognized for an anti-microbial agent and is used as an active ingredient in several health and cosmetic products. Moreover, α -mangostin displays the interesting anti-cancer properties towards several cancer cell lines such as leukemia [48], lung [35, 49], breast [35, 50, 51], ovary [52], liver [53], skin [54], brain [55], prostate [56], colon [57], and cervical [58, 59] cancer cells (Table 2).

Table 2 Cytotoxicity of α -mangostin towards different cancer cell lines reported during 2003-2020

Cell lines		IC ₅₀ (μ M)	References
Human leukemia	HL60	6.8	[48]
	K562	5-10	[48]
	NB4	5-10	[48]
	U937	5-10	[48]
Lung cancer	A-549	12.5-15	[49]
	NCI-H187	7	[35]
Breast cancer	BC-1	2.2	[35]
	BJMC3879luc2	12	[50]
	T47D	1.1	[51]
Ovarian cancer	SKOV-3	2.5-3	[52]
Liver cancer	HepG2	5.5-14	[53]
Skin cancer	SK-MEL-28	14.4	[54]
Brain cancer	GBM8401	6.4	[55]
	DBTRG-05MG	7.3	[55]
Prostate cancer	LNCaP	5.9	[56]
	22Rv1	6.9	[56]
	DU145	22.5	[56]
	PC3	12.7	[56]
Colon cancer	DLD-1	7.5	[57]
Cervical cancer	SiHa	20	[58]
	HeLa	16*	[59]

*: EC₅₀

It is noteworthy that α -mangostin exhibited a synergistic effect of growth inhibition in the human colon cancer cell (DLD-1) when combining with 5-fluorouracil (5-FU) at low concentration ($< 5 \mu\text{M}$) [13]. Decreasing the clinical dose of 5-FU, thereby dropping the systemic side effects and rising the therapeutic index was observed in the presence of α -mangostin. This finding suggests that using this natural xanthone with chemotherapeutic agents may increase the therapeutic efficacy and minimize the chemotherapy-induced toxicity [60]. Additionally, the short-term chemopreventive effect of α -mangostin had been examined on rats with putative preneoplastic lesions, which was related to colon carcinogenesis. Dietary administration of α -mangostin at 0.02% and 0.05% concentrations that were given on rat groups treated with 1,2-dimethylhydrazine (DMH) significantly suppressed the induction and development of aberrant crypt foci (ACF) [13]. These results indicate that α -mangostin potentially has chemopreventive and anti-tumor effects. However, there is no clinically approved evidence on the use of α -mangostin because it has high hydrophobicity, which limits aqueous solubility, stability in the aqueous system, and low oral bioavailability [61, 62]. To solve these limitations, various researches have been described as the alternative formulation to increase the aqueous solubility and bioavailability, along with possible synthetic methodologies to produce the new series of α -mangostin derivatives.

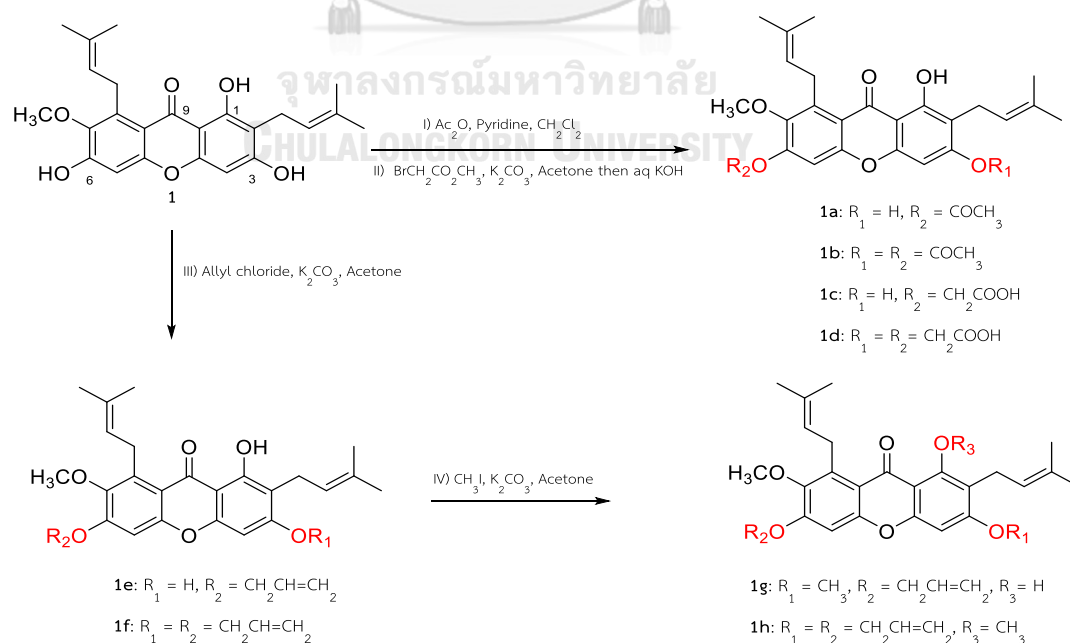
2.4 Syntheses of α -mangostin derivatives

α -Mangostin (**1**) is an oxygenated and prenylated xanthone with a yellow crystallized solid appearance [10]. The chemical structure of α -mangostin consists of xanthone skeleton with prenyl groups at C-2 and C-8, phenolic hydroxy groups at C-1, C-3, C-6, and a methoxy group at C-7. It was firstly isolated by Schmid in 1855 from the mangosteen pericarps and its structure was correctly elucidated in 1958 by Yates and Stout [25]. Numerous α -mangostin derivatives have been synthesized and evaluated the cytotoxicity [9, 10]. The synthesized compounds can be divided into four groups corresponding to the diverse substituents on xanthone core structure

including the phenolic hydroxy groups at C-1, C-3, and C-6, the prenyl groups at C-2 and C-8, the non-substituted aromatic sites at C-4 and C-5, and the methoxy group at C-7.

2.4.1 Modification of hydroxy groups at the positions of C-1, C-3, and C-6

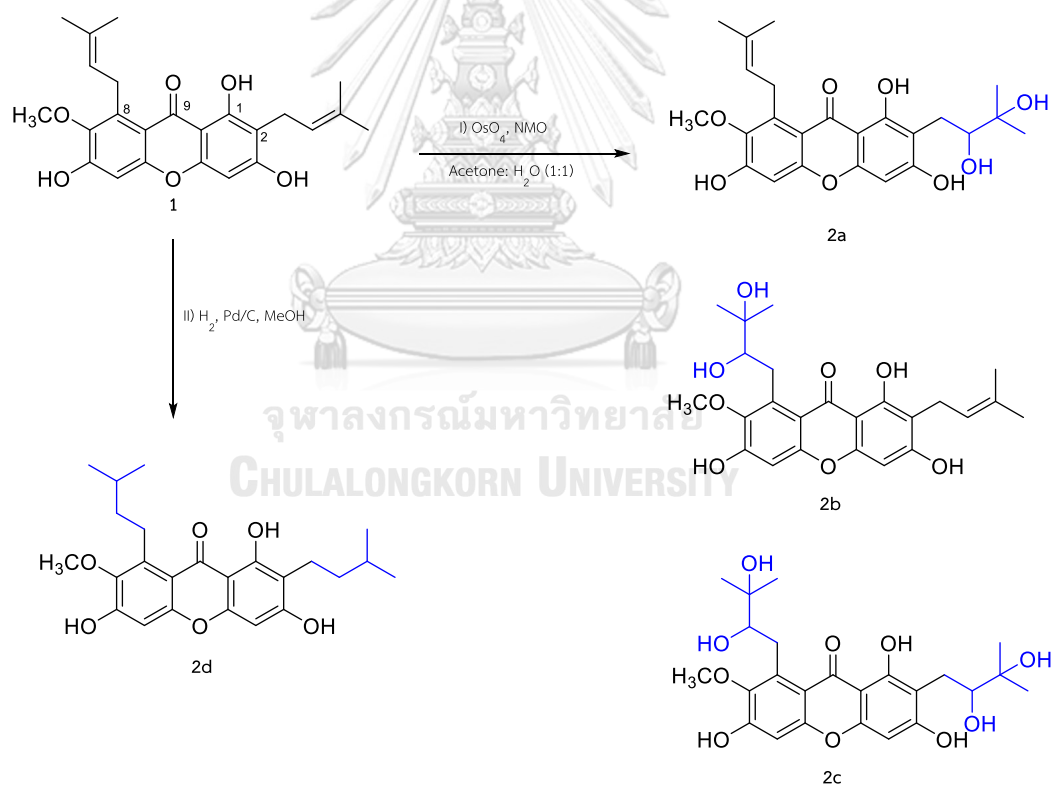
The hydroxy group at C-1 position is less reactive due to the intramolecular hydrogen bond occurs between the hydroxy group of C-1 and carbonyl group of C-9. Thereupon, the modification was mostly taken on C-3 and C-6 positions. α -mangostin was used as a starting material and acetylated with acetic anhydride (Ac_2O) in the presence of pyridine to give **1a** (30%) and **1b** (20%) (Scheme 2(I)). Besides, the introduction of carboxyl at C-3 and C-6 position was performed by methyl bromoacetate and K_2CO_3 followed by basic hydrolysis to produce **1c** (7%) and **1d** (12%) (Scheme 2(II)). Additionally, alkylation of α -mangostin was accomplished by allyl chloride in the presence of potassium carbonate (K_2CO_3) to produce **1e** (59%) and **1f** (20%) (Scheme 2(III)). Furthermore, compounds **1e** and **1f** were methylated with methyl iodide (CH_3I), K_2CO_3 , and acetone to give **1g** (70%) and **1h** (80%) [10] (Scheme 2(IV)).



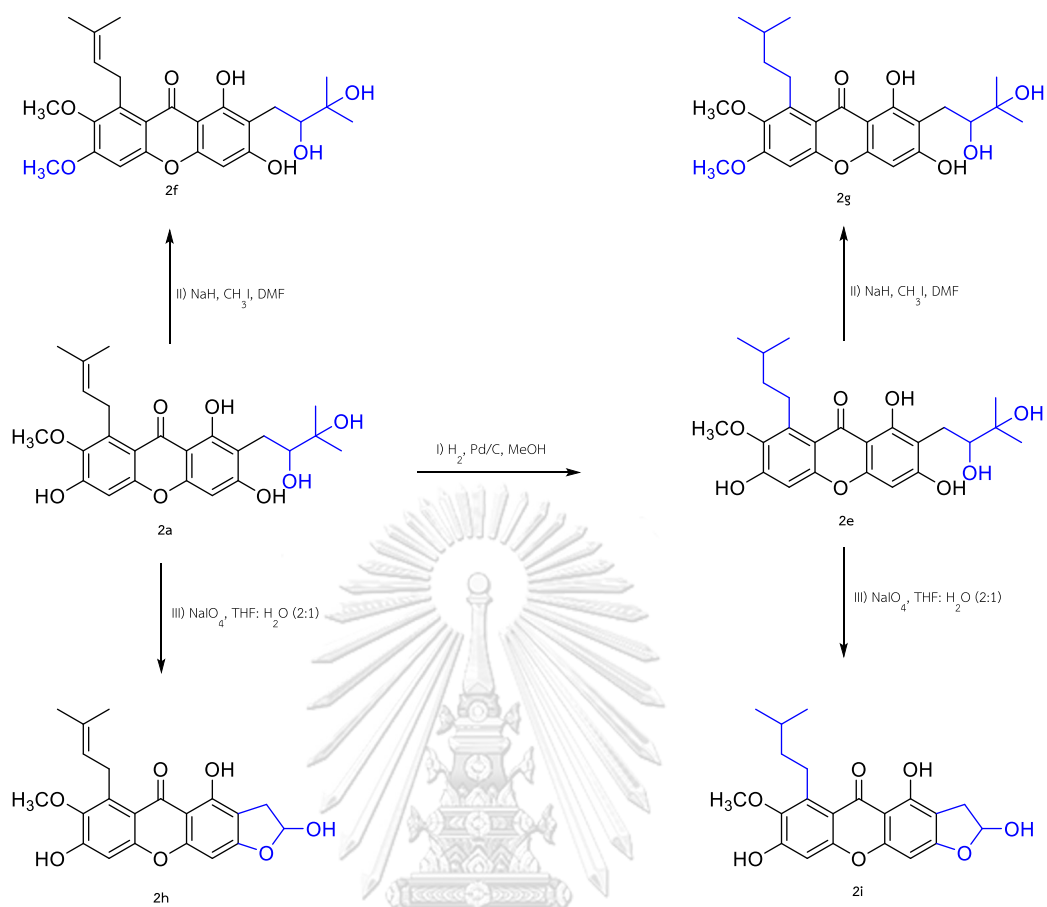
Scheme 2 Syntheses of α -mangostin derivatives **1a-1h**

2.4.2. Modification of prenyl groups at the positions of C-2 and C-8

Oxidation of prenyl groups at C-2 and C-8 positions were synthesized with osmium tetroxide (OsO_4), 4-methylmorpholine-*N*-oxide (NMO) in acetone: H_2O (1:1 v/v) to obtain **2a** (10%), **2b** (12%), and **2c** (78%) (**Scheme 3(I)**) [9]. However, the reduction of prenyl groups was carried out under hydrogenation with H_2 gas and palladium on carbon (Pd/C) as the catalyst to afford compound **2d** (99%) (**Scheme 3(II)**) [10]. Also, compound **2a** was reduced under H_2 gas and Pd/C in MeOH to give compound **2e** (78%) (**Scheme 4(I)**) [9]. Moreover, compounds **2a** and **2e** were methylated with CH_3I , sodium hydride (NaH) in DMF to afford **2f** (60%) and **2g** (60%) (**Scheme 4(II)**) and oxidized with sodium periodate in THF: H_2O (2:1) to give **2h** (60%) and **2i** (60%) (**Scheme 4(III)**) [9].

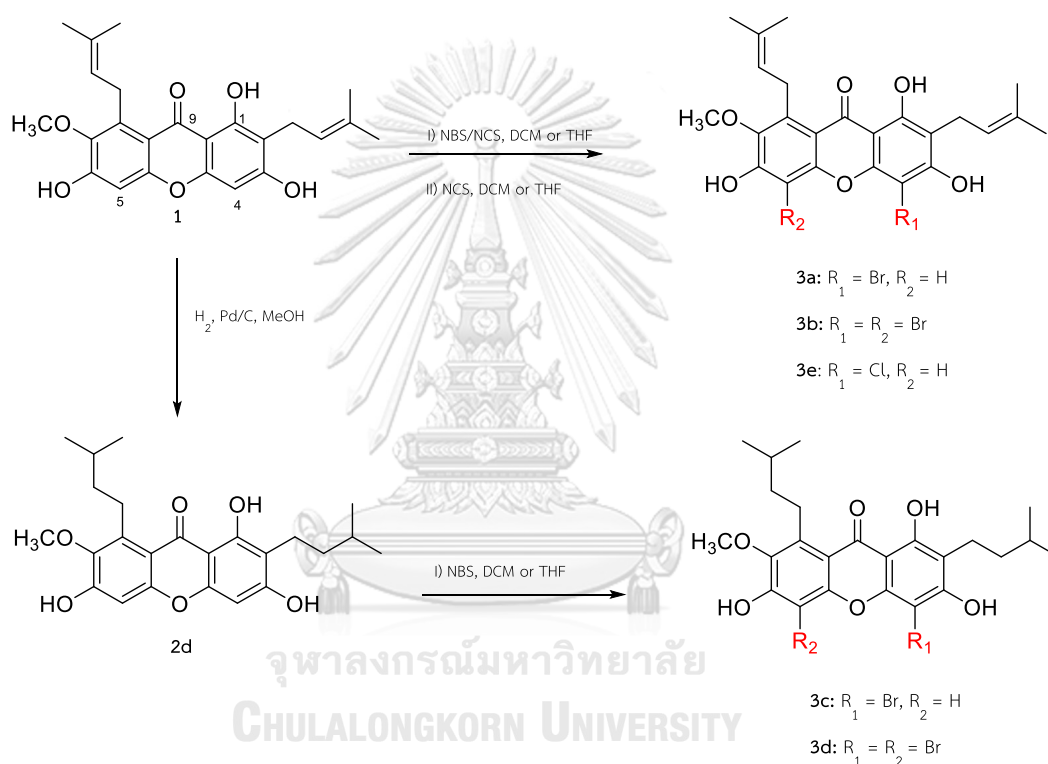


Scheme 3 Syntheses of α -mangostin derivatives **2a-2d**

Scheme 4 Syntheses of α -mangostin derivatives **2e-2i**

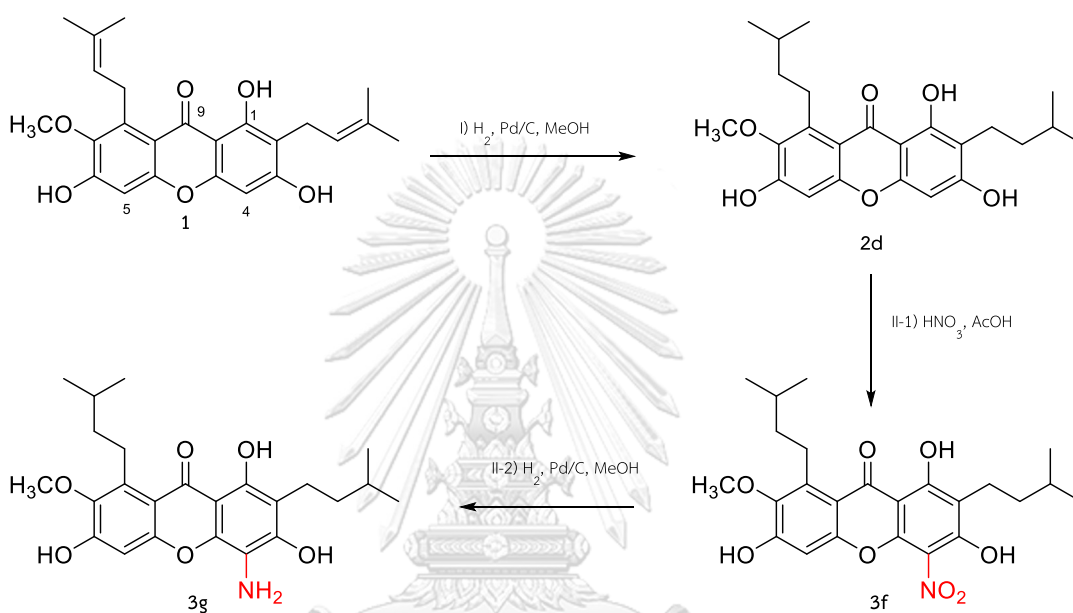
2.4.3 Substitution reaction at the positions of C-4 and C-5

Halogenations at the aromatic C-4 and C-5 positions with bromide of **1** and **2d** were prepared with *N*-bromosuccinimide (NBS) in dichloromethane (DCM), or tetrahydrofuran (THF) to further produce **3a** (12%), **3b** (50%), **3c** (12%) and **3d** (60%) respectively (**Scheme 5 (I)**). Besides, halogenation with chloride of **1** was accomplished by *N*-chlorosuccinimide (NCS) in DCM or THF to afford **3e** (30%) (**Scheme 5 (II)**) [9].



Scheme 5 Syntheses of α -mangostin derivatives **3a-3e**

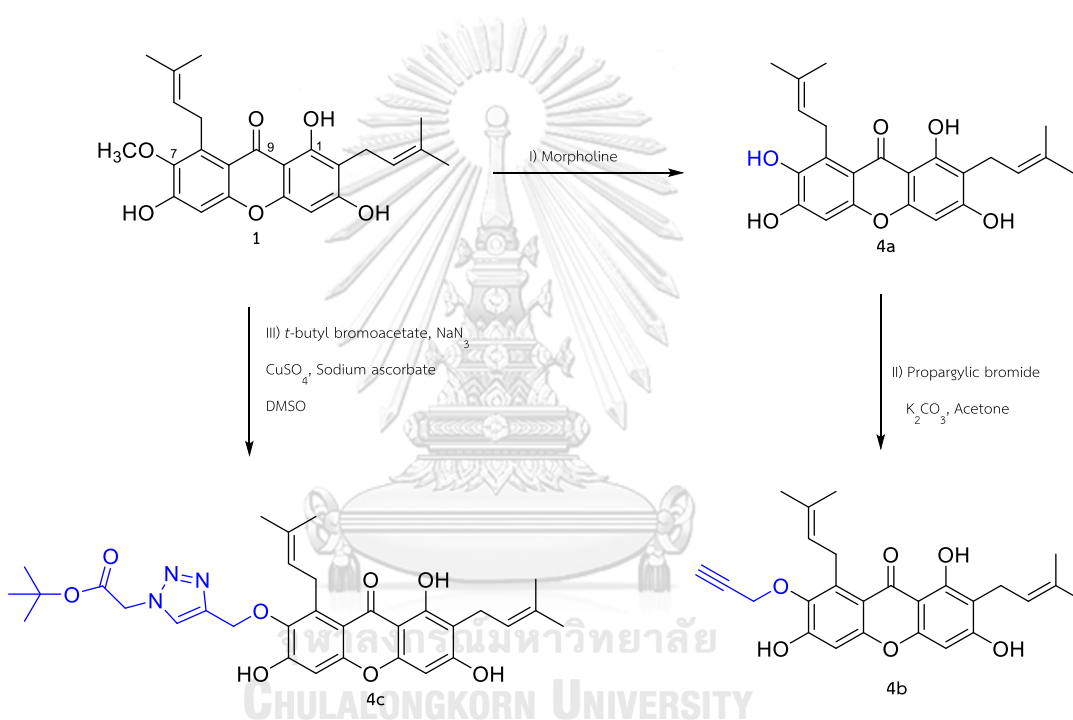
Moreover, nitration of **1** was performed by firstly reduction of prenyl groups at C-2 and C-8 positions to provide **2d** followed by nitration with nitric acid (HNO₃) and acetic acid (AcOH) to afford **3f** (19%) (Scheme 6 (II-1)). Next, compound **3g** (82%) was produced by hydrogenation of **3f** by H₂ and Pd/C [10] (Scheme 6 (II-2)).



Scheme 6 Syntheses of α -mangostin derivatives **3f** and **3g**

2.4.4 Modification of methoxy group at the position of C-7

Demethylation of methoxy group at C-7 of **1** was achieved by using morpholine to obtain **4a** (32%) and followed by the mono-alkylation with propargylic bromide and K_2CO_3 in acetone to afford **4b** (34%) (**Scheme 7 (I-II)**) [10]. Moreover, treatment **1** with *t*-butyl bromoacetate, sodium azide (NaN_3) followed by copper sulphate ($CuSO_4$), and sodium ascorbate in dimethylsulfoxide (DMSO) produced **4c** (19%) through modified click reaction (**Scheme 7 (III)**) [10].



Scheme 7 Syntheses of α -mangostin derivatives **4a-4c**

Moreover, several chemical modifications at C-2, C-3, C-4, C-5, C-6, and C-8 have been reported showing the additional substituents including ether, lactone, and halide [63-68] as shown in the following figures (**Figure 5-8**), which were reported during 2015-2020.

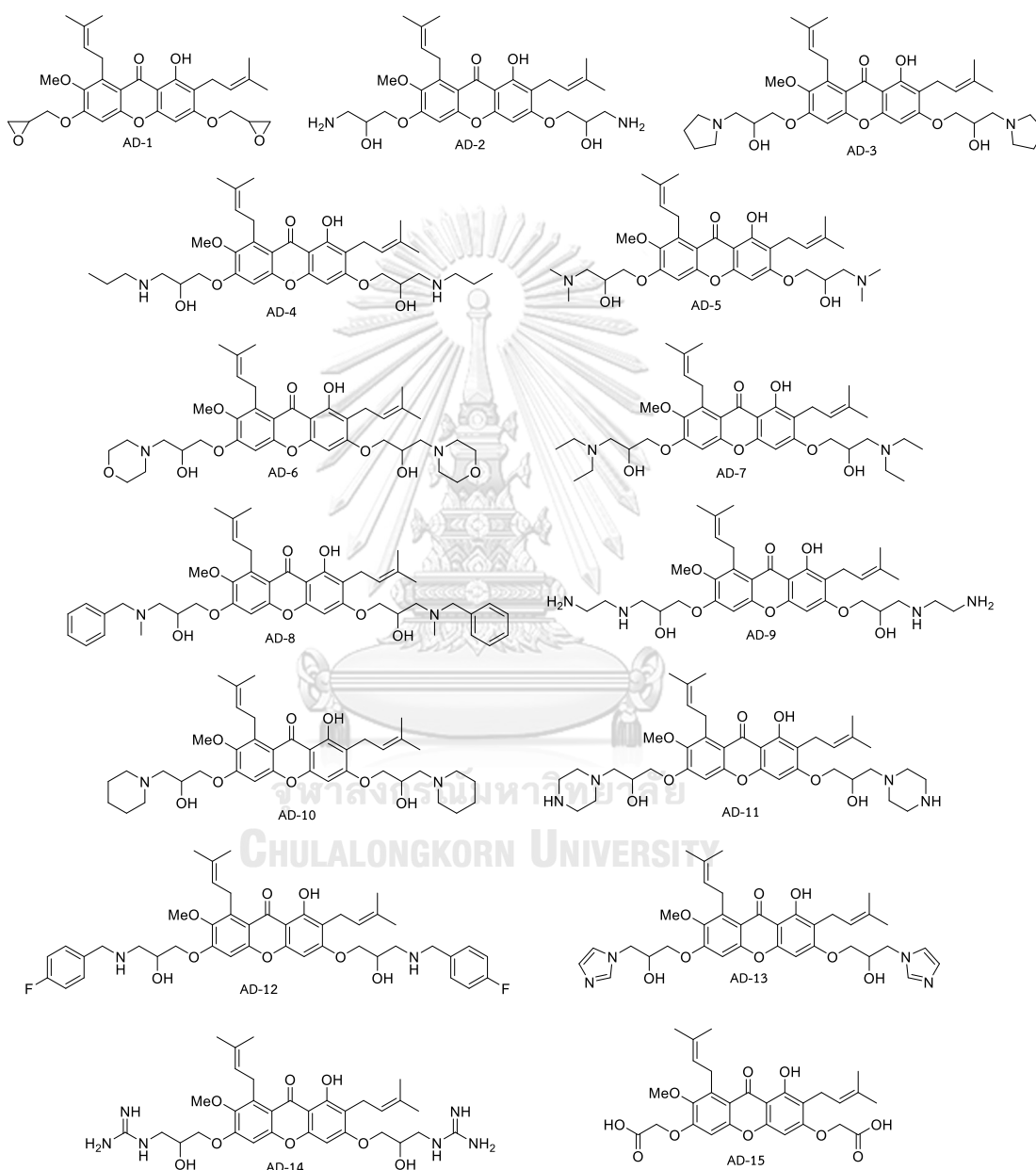


Figure 5 α -Mangostin derivatives (AD) with modification of hydroxy groups of α -mangostin at C-3 and C-6 positions [63]

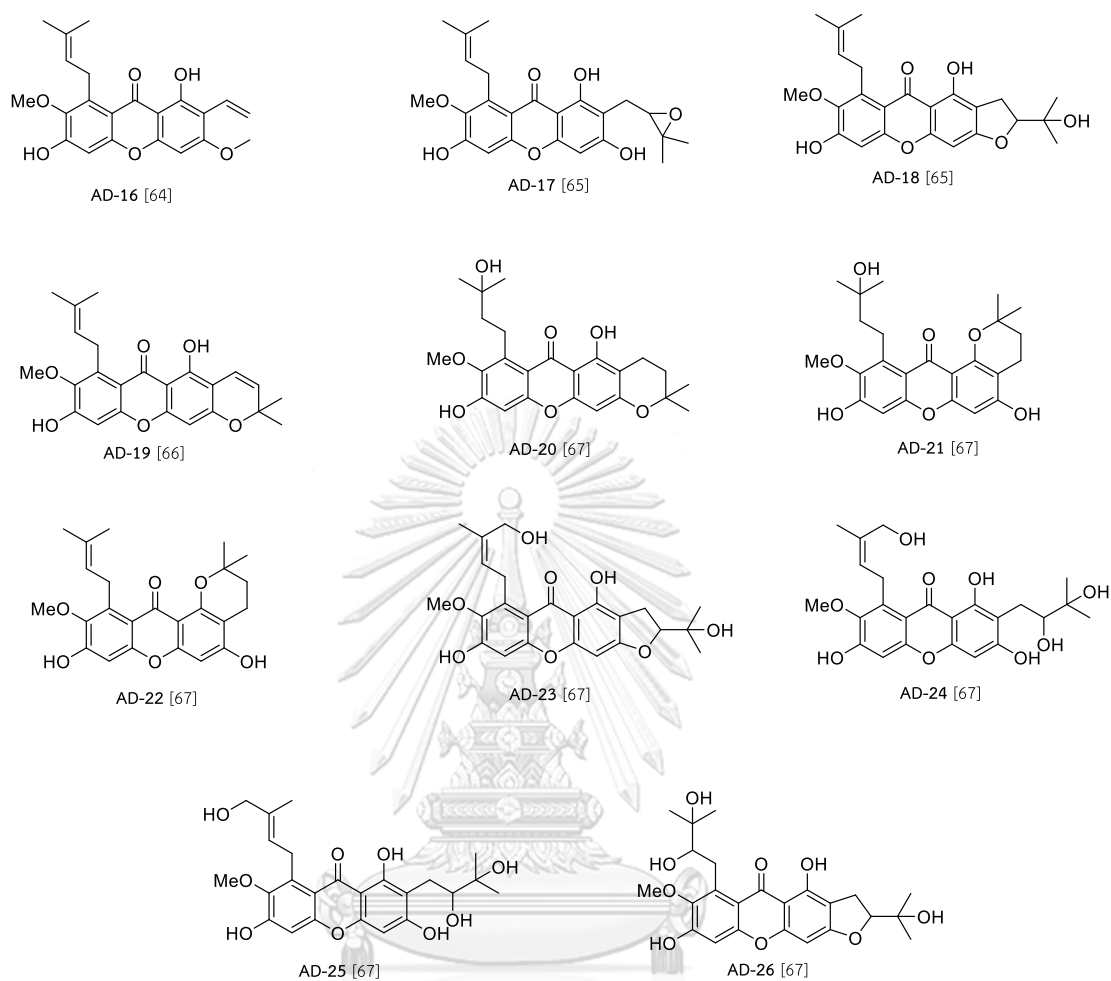


Figure 6 α -Mangostin derivatives (AD) with modification of prenyl groups of α -mangostin at C-2 and C-8 positions

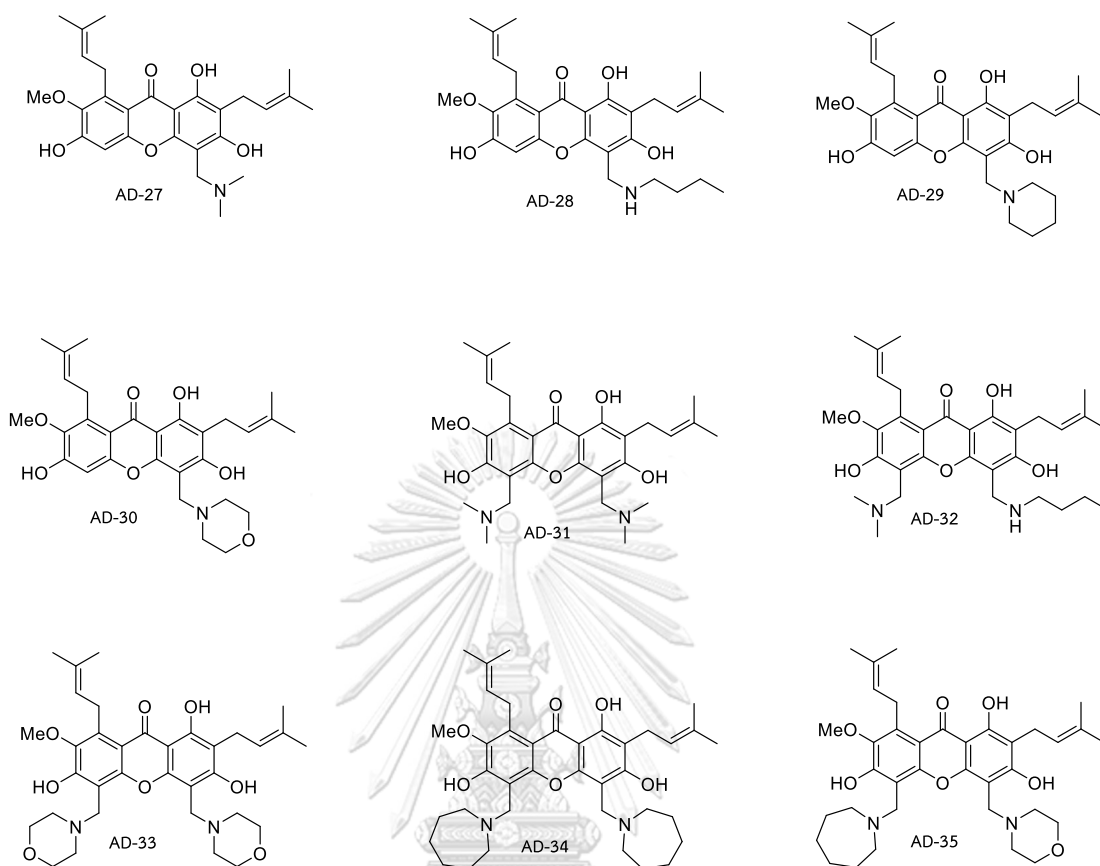


Figure 7 α -Mangostin derivatives (AD) with substitution of aromatic sites of α -mangostin at C-4 and C-5 positions [68]

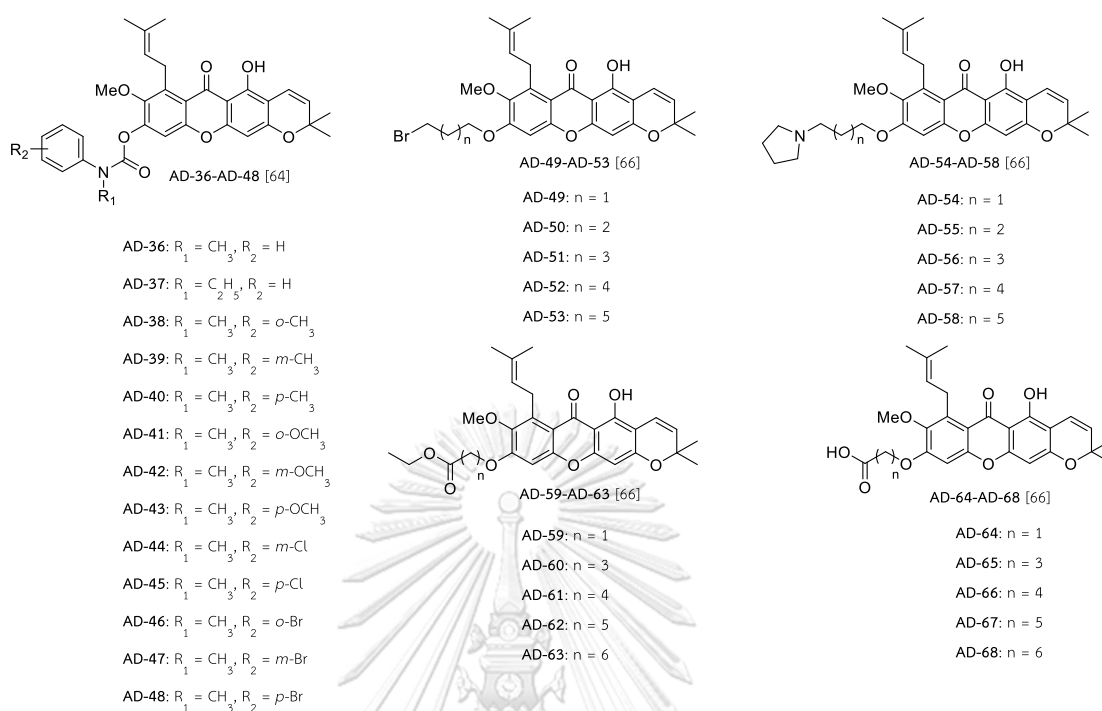


Figure 8 α -Mangostin derivatives (AD) with modification of C-2 and C-6 positions

CHAPTER III RESEARCH METHODOLOGY

Contents

- 3.1 Plant materials
- 3.2 General experimental procedures
 - 3.2.1 Thin-layer chromatography (TLC)
 - 3.2.2 Quick column chromatography (QCC)
 - 3.2.3 Flash column chromatography (FCC)
 - 3.2.4 Nuclear magnetic resonance spectroscopy (NMR)
 - 3.2.5 Mass spectrometry (MS)
 - 3.2.6 Ultraviolet-visible spectrophotometer (UV-vis)
 - 3.2.7 Chemicals and solvents
 - 3.2.8 SwissADME web tool
 - 3.2.9 Cell culture
 - 3.2.10 Statistical analysis
- 3.3 Extraction, isolation, and purification of mangosteen pericarp
- 3.4 Chemical and biological study of α -mangostin derivatives from Smiles rearrangement
 - 3.4.1 Semi-synthesis of α -mangostin derivatives *via* Smiles rearrangement
 - 3.4.1.1 General procedure
 - 3.4.1.2 Reaction condition optimization
 - 3.4.2 Estimation of aqueous solubility and drug-likeness of α -mangostin derivatives from Smiles rearrangement
 - 3.4.3 Cytotoxicity assay against the non-small-cell lung cancer cell lines (H460 and H292)

- 3.4.4 DNA staining assay against the non-small-cell lung cancer cell lines (H460 and H292)
- 3.5 Chemical and biological study of α -mangostin-carbamate prodrugs
 - 3.5.1 Semi-synthesis of α -mangostin derivatives containing carbamate moiety
 - 3.5.1.1 Reaction condition optimization
 - 3.5.1.2 Semi-synthesis of α -mangostin derivatives containing carbamate motif
 - 3.5.1.3 General procedure
 - 3.5.2 Estimation of aqueous solubility and drug-likeness of α -mangostin derivatives containing carbamate moiety
 - 3.5.3 Detection of stability of α -mangostin derivatives by UV-vis spectrophotometer
 - 3.5.4 Cytotoxicity assay against the non-small-cell lung cancer cell line (H460)

3.1 Plant materials

Around 1.5 kg of dried mangosteen pericarps were powdered by grinding machine using the sieve with 0.5 mm in diameter. The resulting powder was kept at room temperature.

3.2 General experimental procedures

3.2.1 Thin-layer chromatography (TLC)

Technique	: One-dimension, ascending method
Adsorbent	: Silica gel 60 F ₂₅₄ precoated plate of aluminium
Layer thickness	: 0.2 mm
Length	: 5 cm
Temperature	: Normal room temperature (30-35°C)
Detection	: Ultraviolet light using both short-wavelength 254 nm and long-wavelength 366 nm.

3.2.2 Quick column chromatography (QCC)

Adsorbent	: Silica gel 60 (0.040-0.063 mm particle size)
Column size	: 11 cm in diameter, 4 cm in length for sample size of ~30 g
Packing column	: 200 g of silica was suspended in an eluent for 30 minutes to prepare the wet-packing column. The slurry was stirred and poured into the 500 mL Büchner funnel, which was connected to the vacuum adapter from the aspirator pump. The solvent was drained by gravity force followed by reduced pressure and the funnel was tapped to pack the adsorbent tightly. The adsorbent was dried completely with the help of an aspirator pump. Finally, the height of the packing column was obtained around 5-7 cm of the funnel.

Sample loading : The sample was mixed with silica gel and a small amount of volatile CH_2Cl_2 was added to obtain a homogeneous fine powder. It was placed into the packing column and the surface was pressed in order to compact and obtain the uniform surface of the powder. The top of the surface was covered with cotton to avoid cracking of the loading surface while pouring the solvent. The eluent was drained by reduced pressure.

Detection : TLC technique as mentioned above was applied to monitor each fraction.

3.2.3 Flash column chromatography (FCC)

Adsorbent : Silica gel 60 (0.040-0.063 mm particle size)

Column size : A) Around 2 cm in diameter with 30 cm in length for the sample size of 20-50 mg (silica gel ~20 g)

B) Around 3 cm in diameter with 50 cm in length for the sample size of 0.2-0.8 g (silica gel ~30 g)

C) Around 5 cm in diameter with 50 cm in length for the sample size of 2-5 g (silica gel ~60 g)

Packing column : The adsorbent was suspended in an eluent for 30 minutes to prepare the wet-packing column. The slurry was stirred and poured into the column and the eluent was drained by positive pressure using a mechanic air pump. The column was tapped to pack the adsorbent tightly and the height of the packing column was obtained around 15 cm of the column. The flow rate by compressed air was adjusted to 1-2 mL/min. The adsorbent was always saturated with solvent during sample loading and purification.

Detection : TLC technique as mentioned above was applied to monitor each fraction.

3.2.4 Nuclear magnetic resonance spectroscopy (NMR)

Nuclear magnetic resonance (NMR) spectroscopy such as ^1H NMR and ^{13}C NMR were recorded on a Bruker Avance DPX-300 instrument using deuterated acetone $(\text{CD}_3)_2\text{CO}$ as solvent and solvent signals served as δ_{H} 2.04, δ_{C} 29.8 and δ_{C} 206.3. The measurement was done under the service of the Scientific and Technological Research Equipment Center, Chulalongkorn University, Bangkok, Thailand.

3.2.5 Mass spectrometry (MS)

High-resolution electrospray ionization mass spectra (HRESIMS) were obtained with a Bruker micrOTOF instrument. To confirm the molecular formula of the compounds, the exact molecular weight was calculated by mass spectra. The measurement was done under the service of the Department of Chemistry, Faculty of Science, Mahidol University, Bangkok, Thailand.

3.2.6 Ultraviolet-visible spectrophotometer (UV-vis)

UV-vis absorption spectra were recorded by Agilent Cary 60 UV-Vis spectrophotometer at the Pharmaceutical Research Instrument Center, Faculty of Pharmaceutical Sciences, Chulalongkorn University to measure the decomposition rate of the compounds.

3.2.7 Chemicals and solvents

All chemical reagents were purchased from TCI (Tokyo Chemical Industry). Additionally, organic solvents applied throughout this research were commercial grade and purified by distillation prior to use. Specifically, solvents used for semi-synthesis of compounds were analytical reagent (AR) grade or dried over molecular sieves 4\AA . Solvent for UV-vis spectrophotometric measurements were HPLC grade solvents.

3.2.8 SwissADME web tool

The solubility of compounds was calculated by the online SwissADME web tool from Molecular Modelling Group of the Swiss Institute of Bioinformatics (SIB).

3.2.9 Cell culture

All human lung cancer cell lines including H460 and H292 were obtained from American Type Culture Collection (ATCC), Manassas, USA. They were cultured in Roswell Park Memorial Institute (RPMI) medium and maintained in a culture plate with an ultra-flat bottom surface that one may attach the cells with the optimized condition at 37°C in a 5% CO₂ humidified incubator. The medium was supplemented with 10% fetal bovine serum (FBS) and 2 mM L-glutamine, 100 units/mL of penicillin/streptomycin solution, which were procured from Gibco (Gaithersburg, MA, USA). 70-80% confluence of the cells in the culture plate were used to continue experiments. The results of 3-(4,5-Dimethylthiazol-2-yl)-2,5-Diphenyltetrazolium Bromide (MTT) assay were measured at 570 nm by Perkin Elmer VICTOR³ microplate reader (Pharmaceutical Research Instrument Center, Faculty of Pharmaceutical Sciences, Chulalongkorn University). Besides, DNA staining assay was examined by fluorescence microscope Olympus IX51 with DP70 instrument. (Pharmaceutical Research Instrument Center, Faculty of Pharmaceutical Sciences, Chulalongkorn University).

3.2.10 Statistical analysis

Data were performed as mean values and standard deviation. Significance was analyzed by a one-way ANOVA method followed by Tukey HSD post hoc test using SPSS Statistic 22 version (Armonk, NY) software and the significance level was determined at $p < 0.05$. The structures of compounds were drawn by using ChemDraw Professional 16.0 software.

3.3 Extraction, isolation, and purification of mangosteen pericarp

Dried and powdered pericarps of *G. mangostana* (500 g) were packed with the white filter cloth and the package was put into the vessel for the extraction process. To macerate the sample, firstly, the appropriate amount of hexane (non-polar solvent) was added until the sample was completely soaked and macerated for 3 days at room temperature. Next, hexane crude extract and marc were separated. The crude extract was filtered by gravity filtration. The filtrate was evaporated by a rotary evaporator. After that, this process was repeated for one more time and the hexane crude extracts were combined. Thereby, the solid marc was sequentially extracted with ethyl acetate (EtOAc), methanol (MeOH), and a mixture of water: MeOH solvent (1:1 v/v) to obtain the EtOAc crude extract, MeOH crude extract, aqueous crude extract, respectively. Next, all the crude extracts were monitored by TLC. The crude extract showed a substantial amount of α -mangostin was selected for further purification by flash column chromatography (FCC) using silica as a stationary phase and a mixture of hexane and EtOAc (100%:0-0:100%) as a mobile phase system. Then, the obtaining α -mangostin was crystallized in EtOAc.

3.4 Chemical and biological study of α -mangostin derivatives from Smiles rearrangement

3.4.1 Semi-synthesis of α -mangostin derivatives *via* Smiles rearrangement

3.4.1.1 General procedure

α -Mangostin derivatives were semi-synthesized by transforming the OH group of α -mangostin to the NH₂ group *via* Smiles rearrangement (Figure 9). The reaction was performed by adding α -mangostin (1) (1 equiv, 0.49 mmol, 200 mg), 2-chloroacetamide (1.2 equiv, 55 mg), K₂CO₃ (2.5 equiv), and KI (0.2 equiv) into the oven-dried round-bottomed flask. *N,N*-dimethylformamide (DMF, 10 mL) was added and the reaction mixture was reflux at 90°C for 1 h and then 150°C for another 4 h (Figure 9). After the reaction showed completion by TLC monitoring, DMF was removed by dissolving in water (30 mL). The mixture was extracted with EtOAc (4x50 mL) by using a separating funnel. After that, EtOAc layers were combined and dried over anhydrous magnesium sulphate (MgSO₄), filtered and concentrated by rotary evaporator to obtain the crude product. The crude product was purified by flash column chromatography applying silica gel as a stationary phase and a solution of hexane: EtOAc mixture (100%:0-0:100%) as a mobile phase. Each obtaining fraction was checked by TLC using hexane: EtOAc (3:7) as a mobile phase. Subsequently, the purified products were structurally characterized by ¹H and ¹³C NMR, and mass spectrometry and the % yield was calculated.

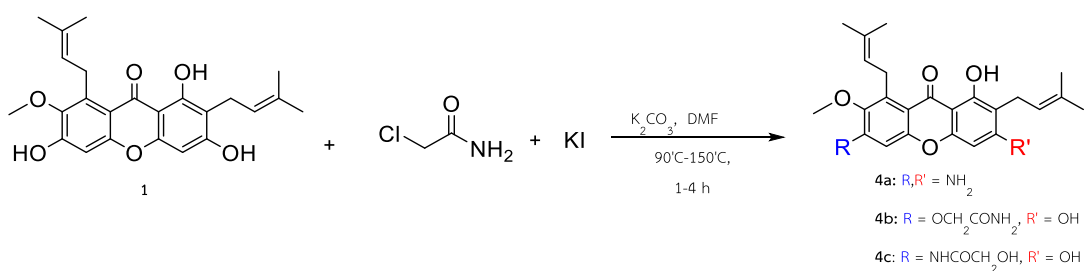


Figure 9 General reaction for Smiles rearrangement

3.4.1.2 Reaction condition optimization

To establish the appropriate reaction condition, a variety of experimental conditions including temperature, reaction time, base, and KI equivalent were optimized. The temperature was controlled under the reflux and microwave apparatus. Besides, examinations of the effects of bases such as K_2CO_3 , KOH, and Cs_2CO_3 were used in this experiment. Moreover, the amount of KI as a catalyst at 0.2 and 0.5 equivalent, and the stoichiometric amount at 1 equivalent were employed in this study (**Table 3**). The optimized condition was analyzed and chosen based on the isolated yield %.

Table 3 Reaction optimization of Smiles rearrangement

Entry	Reaction apparatus	Base	KI equivalent	Step 1: Substitution	Step 2: Rearrangement
1.	Reflux	K_2CO_3	0.2	90°C, 1h	150°C, 4h
2.	Microwave	K_2CO_3	0.2	1 min, 5 times	150°C, 4h
3.	Reflux	K_2CO_3	0.5	90°C, 1h	150°C, 4h
4.	Reflux	K_2CO_3	1	90°C, 1h	150°C, 4h
5.	Reflux	K_2CO_3	1	90°C, 1h	150°C, 10h
6.	Reflux	KOH	0.2	90°C, 1h	150°C, 4h
7.	Reflux	KOH	1	90°C, 1h	150°C, 4h
8.	Reflux	Cs_2CO_3	0.2	90°C, 1h	150°C, 4h
9.	Reflux	Cs_2CO_3	1	90°C, 1h	150°C, 4h

3.4.2 Estimation of aqueous solubility and drug-likeness of α -mangostin derivatives from Smiles rearrangement

The aqueous solubility and drug-likeness of α -mangostin derivatives from Smiles rearrangement were performed by *in silico* computational analysis using the free web tool SwissADME and available at <http://www.swissadme.ch> [69]. The Simplified Molecular Input Line Entry System (SMILES) lists were generated by importing the structure file from ChemDraw Professional 16.0. The aqueous solubility was assessed utilizing three predictive parameters; ESOL, Ali, and SILICOS-IT together with log *S* estimation. The estimation of drug-likeness analysis was established by five different rules of filters from pharmaceutical companies as Lipinski (Pfizer), Ghose (Amgen), Veber (GSK), Egan (Pharmacia), and Muegge (Bayer). The Abbot bioavailability score was measured to estimate the probability of >10 % oral bioavailability in rats or Caco-2 diffusion.

3.4.3 Cytotoxicity assay against the non-small-cell lung cancer cell lines (H460 and H292)

The cytotoxicity of α -mangostin derivatives from Smiles rearrangement was evaluated by *in vitro* 3-(4,5-dimethylthiazol-2-yl)2,5-diphenyltetrazolium bromide (MTT) colorimetric assay which measures the capacity of the mitochondrial enzyme such as succinate dehydrogenase present in viable cells to reduce the tetrazolium compound of MTT to its cell membrane-impermeable purple formazan crystals. Human non-small-cell lung cancer cell lines such as H460 and H292 were seeded in 96-well flat-bottom microtiter plate at the cell density of 1×10^5 cells/well in RPMI medium and allowed to adhere the plate for 24 h at 37°C in a 5% CO₂ incubator. After 24 h, the cells were treated with a series of α -mangostin derivatives with different concentrations and avoid the precipitation of the compounds in the cell culture medium. The test compounds were made by the serial dilution concentration in RPMI containing <0.5% dimethyl sulfoxide (DMSO). Cisplatin was used as a positive control and medium was applied as a negative control. The

treated cells were incubated at 37°C in 5% CO₂ atmosphere for 24 h. After that, the cell viability was determined by adding 100 µL of MTT solution in RPMI medium at 0.4 mg/mL concentration and the test plates were incubated in a dark place at 37°C in a CO₂ incubator for 3 h. After incubation, the liquid media were removed and 100 µL of DMSO was added into each well to dissolve the formazan purple crystals. The intensity of the dissolved formazan crystals as well as the absorbance was measured by using a microplate reader at 570 nm and then the percentage of inhibition and half maximal inhibitory concentration IC₅₀ of this cytotoxicity test was calculated by Excel, Microsoft software. Each experiment was performed in triplicate.

3.4.4 DNA staining assay on against the non-small-cell lung cancer cell lines (H460 and H292)

For DNA staining assay, costaining of Hoechst33342 and propidium iodide (PI) was used to detect apoptotic and necrotic cell death. H460 and H292 cells were seeded with a density of 1×10⁵ cells/well in a 96-well flat-bottom microtiter plate for 24 h at 37°C in a 5% CO₂ incubator. Different concentrations of **α**-mangostin derivatives were treated on the cells for 24 h. After 24 h of treatment, the cells were stained with a concentration of 10 µg/mL Hoechst 33342 and 5 µg/mL PI dyes for 30 mins at 37°C. The mechanism of cell death was examined by a fluorescence microscope and the percentage of apoptotic cells was determined using the following formula.

$$\% \text{Apoptotic cells} = \frac{A+LA}{T} \times 100$$

A is the number of apoptotic cells

LA is the number of late apoptotic cells

T is the number of total cells

3.5 Chemical and biological study of α -mangostin-carbamate prodrugs

3.5.1 Semi-synthesis of α -mangostin derivatives containing carbamate moiety

3.5.1.1 Reaction condition optimization

In this semi-synthesis of α -mangostin derivatives, carbamate is formed by the nucleophilic addition of the hydroxyl group of α -mangostin to the reactive carbonyl of isocyanate. To optimize the reaction condition, 3-chlorophenyl isocyanate was used as a model study (**Figure 10**). The first step of reaction optimization was finding the suitable solvent for the reaction to obtain the prospective isolated yield, using 5 different types of solvents such as dichloromethane (DCM), ethyl acetate (EtOAc), tetrahydrofuran (THF), toluene, and *N,N*-dimethylformamide (DMF). The reaction was performed as described in the general procedure without using a base. The reaction mixture was stirred at room temperature for 17 h. Then, it was heated at 40°C and stirred for another 9 h. Secondly, the reaction was optimized by focusing on the base as a catalyst, utilizing K_2CO_3 and triethylamine (TEA). In this optimization (**Table 4**), the reaction was added to the appropriate solvent and stirred at room temperature for 4 h. Sequentially, the temperature and reaction time were determined.

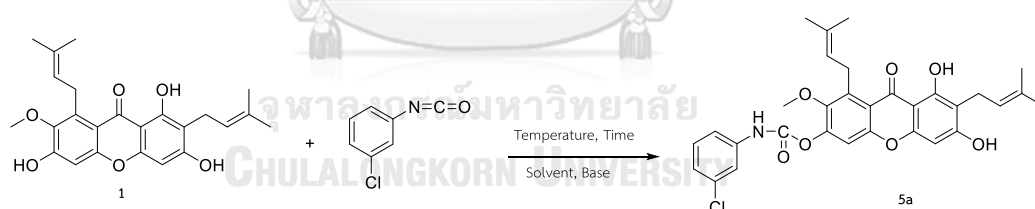


Figure 10 General reaction for the synthesis of carbamate from 3-chlorophenyl isocyanate

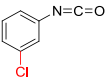
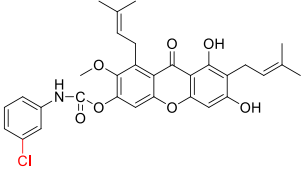
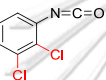
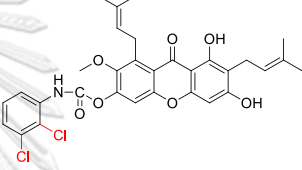
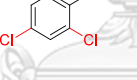
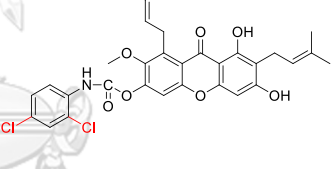
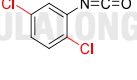
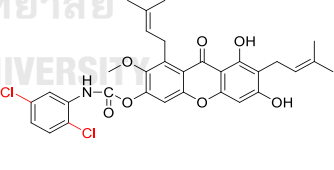
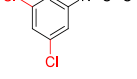
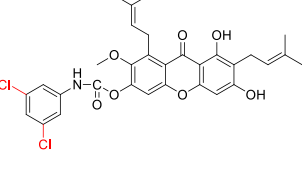
Table 4 Optimization conditions for carbamate formation

Entry	Solvent	Base	Temperature and time
1.	DCM	-	r.t., 17h then 40°C 9h
2.	EtOAc	-	r.t., 17h then 40°C 9h
3.	THF	-	r.t., 17h then 40°C 9h
4.	Toluene	-	r.t., 17h then 40°C 9h
5.	DMF	-	r.t., 17h then 40°C 9h
6.	Solvent	K ₂ CO ₃	r.t., 4h
7.	Solvent	TEA	r.t., 4h

3.5.1.2 Semi-synthesis of α -mangostin derivatives containing carbamate motif

After optimization of the solvent, base, temperature, and reaction time, the best condition was chosen and the semi-synthesis of α -mangostin derivatives containing carbamate moiety using various chlorinated isocyanate reagents were investigated (**Table 5**).

Table 5 Structures of chlorinated isocyanate reagents and the corresponding α -mangostin derivatives containing carbamate moiety

Entry	Isocyanate reagents	Corresponding α -mangostin derivatives
1.	 3-chlorophenyl isocyanate	 5a
2.	 2,3-dichlorophenyl isocyanate	 5b
3.	 2,4-dichlorophenyl isocyanate	 5c
4.	 2,5-dichlorophenyl isocyanate	 5d
5.	 3,5-dichlorophenyl isocyanate	 5e

3.5.1.3 General procedure

α -mangostin (**1**) (1 equiv, 0.12 mmol, 50 mg) was added into an oven-dried round-bottomed flask containing a magnetic stirrer and was dissolved in the dried solvent (10 mL). Then, isocyanate reagent (3 equiv) and base (0.5 equiv) were added into the reaction mixture. The reaction was stirred at an appropriate temperature and time. After that, the product was monitored by TLC using hexane: EtOAc (7:3) as a developing system. After completion, the reaction was concentrated and purified by flash column chromatography using silica gel as a stationary phase and a mixture of hexane and EtOAc as the mobile phase. Subsequently, the purified products (**Figure 11**) were structurally characterized by ^1H and ^{13}C NMR, and mass spectrometry and the % yield was calculated.

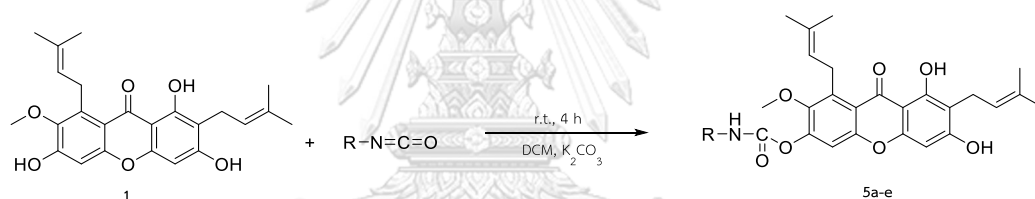


Figure 11 Carbamate formation

3.5.2 Estimation of aqueous solubility and drug-likeness of α -mangostin derivatives containing carbamate moiety

The estimation of aqueous solubility and drug-likeness of α -mangostin derivatives containing carbamate moiety was performed as described in section **3.4.2**

3.5.3 Detection of stability of α -mangostin derivatives by UV-vis spectrophotometer

The samples used in this experiment were **5a**, **5b**, and **5e** regarding the availability of the compound. They were prepared in 0.04 mM concentration and dissolved separately in two different solvents such as analytical grade chloroform (CHCl_3) and methanol (MeOH) to detect their stabilities by time-dependent. The time

was set up at 20 mins and the data were collected every 2 mins. The stability was measured by comparing the absorbance peak of the compounds.

3.5.4 Cytotoxicity assay against the non-small-cell lung cancer cell line (H460)

The cytotoxicity of α -mangostin derivatives containing carbamate moiety was examined by MTT assay as described in section 3.4.3. The precipitation of compounds in the cell culture medium was not observed in this experiment and the maximal concentration dose range was 80 μ M. The cells were treated with the test compound prepared in the serial dilution concentration in RPMI containing <0.5% dimethyl sulfoxide (DMSO). Finally, the IC_{50} of this cytotoxicity test was calculated by Excel, Microsoft software.



CHAPTER IV RESULTS AND DISCUSSION

Contents

- 4.1. Extraction, purification, and structure determination of isolated compounds from mangosteen pericarp
- 4.2. Chemical and biological study of α -mangostin derivatives from Smiles rearrangement
 - 4.2.1. Chemical synthesis
 - 4.2.2. Structural determination of α -mangostin derivatives from Smiles rearrangement
 - 4.2.2.1. Structural determination of compound **4a**
 - 4.2.2.2. Structural determination of compound **4b**
 - 4.2.2.3. Structural determination of compound **4c**
 - 4.2.3. Aqueous solubility and drug-likeness of α -mangostin derivatives from Smiles rearrangement
 - 4.2.4. Cytotoxic activity against H460 and H292 cell lines
 - 4.2.5. Quantification of apoptotic cells
- 4.3. Chemical and biological study of α -mangostin-carbamate prodrugs
 - 4.3.1. Chemical synthesis
 - 4.3.2. Structural determination of α -mangostin-carbamate derivatives
 - 4.3.2.1. Structural determination of compound **5a**
 - 4.3.2.2. Structural determination of compound **5b**
 - 4.3.2.3. Structural determination of compound **5c**
 - 4.3.2.4. Structural determination of compound **5d**
 - 4.3.2.5. Structural determination of compound **5e**

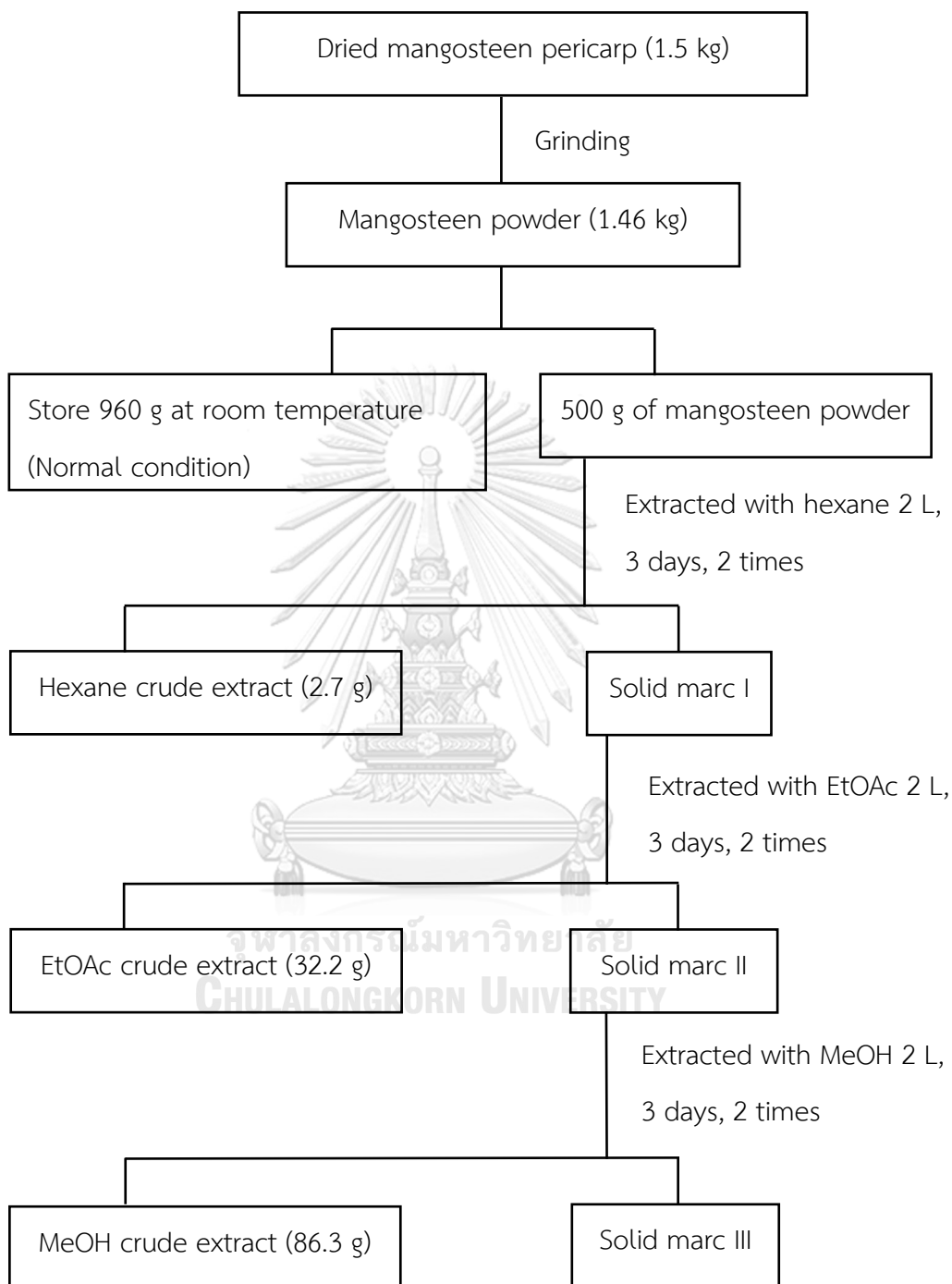
- 4.3.3. Aqueous solubility and drug-likeness of α -mangostin derivatives containing carbamate moiety
- 4.3.4. Stability of α -mangostin derivatives by UV-vis spectrophotometer
- 4.3.5. Cytotoxic activity against H460 cell line



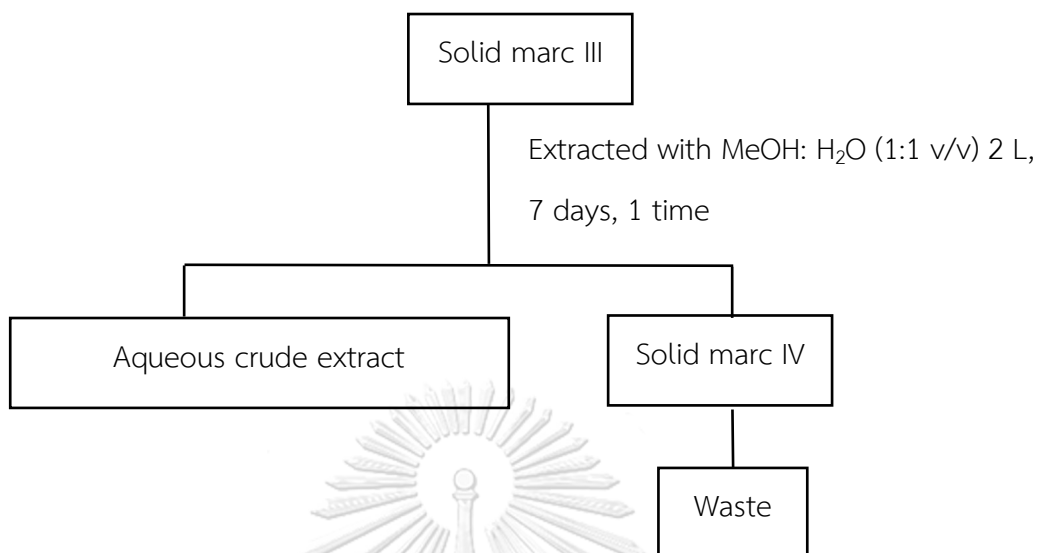
4.1 Extraction, purification, and structure determination of isolated compounds from mangosteen pericarp

In this research, 500 g of mangosteen pericarps were sequentially extracted with four different solvents such as hexane, EtOAc, MeOH, water: MeOH (1:1 v/v), and their crude extracts were detected by TLC (**Scheme 8**). According to the TLC monitoring, the hexane crude extract (2.7 g) and EtOAc crude extract (32.2 g) showed a promising amount of α -mangostin. Thereby, the hexane crude extract (2.7 g) was further chromatographed to afford nine fractions, H1-H9. Fraction H2 (0.23 g) was then separated by flash column chromatography (FCC) over silica gel with a gradient mixture of hexane and EtOAc to give six sub-fractions, H2A-H2F. Finally, it provided α -mangostin (**1**, 1.03 g) in the fractions of H5, H6, and H2D, along with two pure mangosteen xanthenes such as X-1 (13 mg) and X-2 (4.3 mg) (**Scheme 9**).

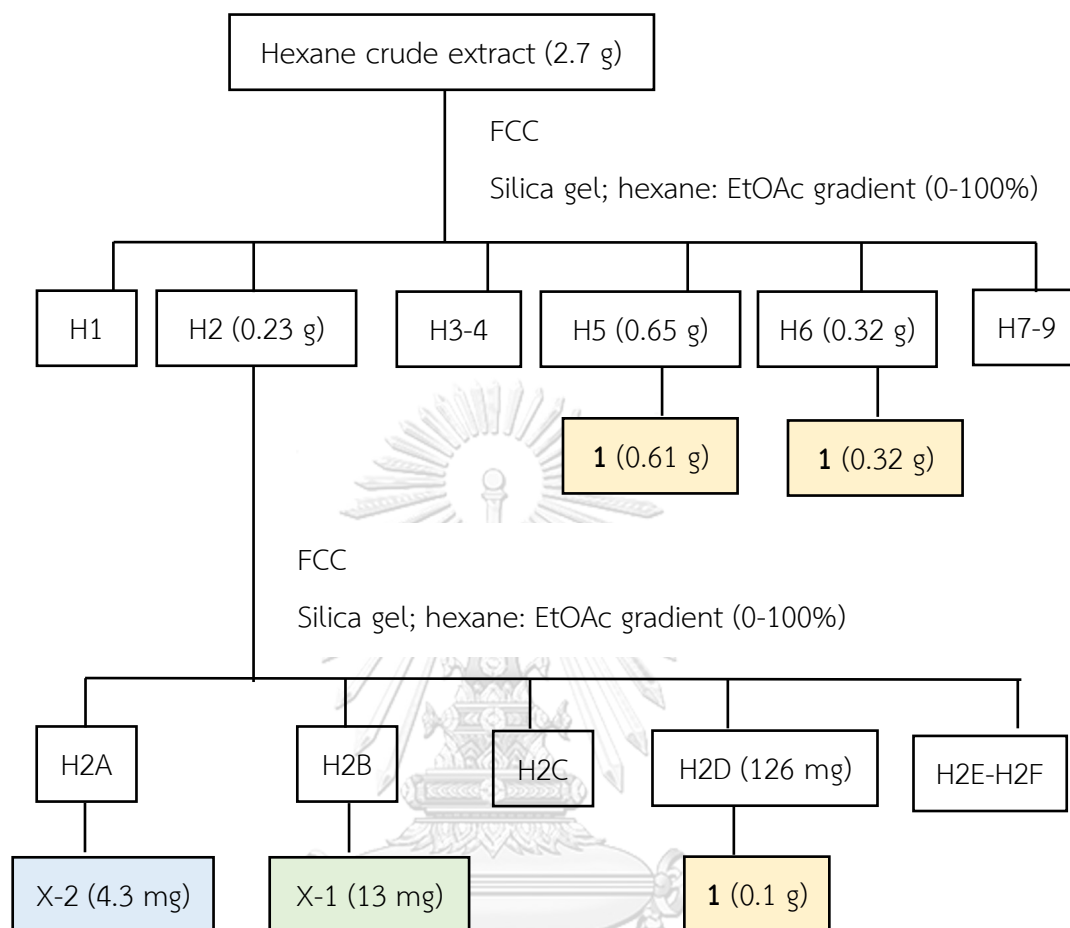
In parallel, the EtOAc crude extract (32.2 g) was fractionated by quick column chromatography (QCC). Silica gel was used as a stationary phase and eluted with a gradient mixture of hexane-EtOAc (0%-100%) as the mobile phase. Each fraction was collected at 250 mL and monitored by TLC. In this step, the ten fractions were obtained and labeled as fractions A-J (**Scheme 10**). Fractions C-D were precipitated and recrystallized in EtOAc to afford α -mangostin. The fractions containing a mixture of α -mangostin were purified by FCC over silica gel with a gradient mixture of hexane and EtOAc (0%-100%). Two pure mangosteen xanthenes were obtained including α -mangostin (**1**, 14.79 g) in the purified fractions of C1A, C2, D1, E1, and F1A, and X-1 (20 mg) in C1B.



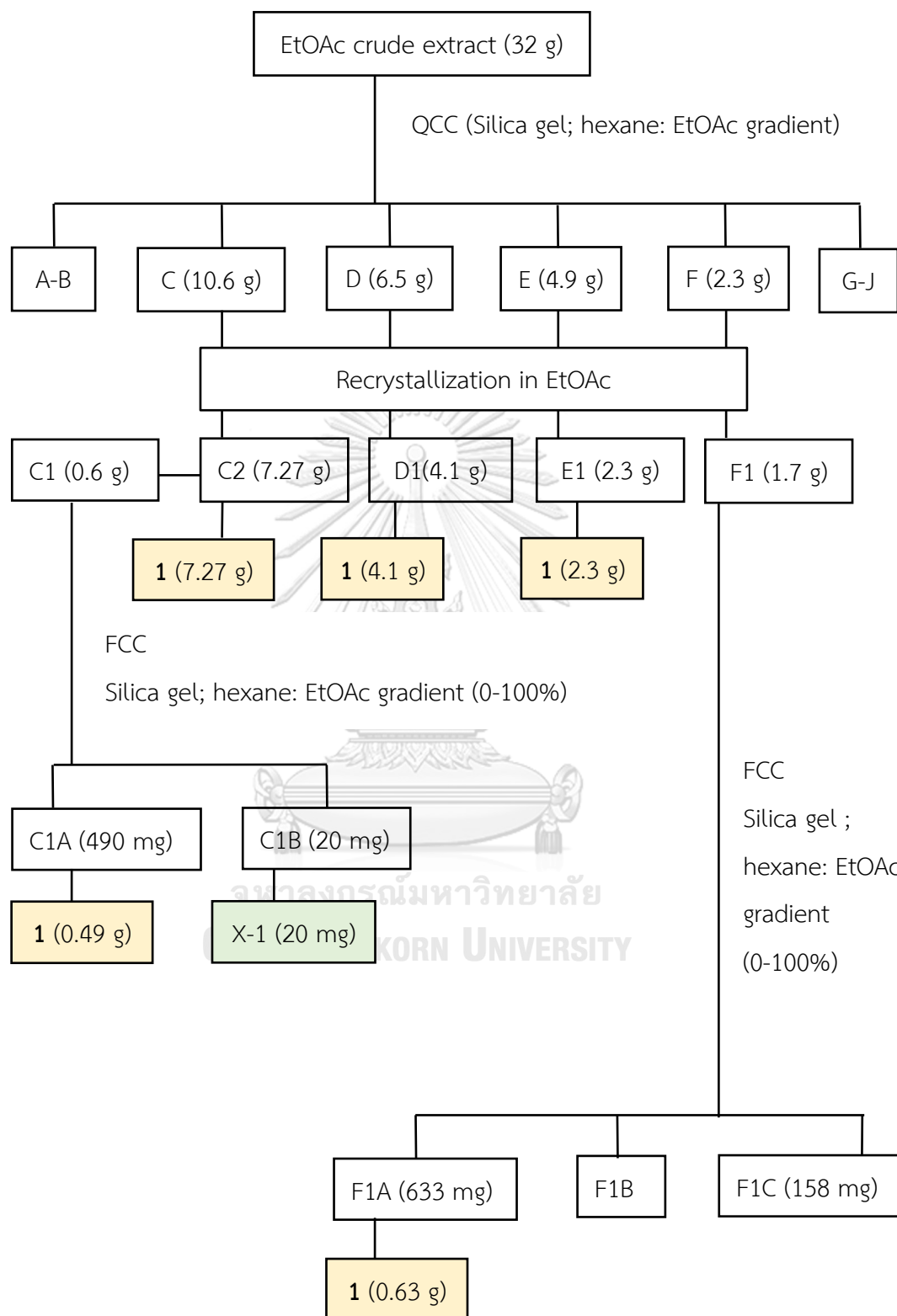
Scheme 8 Extraction of *G. mangostana* pericarp



Scheme 8 Extraction of *G. mangostana* pericarp (continued)



Scheme 9 Separation of hexane crude extract of *G. mangostana*



Scheme 10 Separation of EtOAc crude extract of *G. mangostana*

α -mangostin and two xanthones were isolated from the pericarps of mangosteen. The proton NMR of α -mangostin (Figure 12 and Table 6) was displayed. The observed spectra were identified and matched with previously reported data [36, 70]

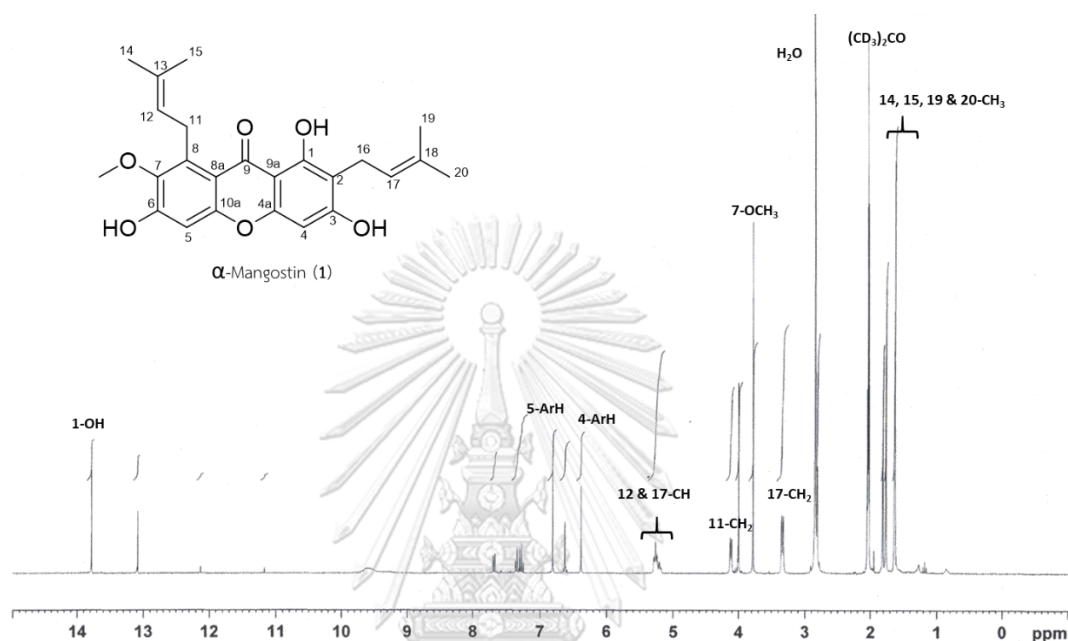


Figure 12 ^1H NMR (300 MHz) spectrum of compound 1 in $(\text{CD}_3)_2\text{CO}$

Table 6 ¹H NMR spectral data of compound **1***

Position	α -mangostin [36, 70]	Compound 1
1	13.78 (1H, s, OH)	13.80 (1H, s, OH)
5	6.82 (1H, s)	6.82 (1H, s)
4	6.40 (1H, s)	6.39 (1H, s)
12	5.27 (1H, t)	5.26 (1H, m) and 5.20 (1H, m)
17	5.27 (1H, t)	
11	4.13 (2H, d, <i>J</i> = 6.5 Hz)	4.12 (2H, d, <i>J</i> = 6.3 Hz)
7-OCH ₃	3.80 (3H, s)	3.79 (3H, s)
16	3.35 (2H, d, <i>J</i> = 7.3 Hz)	3.34 (2H, d, <i>J</i> = 7.2 Hz)
20	not report	1.81 (3H, s), 1.77 (3H, s), 1.63 (3H, s) and 1.63 (3H, s)
15	not report	
14	1.81 (3H, s)	
19	1.65 (3H, s)	

*NMR data from experiment and reference were measured with (CD₃)₂CO.

Besides the goal of isolation of **α**-mangostin for chemical modification study, the structures of pure compounds from fraction X-1 (**Figure 13 and Table 7**) and X-2 (**Figure 14 and Table 8**) were also initially determined by proton NMR. The proton NMR of compound from fraction X-1 displayed one OH, two methoxy groups, two aromatic protons, one prenyl olefin, one geranyl olefin, and five methyl groups. Also, the proton NMR of compound from fraction X-2 displayed three OH groups with downfield peaks, five aromatic protons, two prenyl olefins, and five methyl groups. They were regarded as the xanthones from mangosteen pericarp. To elucidate the structure of these pure compounds, further determination by spectroscopic techniques is needed in the future.

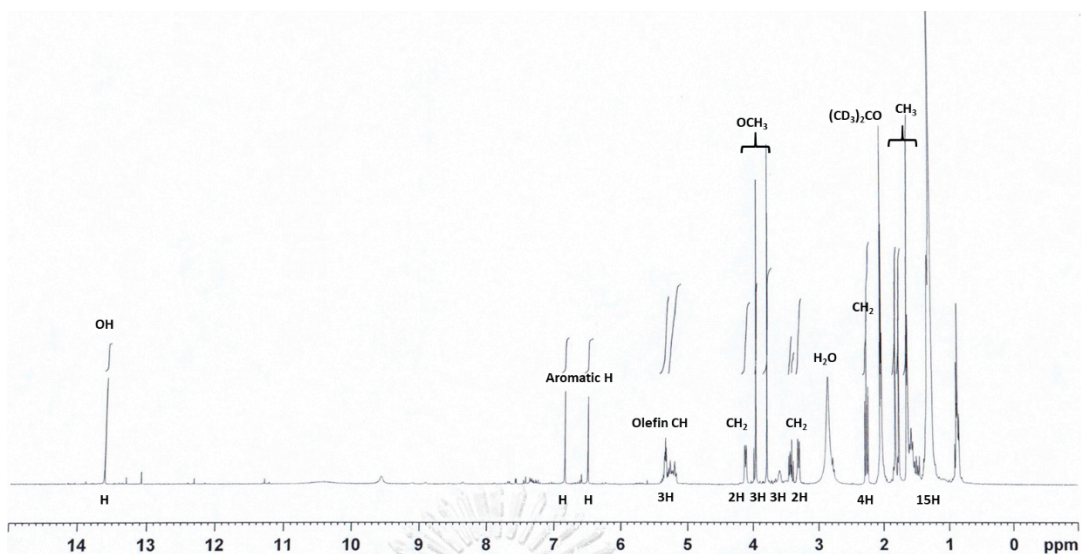


Figure 13 ^1H NMR (300 MHz) spectrum of compound from fraction X-1 in $(\text{CD}_3)_2\text{CO}$

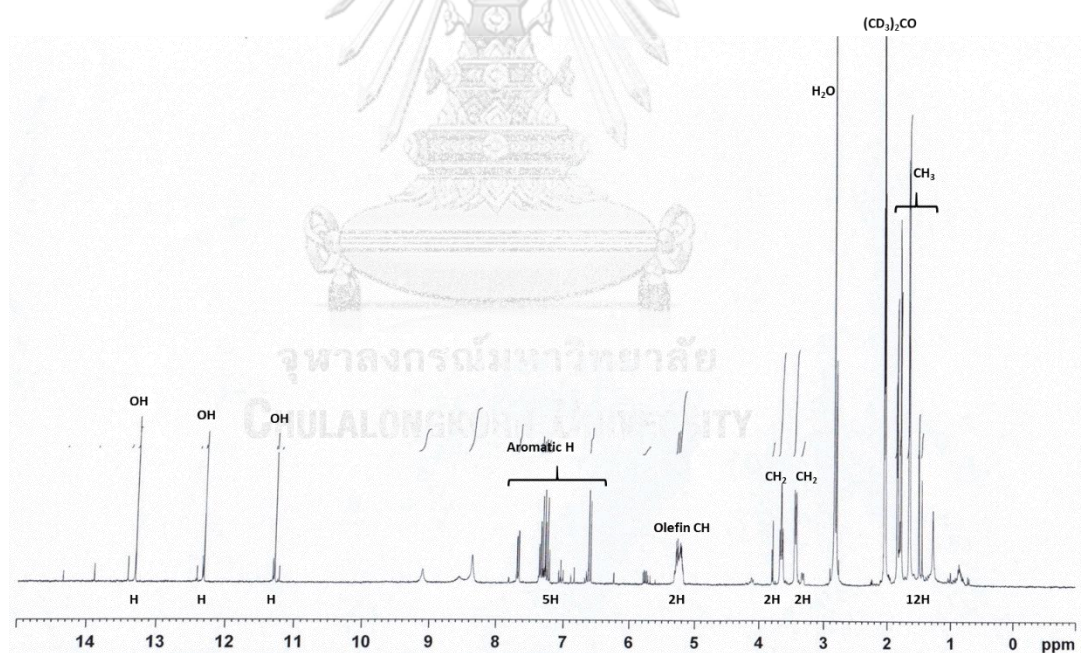


Figure 14 ^1H NMR (300 MHz) spectrum of compound from fraction X-2 in $(\text{CD}_3)_2\text{CO}$

Table 7 ^1H NMR spectral data of fraction X-1 in $(\text{CD}_3)_2\text{CO}$

Peak	δ_{H} (ppm, mult., J in Hz)	Functional group
1	13.63 (1H, s)	OH
2	6.85 (1H, s)	Ar-H
3	6.50 (1H, s)	Ar-H
4	5.35 (1H, s)	=CH
5	5.33 (1H, s)	=CH
6	5.32 (1H, s)	=CH
7	4.12 (2H, d, $J = 6.6$ Hz)	CH_2
8	3.96 (3H, s)	OCH_3
9	3.79 (3H, s)	OCH_3
10	3.42 (2H, m)	CH_2
11	3.31 (2H, d, $J = 7.2$ Hz)	CH_2
12	2.27 (4H, t, $J = 7.2$ Hz)	CH_2
13	1.82 (3H, s)	CH_3
14	1.77 (3H, s)	CH_3
15	1.65 (3H, s)	CH_3
16	1.64 (3H, s)	CH_3
17	1.63 (3H, s)	CH_3

Table 8 ^1H NMR spectral data of fraction X-2 in $(\text{CD}_3)_2\text{CO}$

Peak	δ_{H} (ppm, mult., J in Hz)	Functional group
1	13.32 (1H, s)	OH
2	12.33 (1H, s)	OH
3	11.30 (1H, s)	OH
4	7.69 (1H, dd, $J = 9.6$ Hz)	Ar-H
5	7.21-7.34 (2H, m)	Ar-H
6	6.60-6.63 (2H, d)	Ar-H
7	5.27 (2H, m)	=CH
8	3.66 (2H, overlapped)	CH_2
9	3.34 (2H, d, $J = 6.9$ Hz)	CH_2
11	1.85 (3H, s)	CH_3
12	1.80 (3H, s)	CH_3
13	1.65 (6H, s)	CH_3
14	1.50 (3H, s)	CH_3

Regarding the purification of mangosteen pericarps, the overall α -mangostin (**1**) was obtained at 15.8 g as a yellow powder with 80-90% purity and the yield of this isolation protocol was 3.3% weight by dry weight.

4.2 Chemical and biological study of α -mangostin derivatives from Smiles rearrangement

4.2.1 Chemical synthesis

In this research, the isolated α -mangostin from mangosteen pericarps was employed as the starting material for the semi-synthesis *via* Smiles rearrangement. Smiles rearrangement is an intramolecular nucleophilic aromatic substitution reaction. The rearrangement is occurred by a nucleophile A displaces aromatic electrophile B under a basic condition (**Figure 15**). The nucleophilic group in this rearrangement involves alcohol, phenol, amine, amide, and sulfonamide, while the leaving group is often an ether, sulfide, sulfoxide, or sulfone [71].

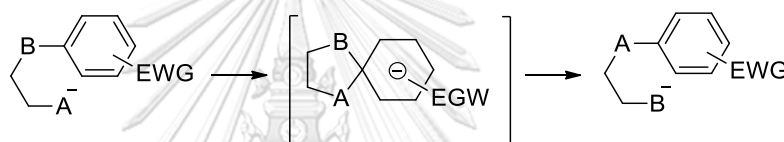


Figure 15 Smiles rearrangement mechanism

The optimized condition was confirmed by the isolated yield and it provided three products including 3, 6-diamino-1-hydroxy-7-methoxy-2, 8-bis (3-methylbut-2-en-1-yl)-9H-xanthen-9-one (**4a**), 2-((6,8-dihydroxy-2-methoxy-1, 7-bis (3-methylbut-2-en-1-yl)-9-oxo-9H-xanthen-3-yl)oxy) acetamide (**4b**), *N*-(6,8-dihydroxy-2-methoxy-1, 7-bis (3-methylbut-2-en-1-yl)-9-oxo-9H-xanthen-3-yl)-2-hydroxy acetamide (**4c**) (**Figure 16**). This semi-synthesis by Smiles rearrangement for the formation of **4a**, **4b**, and **4c**, performed with three steps, one-pot reaction, demonstrated that firstly, α -mangostin (**1**) was substituted with 2-chloroacetamide with the help of catalyst KI to produce **4b** as a nucleophilic substituted product. Besides, **4b** was rearranged under the basic condition and reflux at 150°C to afford **4c** as rearrangement product followed by the hydrolysis of **4c** in the presence of the base to produce **4a** as the final product. This reaction was aimed to synthesize monoamine at C-6 of α -mangostin (**1**). However, the diamine **4a** was obtained and the compounds **4b** and **4c** were also found unexpectedly.

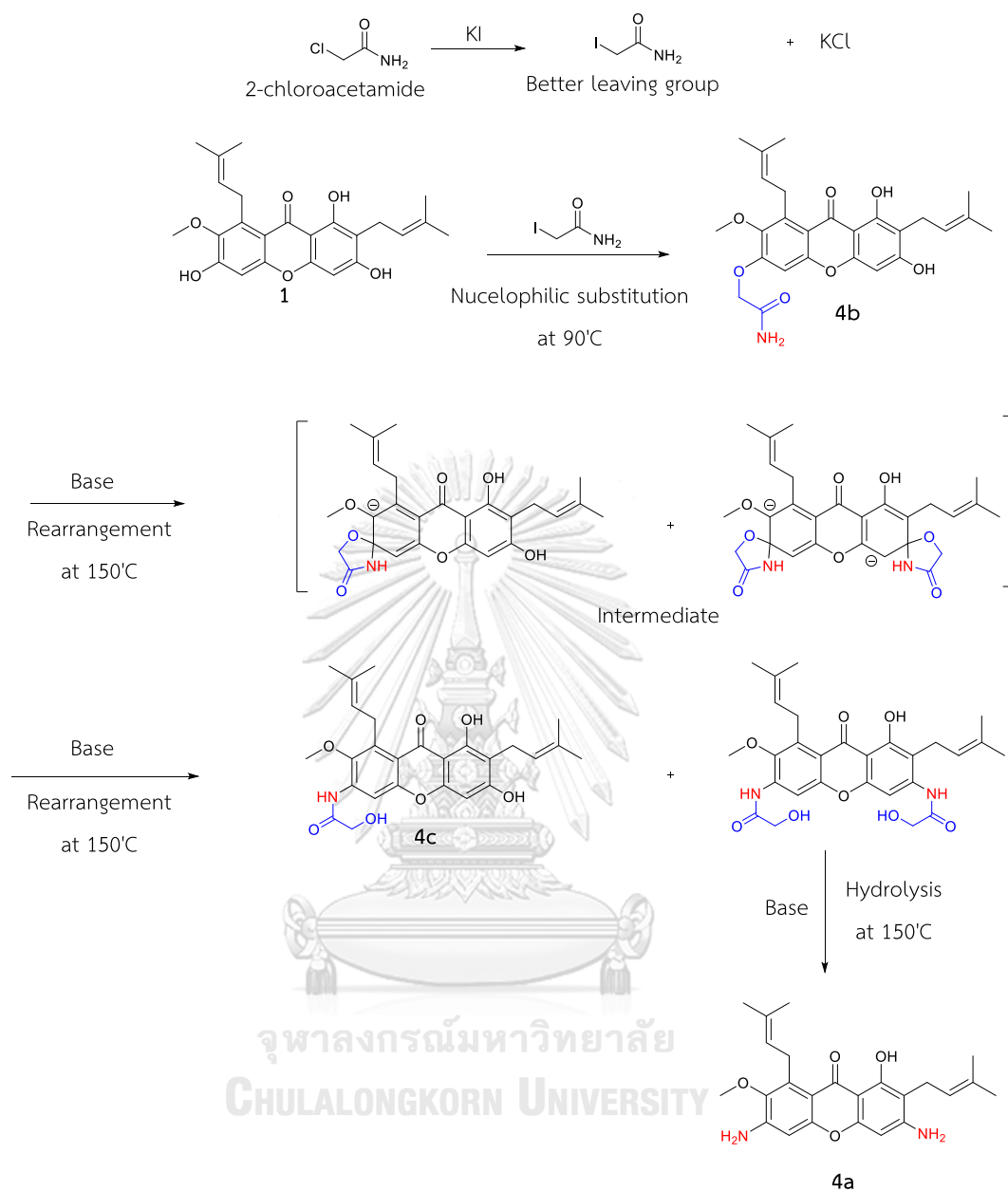


Figure 16 Semi-synthesis and proposed mechanism of **4a**, **4b**, and **4c** via Smiles rearrangement of α -mangostin

The optimized condition results were summarized as shown in **Table 9**. The percentage of the yields of the products was dependent on the conditions. This finding firstly suggested that using K_2CO_3 as base and changing the amount of KI, which was the catalyst at 0.2, 0.5 and 1 equivalent promoted the formation of **4b** from substitution step (**Table 9**, Entries 1-3). The catalytic KI seemed to provide better results based on the ratio of **4a:4b:4c**. Nonetheless, increase the reflux time up to 10 h did not affect the rearrangement step (**Table 9**, Entry 4). Moreover, using the base as KOH along with 0.2 equivalent of KI was significantly promoted rearrangement and hydrolysis to obtain **4a** at the highest ratio (**Table 9**, Entry 5) whereas employing KI 1 equivalent did not affect the production of **4a** notably (**Table 9**, Entry 6). Another entry of alternating base as Cs_2CO_3 and KI (**Table 9**, Entries 7 and 8) provided the highest production of **4c** when 1 equivalent of KI was used. Using the microwave apparatus (**Table 9**, Entry 9) reduced the reaction time to produce **4a** significantly. Interestingly, the optimized condition to produce the highest amount of **4a** and **4c** based on isolated yield was using Cs_2CO_3 and KI in 0.2 equivalent (**Table 9**, Entry7).

Table 9 Percent yields of compounds 4a, 4b, and 4c

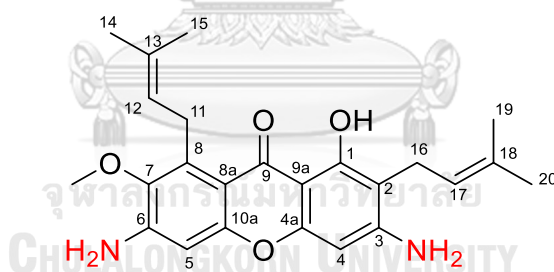
Entry	Apparatus	Base	KI (equiv)	Yield (% and weight)			%Yield in ratio of 4a:4b:4c
				4a	4b	4c	
1	Reflux	K ₂ CO ₃	0.2	9 (17 mg)	20 (46 mg)	17 (38 mg)	1: 2.2: 1.9
2	Reflux	K ₂ CO ₃	0.5	12 (25 mg)	27 (61 mg)	26 (59 mg)	1: 2.3: 2.2
3	Reflux	K ₂ CO ₃	1	17 (34 mg)	25 (58 mg)	21 (48 mg)	1: 1.5: 1.2
4	Reflux (10 h)	K ₂ CO ₃	1	16 (31 mg)	20 (45 mg)	18 (41 mg)	1: 1.3: 1.1
5	Reflux	KOH	0.2	23 (47 mg)	3 (6 mg)	13 (31 mg)	7.7: 1: 4.3
6	Reflux	KOH	1	16 (31 mg)	17 (40 mg)	21 (49 mg)	1: 1.1: 1.3
7	Reflux	Cs ₂ CO ₃	0.2	35 (69 mg)	14 (33 mg)	36 (83 mg)	2.5: 1: 2.6
8	Reflux	Cs ₂ CO ₃	1	4 (8 mg)	20 (45 mg)	33 (75 mg)	1: 5: 8.3
9	Microwave	K ₂ CO ₃	0.2	17 (35 mg)	4 (9 mg)	3 (6 mg)	5.7: 1.3: 1

4.2.2 Structural determination of α -mangostin derivatives from Smiles rearrangement

4.2.2.1 Structural determination of compound **4a**

Compound **4a** was obtained as brown amorphous gum. The molecular weight was identified by HRESIMS (**Figure 29** in Appendix) as $C_{24}H_{28}N_2NaO_4$ at m/z 431.1920 $[M+Na]^+$ (calculated for $C_{24}H_{28}N_2NaO_4$ 431.1941); 409.2033 $[M+H]^+$ (calculated for $C_{24}H_{29}N_2O_4$ 409.2122).

The 1H NMR spectrum of this compound (**Figure 30** in Appendix and **Table 10**) displayed the signal of a hydroxy group at δ 14.2 (1-OH), two amine signals at δ 5.69 and δ 5.37 ppm, and methoxy group at δ 3.71 (7-OCH₃). The ^{13}C NMR spectrum (**Figure 31** in Appendix and **Table 10**) exhibited signals for twenty-four carbons, comprising a conjugated carbonyl carbon at δ 181.73 (C-9), twelve aromatic carbons, a methoxy carbon, four olefinic carbons, two methylene carbons, and four methyl carbons.



3,6-diamino-1-hydroxy-7-methoxy-2,8-bis(3-methylbut-2-en-1-yl)-9H-xanthen-9-one (**4a**); Brown amorphous gum; 35% yield; R_f 0.89 (EtOAc:hexane = 7:3); 1H NMR (300 MHz, Acetone- d_6): δ ppm 14.2 (1H, s, OH), 6.55 (1H, s), 6.12 (1H, s), 5.69 (2H, s, NH₂), 5.37 (2H, s, NH₂), 5.29 (1H, t, J = 6.6 Hz), 5.14 (1H, t, J = 6.9 Hz), 4.07 (2H, d, J = 6.3 Hz), 3.71 (3H, s), 3.29 (2H, d, J = 6.6 Hz), 1.80 (3H, s), 1.79 (3H, s), 1.66 (3H, s), 1.63 (3H, s); ^{13}C NMR (300 MHz, Acetone- d_6): δ ppm 181.7, 161.2, 156.8, 156.0, 154.3, 148.7, 142.7, 136.8, 132.5, 130.7, 125.5, 123.0, 108.9, 106.5, 101.3, 99.1, 91.09, 60.2, 26.8, 25.9, 25.8, 22.2, 18.3, 17.9; HRMS (ESI) m/z calculated for $C_{24}H_{28}N_2NaO_4$ 431.1941

[M+Na]⁺ found 431.1920 and calculated for C₂₄H₂₉N₂O₄ 409.2122 [M+H]⁺ found 409.2033.

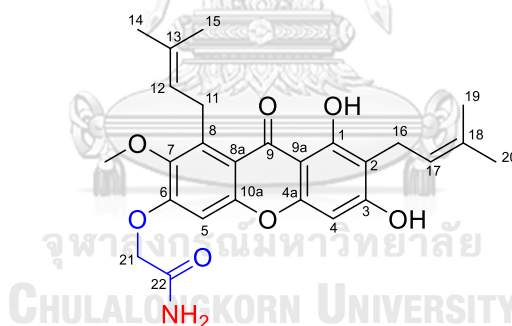
Table 10 NMR spectral data of compound **4a** in (CD₃)₂CO

Position	δ_{H} of 1 [70]	δ_{H} of 4a
1	13.78 (1H, s, OH)	14.2 (1H, s, OH)
5	6.82 (1H, s)	6.55 (1H, s)
4	6.40 (1H, s)	6.12 (1H, s)
3	-	5.69 (2H, s, NH ₂)
6	-	5.37 (2H, s, NH ₂)
12	5.27 (1H, t)	5.29 (1H, t, <i>J</i> = 6.6 Hz)
17	5.27 (1H, t)	5.14 (1H, t, <i>J</i> = 6.9 Hz)
11	4.13 (2H, d, <i>J</i> = 6.5 Hz)	4.07 (2H, d, <i>J</i> = 6.3 Hz)
7-OCH ₃	3.80 (3H, s)	3.71 (3H, s)
16	3.35 (2H, d, <i>J</i> = 7.3 Hz)	3.29 (2H, d, <i>J</i> = 6.6 Hz)
14	1.81 (3H, s)	1.80 (3H, s)
19	1.65 (3H, s)	1.79 (3H, s)
20	not report	1.66 (3H, s)
15	not report	1.63 (3H, s)

4.2.2.2 Structural determination of compound **4b**

Compound **4b** was obtained as brown amorphous gum. The HRESIMS (Figure 32 in Appendix) presented $[M+Na]^+$ at 490.1883 (calculated for $C_{26}H_{29}NNaO_7$ 490.1836), $[M+H]^+$ at 468.2046 (calculated for $C_{26}H_{30}NO_7$ 468.2017), suggesting the molecular formula.

The 1H NMR spectrum of this compound (Figure 33 in Appendix and Table 11) displayed the amide signal at δ 9.57 ppm (2H, s, NH_2), the signal of methylene beside amide group at δ 4.23 (2H, s, H-21) and methoxy group at δ 3.83 (7-O CH_3). The ^{13}C NMR spectrum (Figure 34 in Appendix and Table 11) exhibited signals for twenty-six carbons, comprising a conjugated carbonyl carbon at δ 182.7 (C-9) and an amide carbonyl carbon at δ 171.8 (C-22), twelve aromatic carbons, four olefinic carbons, two methylene carbons, a methylene ether carbon, a methoxy carbon, and four methyl carbons.



2-((6,8-dihydroxy-2-methoxy-1,7-bis(3-methylbut-2-en-1-yl)-9-oxo-9H-xantho-3-yl)oxy) acetamide (**4b**); Brown amorphous gum; 14% yield; R_f 0.73 (EtOAc:hexane = 7:3); 1H NMR (300 MHz, Acetone- d_6): δ ppm 13.60 (1H, s, OH), 9.57 (2H, s, NH_2), 8.41 (1H, s), 6.43 (1H, s), 5.27 (m), 5.27 (m), 4.23 (2H, s), 4.11 (2H, d, $J = 6$ Hz), 3.83 (3H, s), 3.34, (2H, d, $J = 7.2$ Hz), 1.81 (3H, s), 1.77 (3H, s), 1.64 (3H, s), 1.64 (3H, s); ^{13}C NMR (300 MHz, Acetone- d_6): δ ppm 182.7, 171.8, 163.3, 161.6, 155.8, 155.7, 144.4, 138.1, 137.1, 131.8, 131.4, 124.5, 123.4, 114.4, 111.2, 105.8, 103.8, 93.3, 63.1, 62.0, 26.9, 25.9,

25.9, 22.0, 18.3, 17.9; HRMS (ESI) m/z calculated for $C_{26}H_{29}NNaO_7$ 490.1836 $[M+Na]^+$ found 490.1883 and calculated for $C_{26}H_{30}NO_7$ 468.2017 $[M+H]^+$ found 468.2046.

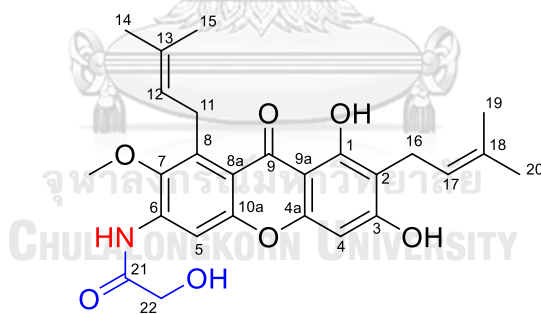
Table 11 NMR spectral data of compound **4b** in $(CD_3)_2CO$

Position	δ_H of 1 [70]	δ_H of 4b
1	13.78 (1H, s, OH)	13.60 (1H, s, OH)
5	6.82 (1H, s)	8.41 (1H, s)
4	6.40 (1H, s)	6.43 (1H, s)
12	5.27 (1H, t)	5.27 (m)
17	5.27 (1H, t)	5.27 (m)
11	4.13 (2H, d, $J = 6.5$ Hz)	4.11 (2H, d, $J = 6$ Hz)
7-OCH ₃	3.80 (3H, s)	3.83 (3H, s)
16	3.35 (2H, d, $J = 7.3$ Hz)	3.34 (2H, d, $J = 7.2$ Hz)
14	1.81 (3H, s)	1.81 (3H, s)
19	1.65 (3H, s)	1.77 (3H, s)
20	not report	1.64 (3H, s)
15	not report	1.64 (3H, s)
21	-	4.23 (2H, s)
22	-	9.57 (2H, s, NH ₂)

4.2.2.3 Structural determination of compound **4c**

Compound **4c** was obtained as a yellow amorphous solid. The HRESIMS (Figure 35 in Appendix) presented $[M+Na]^+$ at 490.1830 (calculated for $C_{26}H_{29}NNaO_7$ 490.1836), suggesting the molecular formula.

The 1H NMR spectrum of this compound (Figure 36 in Appendix and Table 12) displayed the amide signal at δ 9.70 ppm (1H, br s, NH), the signal of methylene beside amide group at δ 4.65 (2H, s, H-22) and methoxy group at δ 3.79 (7-OCH₃). The ^{13}C NMR spectrum (Figure 37 in Appendix and Table 12) exhibited signals for twenty-six carbons, comprising a conjugated carbonyl carbon at δ 182.9 (C-9) and an amide carbonyl carbon at δ 170.0 (C-21), twelve aromatic carbons, four olefinic carbons, two methylene carbons, a methylene ether carbon, a methoxy carbon, and four methyl carbons. Note that, the structure of **4c** is proposed. However, further determination by 2-dimensional NMR spectroscopic techniques is needed to confirm substitution at C-3 and C-6 of **4c**.



N-(6,8-dihydroxy-2-methoxy-1,7-bis(3-methylbut-2-en-1-yl)-9-oxo-9H-xanthen-3-yl)-2-hydroxyacetamide (**4c**); yellow amorphous solid; 36% yield; *R*_f 0.0.6 (EtOAc:hexane = 7:3); 1H NMR (300 MHz, Acetone-*d*₆): δ ppm 13.71 (1H, s, OH), 9.70 (1H, br s, NH), 6.85 (1H, s), 6.48 (1H, s), 5.25 (m), 5.25 (m), 4.65 (2H, s), 4.11 (2H, d, *J* = 6.3 Hz), 3.79 (3H, s), 3.41 (2H, d, *J* = 6.6 Hz), 1.82 (3H, s), 1.79 (3H, s), 1.65 (3H, s), 1.65 (3H, s); ^{13}C NMR (300 MHz, Acetone-*d*₆): δ ppm 182.9, 170.0, 162.5, 160.8, 157.7, 156.3, 156.0, 144.7, 138.1, 131.9, 131.5, 124.6, 123.6, 112.1, 112.0, 104.6, 102.7, 90.8, 68.3, 61.3, 26.9, 25.9, 25.8,

22.0, 18.2, 17.9; HRMS (ESI) m/z calculated for $C_{26}H_{29}NNaO_7$ 490.1836 $[M+Na]^+$ found 490.1830.

Table 12 NMR spectral data of compound **4c** in $(CD_3)_2CO$

Position	δ_H of 1 [70]	δ_H of 4c
1	13.78 (1H, s, OH)	13.71 (1H, s, OH)
6	-	9.70 (1H, br s, NH)
5	6.82 (1H, s)	6.85 (1H, s)
4	6.40 (1H, s)	6.48 (1H, s)
12	5.27 (1H, t)	5.25 (m)
17	5.27 (1H, t)	5.25 (m)
11	4.13 (2H, d, $J = 6.5$ Hz)	4.11 (2H, d, $J = 6.3$ Hz)
7-OCH ₃	3.80 (3H, s)	3.79 (3H, s)
16	3.35 (2H, d, $J = 7.3$ Hz)	3.41 (2H, d, $J = 6.6$ Hz)
14	1.81 (3H, s)	1.82 (3H, s)
19	1.65 (3H, s)	1.79 (3H, s)
20	not report	1.65 (3H, s)
15	not report	1.65 (3H, s)
22	-	4.65 (2H, s)

4.2.3 Aqueous solubility and drug-likeness of α -mangostin derivatives from Smiles rearrangement

The general physicochemical properties and aqueous solubility of α -mangostin and its derivatives from Smiles rearrangement were presented (**Table 13**). The aqueous solubility of the compounds was evaluated by log *S* depended on three predictive parameters involving ESOL, Ali, and SILICOS-IT. The predicted aqueous solubility of the derivatives was improved when compared with starting material α -mangostin by ESOL method. The solubility (mol/L) values of the derivatives **4a**, **4b**, and **4c** showed better aqueous solubility than α -mangostin with 2.6, 2.2, and 3.9 folds respectively and both **4a** and **4c** were concluded as moderately soluble. It was regarded as modification of α -mangostin at C-3 and C-6 positions with amine and amide moieties potentially improved the aqueous solubility.

The estimation of the drug-likeness of α -mangostin derivatives from Smiles rearrangement was showed (**Table 14**). All compounds proved to conform with rules of Lipinski filters, which was considered as the principal pattern of all drug-likeness means, accomplished from the drug discovery screens of Pfizer. Also, the compounds had no violations of the Veber rules but had variable and acceptable rates in Ghose and Egan. The Abbot bioavailability score (ABS) showed 0.55 in all compounds mean the probability of the compounds had oral bioavailability in rat >10 % and measurable CaCO₂ permeability.

Table 13 General physicochemical properties and aqueous solubility of α -mangostin derivatives from Smiles rearrangement

Properties	1	4a	4b	4c
Formula	$C_{24}H_{26}O_6$	$C_{24}H_{28}N_2O_4$	$C_{26}H_{29}NO_7$	$C_{26}H_{29}NO_7$
1. Molecular weight (MW)	410.46	408.49	467.51	467.51
2. Numbers of heavy atoms (HA)	30	30	34	34
3. Numbers of rotatable bonds (RB)	5	5	8	8
4. Numbers of H-bond acceptors (HBA)	6	4	7	7
5. Numbers of H-bond donors (HBD)	3	3	3	4
6. Log <i>S</i> (ESOL)	-6.35	-5.93	-6.01	-5.76
6.1 Solubility (mg/mL)	1.83×10^{-04}	4.82×10^{-04}	4.62×10^{-04}	8.13×10^{-04}
6.2 Solubility (mol/L)	4.46×10^{-07}	1.18×10^{-06}	9.87×10^{-07}	1.74×10^{-06}
6.3 Class (ESOL)	Poorly soluble	Moderately soluble	Poorly soluble	Moderately soluble

Table 13 General physicochemical properties and aqueous solubility of α -mangostin derivatives from Smiles rearrangement (continued)

Properties	1	4a	4b	4c
7. Log S (Ali)	-8.16	-7.73	-8.08	-7.61
7.1 Solubility (mg/mL)	2.84×10^{-06}	7.62×10^{-06}	3.92×10^{-06}	1.15×10^{-05}
7.2 Solubility (mol/L)	6.91×10^{-09}	1.87×10^{-08}	8.38×10^{-09}	2.46×10^{-08}
7.3 Class (Ali)	Poorly soluble	Poorly soluble	Poorly soluble	Poorly soluble
8. Log S (SILICOS-IT)	-6.14	-6.58	-6.4	-6.49
8.1 Solubility (mg/mL)	2.97×10^{-04}	1.09×10^{-04}	1.88×10^{-04}	1.51×10^{-04}
8.2 Solubility (mol/L)	7.23×10^{-07}	2.66×10^{-07}	4.02×10^{-07}	3.23×10^{-07}
8.3 Class (SILICOS-IT)	Poorly soluble	Poorly soluble	Poorly soluble	Poorly soluble

Table 14 Drug-likeness parameters of α -mangostin derivatives from Smiles rearrangement

Properties	α -Mangostin	4a	4b	4c
Lipinski	Yes	Yes	Yes	Yes
	0 violation	0 violation	0 violation	0 violation
Ghose	Yes	Yes	No	No
			1 violation	1 violation
			MR>130	MR>130
Veber	Yes	Yes	Yes	Yes
Egan	Yes	Yes	No	Yes
			1 violation	
			TPSA >131.6	
Muegge	No	No	No	No
	1 violation	1 violation	1 violation	1 violation
	XLOGP3 >5	XLOGP3 >5	XLOGP3 >5	XLOGP3 >5
ABS	0.55	0.55	0.55	0.55

ABS = Abbot Bioavailability Score, MR = Molar refractivity, TPSA = Topological polar surface area, XLOGP3 = Atomistic and knowledge-based method calculated Log *P* by XLOGP program.

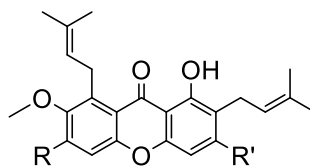
4.2.4 Cytotoxic activity against H460 and H292 cell lines

Human non-small cell lung cancer cell line H460 is adenocarcinoma cell type with highly metastatic nature [72]. Also, another cell line H292 is mucoepidermoid pulmonary carcinoma cell with metastatic type [73].

The cytotoxic experiments with human non-small cell lung cancer cell lines including H292 and H460 were first carried out with the same dose of all compounds with the treatment at 0, 10, 20, 40, 80, 160, and 320 μM . The preparation of serial dilution solution did not find the precipitation of test compounds in RPMI culturing media with <0.5% dimethyl sulfoxide (DMSO). Unexpectedly, precipitation was occurred on compound **4a** at 160 μM and **4c** at 20 μM , while compound **4b** was completely soluble in the cell-cultured aqueous media. Considering precipitation cautions when the compounds were treated into the cell assay, the dose of precipitation was excluded, and the experiment was continued with the specific dose ranges (Table 15). Thus, IC_{50} of compounds **4a** and **4c** were predicted based upon experimental observation along with theoretical estimation. The cytotoxic activity results were shown in Table 16. It could be noted that chemical modification of α -mangostin on the position of C-3 and C-6 hydroxy groups into amine groups decreased the cytotoxic activity dramatically. It also claimed that the hydroxy groups on α -mangostin were important for the cytotoxic activity on human non-small cell lung cancer cell lines.

Table 15 Dose of precipitation and treatment of α -mangostin derivatives from Smiles rearrangement

Compound	Precipitation dose (μM)	Treatment dose (μM)
α -mangostin	> 80	0, 10, 20, 30, 40, 50
4a	160	0, 10, 20, 30, 40, 50, 60, 70, 80
4b	> 640	0, 20, 40, 80, 160, 320, 640
4c	20	0, 0.625, 1.25, 2.5, 5, 10



1 (R, R' = OH)

4a (R, R' = NH₂)

4b (R = OCH₂CONH₂, R' = OH)

4c (R = NHCOCH₂OH, R' = OH)

Table 16 Cytotoxic activity of α -mangostin derivatives from Smiles rearrangement

Compound	IC ₅₀ ± S.D. (μM)	
	H460	H292
1	26.16±0.74	25.07±2.15
4a	1166.17±43.38*	297.66±37.34*
4b	265.48±25.22	280.48±17.59
4c	26.50±12.42*	13.89±2.55*
Cisplatin	55.71±0.26	48.81±0.93

* The reported data are predicted IC₅₀. H460 and H292 are non-small cell lung cancer cell lines.

4.2.5 Quantification of apoptotic cells

Hoechst33342 is a cell-permeable nucleic acid dye that emits blue fluorescence to detect nuclear chromatin condensation and DNA fragmentation by staining the condensed pyknotic nuclei in apoptotic cells [74]. PI is a red fluorescent DNA-binding dye that is used to distinguish between late apoptotic or necrotic cells and normal cells in population because it cannot permeate the cell membrane of viable cells. It can only stain the cells in the condition of the plasma membrane with high permeability and lack integrity [74].

The morphological changes in the cell nuclei after treatment induced significant apoptosis whereas necrotic cells were less detected (**Figure 17** and **18**). The percentage of apoptotic cells was determined, and the results were presented as apoptotic mode of cell death (**Figure 19** and **20**). The dose range of the costaining assay was similar concentration with MTT assay. Hence, the dose of compounds **4a** and **4c** had limitations but it demonstrated the mode of cell death with apoptosis. Additionally, by this Hoechst33342/PI staining assay, the percentage of apoptotic cells confirmed the IC_{50} of cytotoxic assay of compounds **1** and **4a** on both cell lines. It also claimed that the cytotoxicity of the cells was concerned with the cell death of apoptosis.

Regarding the cytotoxic activity of compounds **4a**, **4b**, and **4c**, the new series of α -mangostin derivatives show no cellular toxicity to human non-small cell lung cancer cell lines. Thus, these compounds cannot be developed as anti-lung cancer agents. Toward the future study, **4a**, **4b**, and **4c** would be further exploring their biological application toward lung disease such as tuberculosis, and malaria to promote human health benefit.

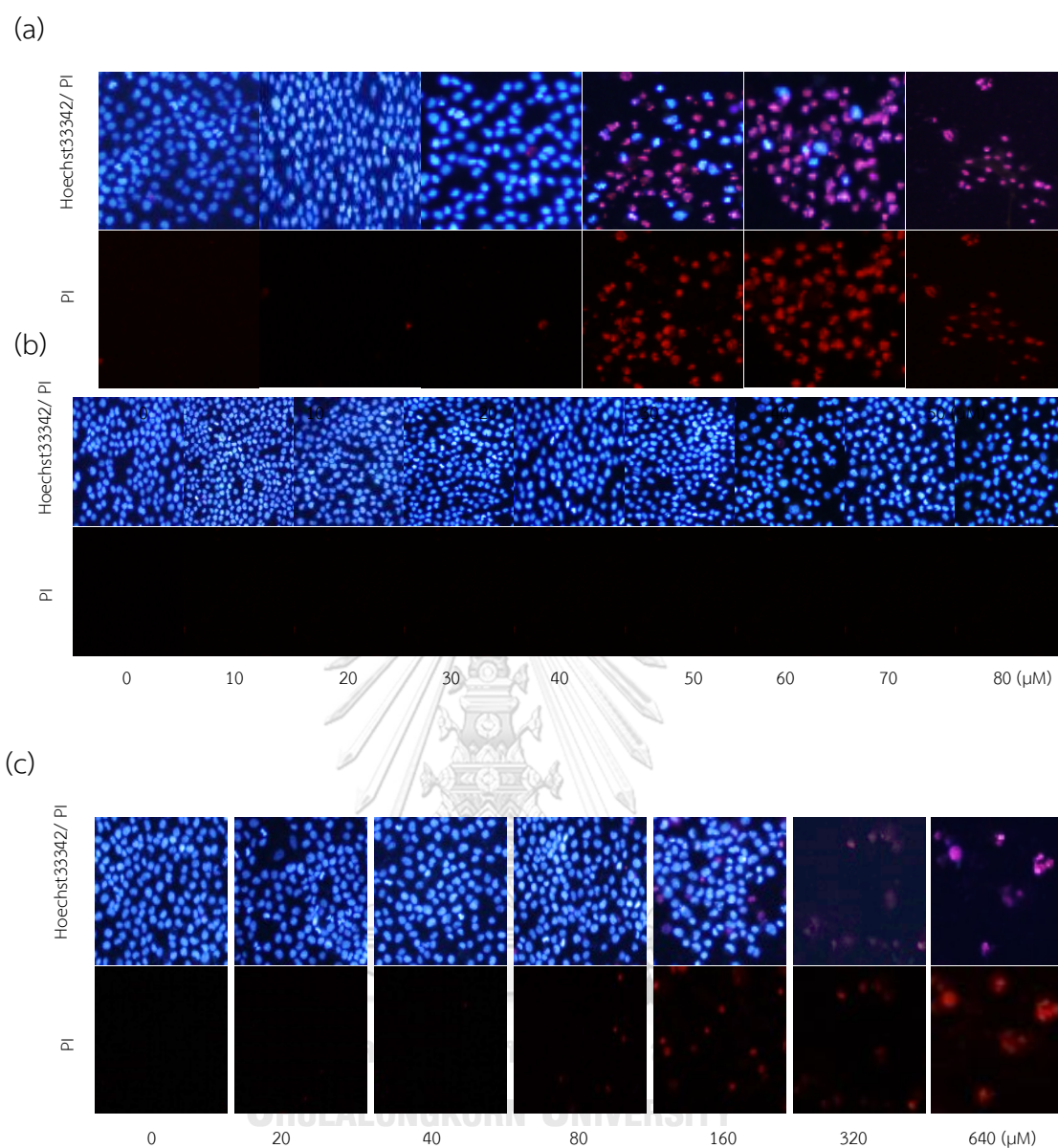


Figure 17 Morphological changes in the H460 cell nuclei detected with costaining of Hoechst33342/PI under the fluorescence microscope (a) α -mangostin, (b) **4a**, (c) **4b**, and (d) **4c**.

(d)

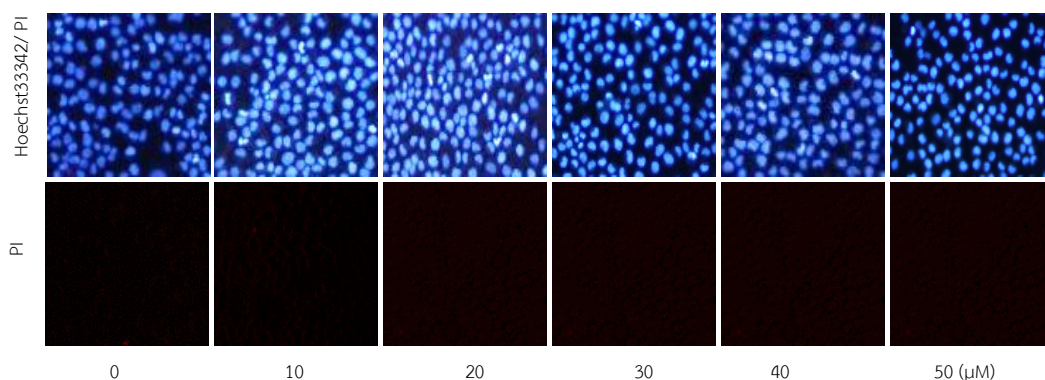
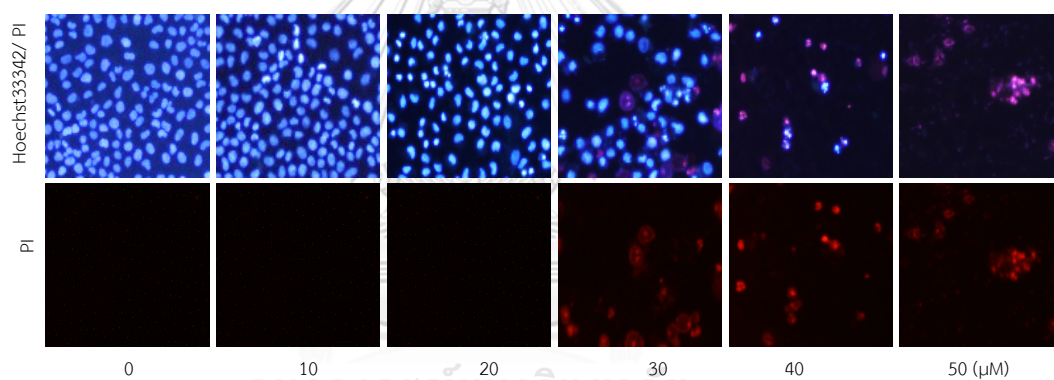


Figure 17 Morphological changes in the H460 cell nuclei detected with costaining of Hoechst33342/PI under the fluorescence microscope (continued)

(a)



(b)

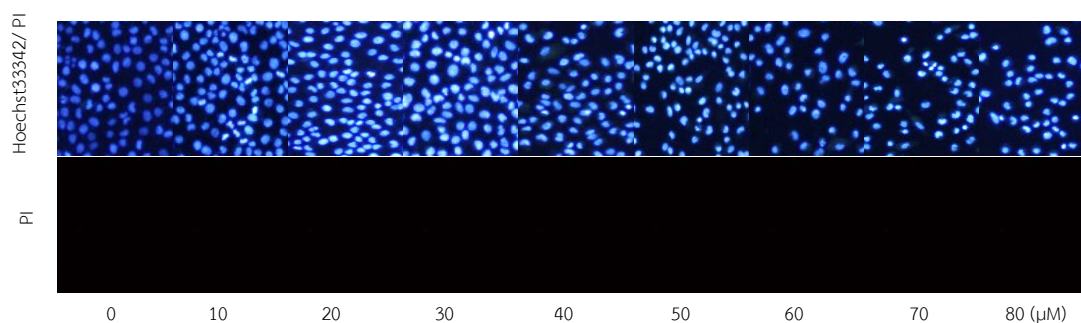
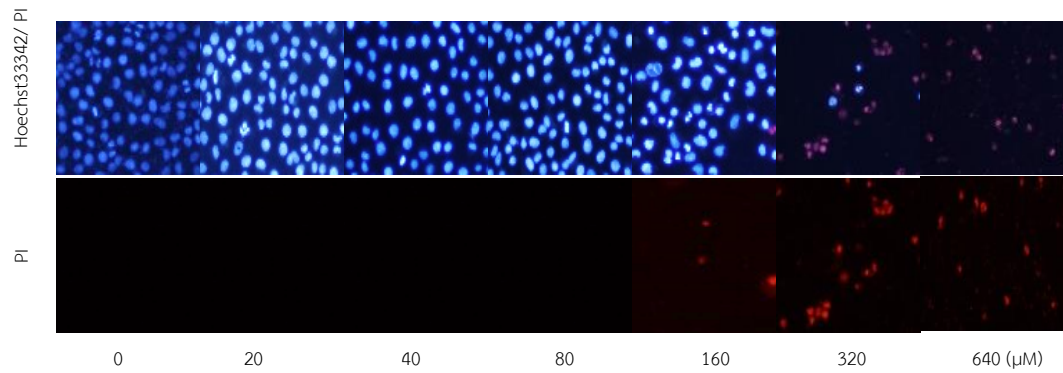


Figure 18 Morphological changes in the H292 cell nuclei detected with costaining of Hoechst33342/PI under the fluorescence microscope (a) α -mangostin, (b) 4a, (c) 4b, and (d) 4c.

(C)



(d)

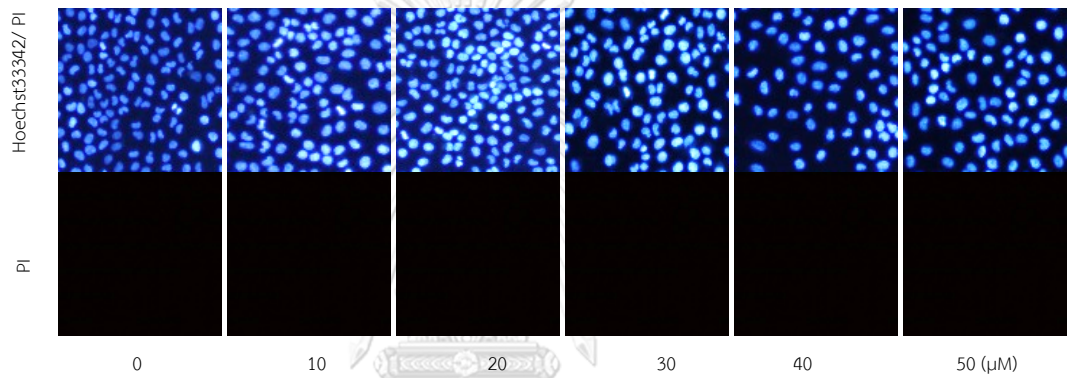


Figure 18 Morphological changes in the H292 cell nuclei detected with costaining of Hoechst33342/PI under the fluorescence microscope (continued)

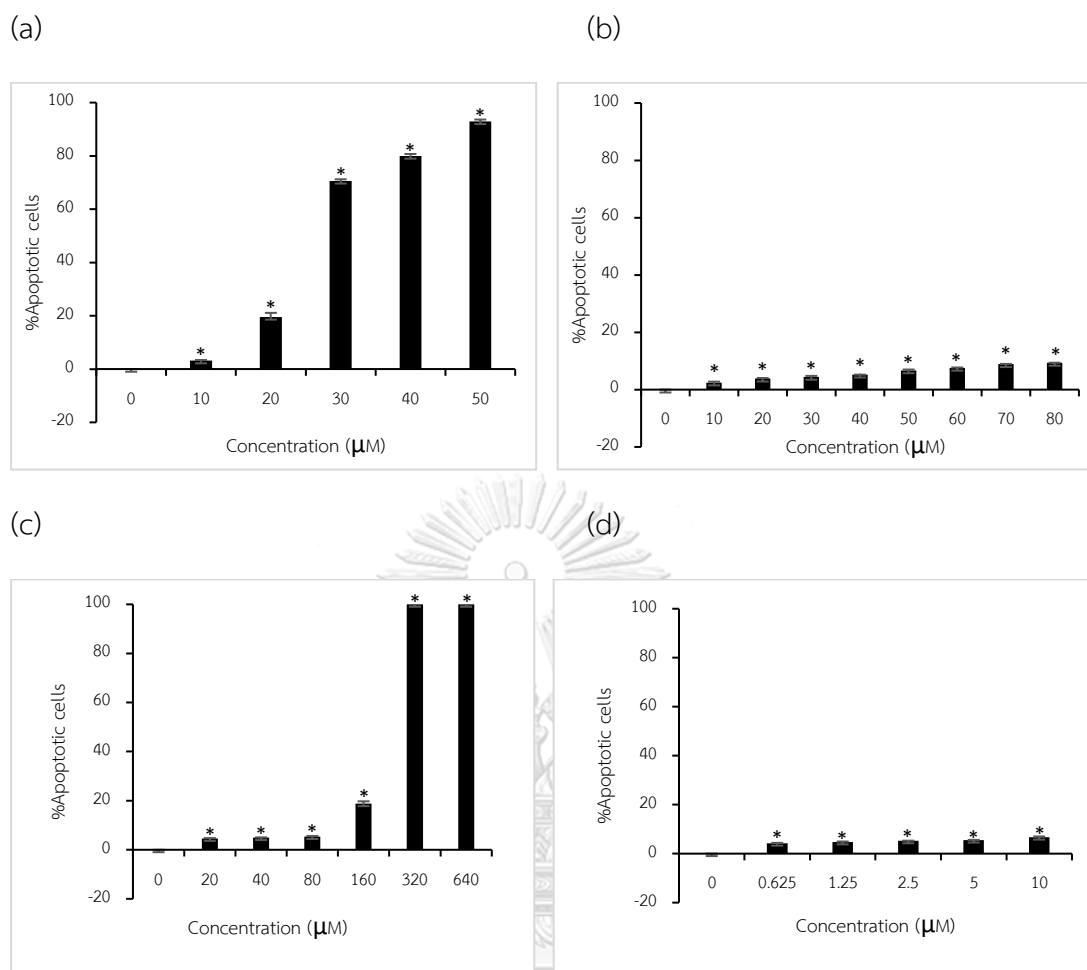


Figure 19 Percentage of apoptotic cells death in H460 cells

(a) α -mangostin, (b) 4a, (c) 4b, and (d) 4c. Data are expressed as mean \pm S.D., * p -value < 0.05 versus control group.

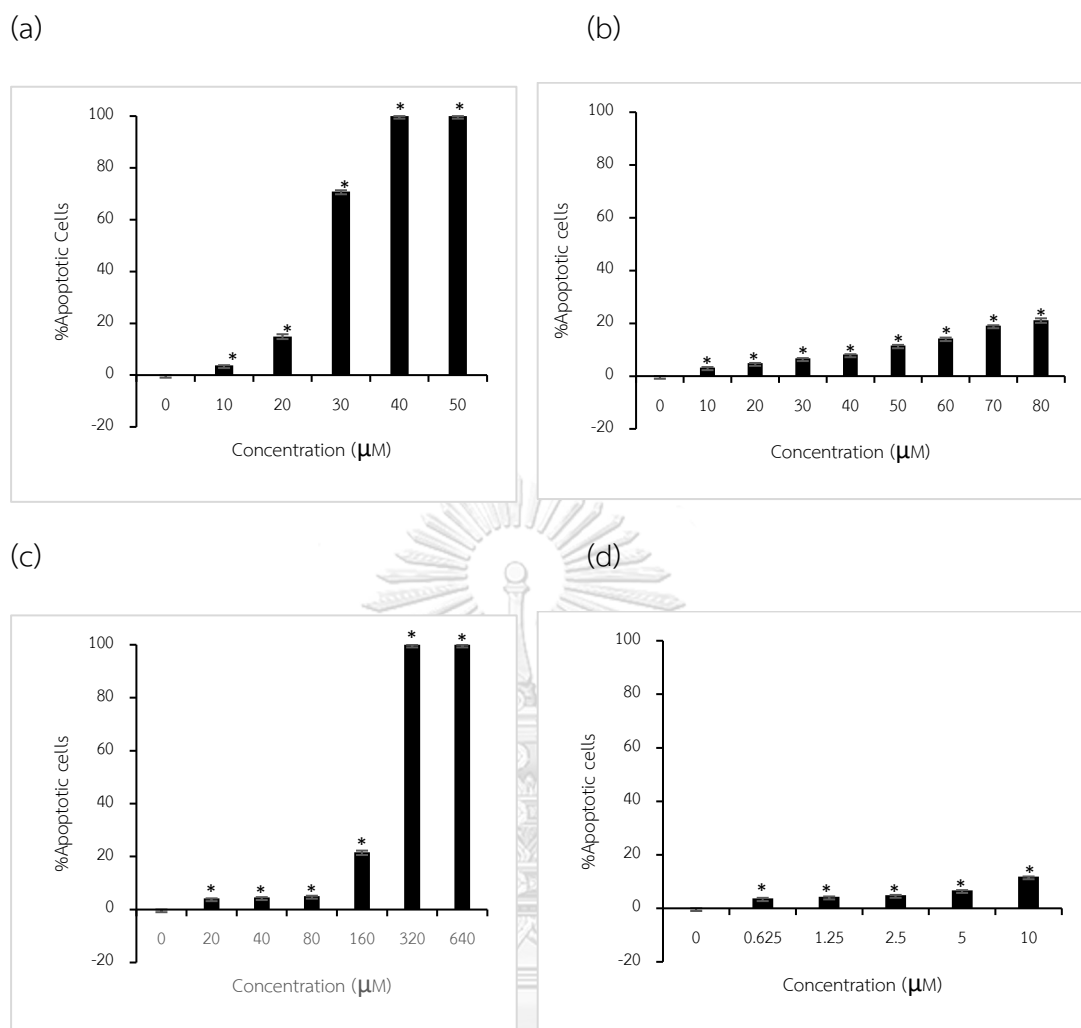


Figure 20 Percentage of apoptotic cells death in H292 cells

(a) α -mangostin, (b) 4a, (c) 4b, and (d) 4c. Data are expressed as mean \pm S.D., * p -value $<$ 0.05 versus control group.

4.3 Chemical and biological study of α -mangostin-carbamate prodrugs

4.3.1 Chemical synthesis

Carbamate derivatives have gained much interest in recent years because of their applications in drug design. There are several methods for synthesis of carbamates such as Hofmann rearrangement, Curtius rearrangement, and the use of specific reagents such as phosgene, isocyanate, and alkyl chloroformates [12]. In this semi-synthesis of α -mangostin derivatives, carbamate was formed by the nucleophilic addition of the hydroxy group of α -mangostin to the reactive carbonyl of isocyanate.

For the semi-synthesis of α -mangostin-carbamate prodrugs, the optimized condition was investigated by solvent, base, temperature, and reaction time with 3-chlorophenyl isocyanate as the model study. The reaction was firstly optimized by using five different solvents at the same condition of temperature and reaction time. Then, the results were measured by densitometry on TLC with ImageJ software and the solvent was chosen by the % yield of the products (**Table 17**). As the results, dichloromethane (DCM) promoted the highest yield of the designed α -mangostin-carbamate derivative. Thus, DCM was chosen as the optimized solvent.

Table 17 Reaction optimization of carbamate formation by solvent

Entry	Solvent	Temperature and time	Yield %
1.	Dichloromethane (DCM)	r.t., 17h then 40°C, 9h	68
2.	Ethyl acetate (EtOAc)	r.t., 17h then 40°C, 9h	21
3.	Tetrahydrofuran (THF)	r.t., 17h then 40°C, 9h	29
4.	Toluene	r.t., 17h then 40°C, 9h	34
5.	Dimethylformamide (DMF)	r.t., 17h then 40°C, 9h	66

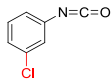
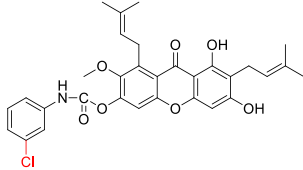
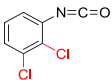
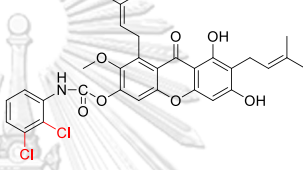
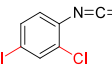
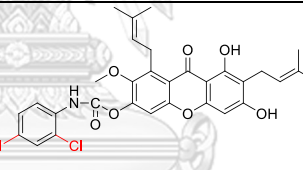

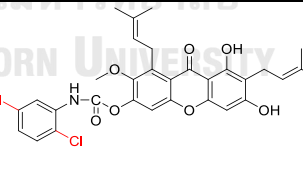
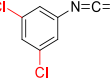
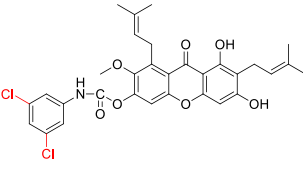
Secondly, the reaction was optimized by base (0.5 equiv) utilizing an inorganic base such as K_2CO_3 and an organic base such as triethylamine (TEA) with the selected solvent such as DCM. It was noted that using the organic base such as triethylamine did not promote carbamate formation of α -mangostin (**Table 18**).

Table 18 Reaction optimization of carbamate formation by the base

Entry	Base	Temperature and time	Yield %
1.	K_2CO_3	r.t., 4h	89
2.	TEA	r.t., 4h	No product

After exploring and optimizing reaction conditions, the series of α -mangostin-carbamate prodrugs were prepared with the various chlorinated isocyanate reagents including 3-chlorophenyl isocyanate, 2,3-dichlorophenyl isocyanate, 2,4-dichlorophenyl isocyanate, 2,5-dichlorophenyl isocyanate and 3,5-dichlorophenyl isocyanate. The optimized condition was α -mangostin: isocyanate: K_2CO_3 (1:3:0.5) in DCM and the results were investigated (**Table 19**). The obtained products were 6, 8-dihydroxy-2-methoxy-1, 7-bis-(3-methylbut-2-en-1-yl) -9-oxo-9H-xanthen-3-yl- (3-chlorophenyl) carbamate (**5a**), 6, 8-dihydroxy-2-methoxy-1, 7-bis-(3-methylbut-2-en-1-yl) -9-oxo-9H-xanthen-3-yl-(2, 3-dichlorophenyl) carbamate (**5b**), 6, 8-dihydroxy-2-methoxy-1, 7-bis-(3-methylbut-2-en-1-yl) -9-oxo-9H-xanthen-3-yl-(2, 4-dichlorophenyl) carbamate (**5c**), 6, 8-dihydroxy-2-methoxy-1, 7-bis-(3-methylbut-2-en-1-yl) -9-oxo-9H-xanthen-3-yl-(2, 5-dichlorophenyl) carbamate (**5d**), 6, 8-dihydroxy-2-methoxy-1, 7-bis-(3-methylbut-2-en-1-yl)-9-oxo-9H-xanthen-3-yl-(3, 5-dichlorophenyl) carbamate (**5e**), respectively.

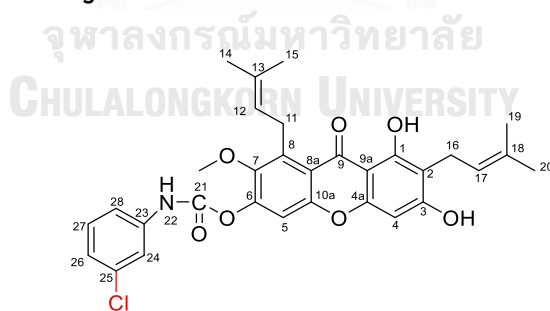
Table 19 Formation of α -mangostin-carbamate derivatives

Entry	Isocyanate reagents	Corresponding α -mangostin derivatives	Yield % and Weight
1.	 3-chlorophenyl isocyanate	 5a	81 (55mg)
2.	 2,3-dichlorophenyl isocyanate	 5b	52 (38mg)
3.	 2,4-dichlorophenyl isocyanate	 5c	23 (16mg)
4.	 2,5-dichlorophenyl isocyanate	 5d	42 (30mg)
5.	 3,5-dichlorophenyl isocyanate	 5e	72 (52mg)

4.3.2 Structural determination of α -mangostin-carbamate derivatives

4.3.2.1 Structural determination of compound **5a**

The product from the model reaction, compound **5a**, was obtained as the yellow amorphous solid. The structure of compound **5a** was firstly determined by ^1H and ^{13}C NMR. The ^1H NMR spectrum of this compound (**Figure 38** in Appendix and **Table 20**) exhibited the amide signal at δ 9.59 ppm, four signals of the aromatic proton from the carbamate ring at δ 7.78 (1H, t, $J = 2.1$ Hz), δ 7.34 (1H, ddd, $J = 9.0, 1.7, 1.2$ Hz), δ 7.27 (1H, t, $J = 7.8$ Hz), and δ 7.01 (1H, ddd, $J = 7.7, 2.1, 1.2$ Hz), two aromatic protons from xanthone core ring revealed at δ 6.89 (1H, s, H-5) and δ 6.39 (1H, s, H-4), together with a methoxy group at δ 3.81 (7-OCH₃). The ^{13}C NMR spectrum (**Figure 39** in Appendix and **Table 20**) indicated the presence of thirty-one carbons with a conjugated carbonyl carbon at δ 183.5 (C-9) and a carbamate carbonyl carbon at δ 151.5 (C-21), eighteen aromatic carbons, four olefinic carbons, two methylene carbons, a methoxy carbon, and four methyl carbons. Unfortunately, the compound **5a** was decomposed to starting compounds during NMR measurement. Thus, ^1H NMR spectra of α -mangostin and compound **5a** were compared as shown in **Figure 21**.



6,8-dihydroxy-2-methoxy-1,7-bis(3-methylbut-2-en-1-yl)-9-oxo-9H-xanthen-3-yl (3-chlorophenyl)carbamate (**5a**); yellow amorphous solid; 81% yield; R_f 0.38 (EtOAc:hexane = 3:7); ^1H NMR (300 MHz, Acetone- d_6): δ ppm 13.86 (1H, s, OH), 9.59 (1H, br s, NH), 7.78 (1H, t, $J = 2.1$ Hz), 7.34 (1H, ddd, $J = 9, 1.7, 1.2$), 7.27 (1H, t, $J = 7.8$), 7.01 (1H, ddd, $J = 7.7, 2.1, 1.2$ Hz), 6.89 (1H, s), 6.39 (1H, s), 5.28 (1H, t, $J = 7.2$

Hz), 5.17 (1H, t, $J = 7.2$ Hz), 4.13 (2H, d, $J = 6.9$ Hz), 3.81 (3H, s), 3.36 (2H, d, $J = 6.9$ Hz), 1.83 (3H, s), 1.72 (3H, s), 1.65 (3H, s), 1.60 (3H, s); ^{13}C NMR (75 MHz, Acetone- d_6): δ ppm 183.5, 161.7, 161.5, 158.2, 156.6, 154.5, 151.5, 144.8, 140.9, 138.3, 135.0, 132.3, 131.7, 131.3, 131.0, 124.4, 124.1, 122.9, 122.5, 119.1, 117.7, 116.9, 102.8, 93.1, 61.3, 26.9, 25.9, 22.7, 21.9, 18.3, 17.8.

Table 20 NMR spectral data of compound **5a** in $(\text{CD}_3)_2\text{CO}$

Position	δ_{H} of 1 [70]	δ_{H} of 5a
1	13.78 (1H, s, OH)	13.86 (1H, s, OH)
5	6.82 (1H, s)	6.89 (1H, s)
4	6.40 (1H, s)	6.39 (1H, s)
12	5.27 (1H, t)	5.28 (1H, t, $J = 7.2$ Hz)
17	5.27 (1H, t)	5.17 (1H, t, $J = 7.2$ Hz)
11	4.13 (2H, d, $J = 6.5$ Hz)	4.13 (2H, d, $J = 6.9$ Hz)
7-OCH ₃	3.80 (3H, s)	3.81 (3H, s)
16	3.35 (2H, d, $J = 7.3$ Hz)	3.36 (2H, d, $J = 6.9$ Hz)
14	1.81 (3H, s)	1.83 (3H, s)
19	1.65 (3H, s)	1.72 (3H, s)
20	not report	1.65 (3H, s)
15	not report	1.60 (3H, s)
Amide of carbamate	-	9.59 (1H, br s, NH)
Aromatic of carbamate	-	7.78 (1H, t, $J = 2.1$ Hz) 7.34 (1H, ddd, $J = 9, 1.7, 1.2$) 7.27 (1H, t, $J = 7.8$) 7.01 (1H, ddd, $J = 7.7, 2.1, 1.2$ Hz)

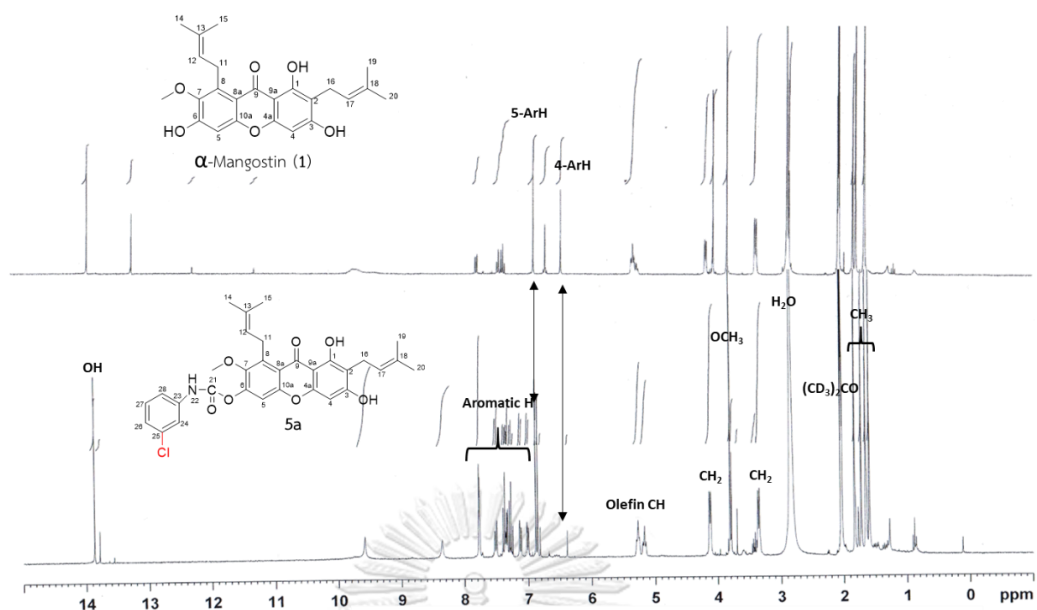
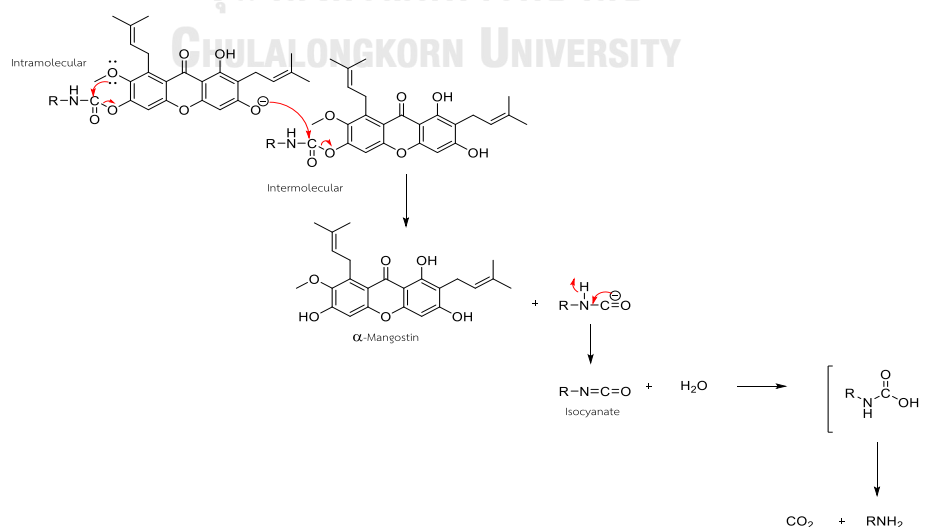


Figure 21 Comparison of ^1H NMR (300 MHz) spectrum of compounds **1** and **5a**

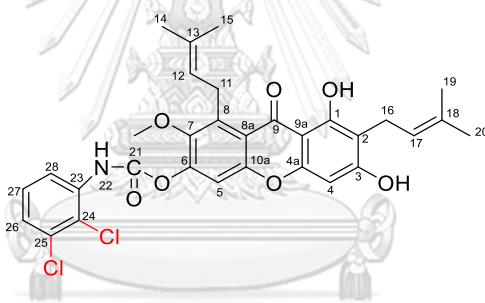
Regarding the decomposition, the hydrolysis of carbamate bond was proposed as self-hydrolysis with either intramolecular hydrolysis by methoxy group at C-7 or intermolecular hydrolysis by free hydroxyl group at C-3 and turned back to **α -mangostin** precursor and isocyanate [75]. Besides, in the presence of water, isocyanate was hydrolyzed into amine [76] (**Scheme 11**).



Scheme 11 Proposed mechanism of carbamate hydrolysis

4.3.2.2 Structural determination of compound **5b**

The compound **5b** was obtained as the yellow amorphous solid and its structure was determined by ^1H NMR (Figure 40 in Appendix and Table 21). The NMR spectrum expressed the signal of amide at δ 9.71 (1H, br s) ppm, and a methoxy group at δ 3.81 (3H, s). The differences between the model product **5a** and **5b** were the proton coupling of *ortho* and *meta* position in the aromatic ring of carbamate. In this compound **5b**, the three aromatic protons from the carbamate ring revealed at δ 7.96 (1H, dd, $J = 6.6, 3.0$ Hz), δ 7.42 (1H, overlapped), and δ 7.41 (1H, overlapped). The two aromatic protons from xanthone core ring revealed at δ 6.89 (1H, s, H-5) and δ 6.39 (1H, s, H-4) respectively. This compound **5b** also decomposed and turned back to α -mangostin as in Figure 22.



6,8-dihydroxy-2-methoxy-1,7-bis (3-methylbut-2-en-1-yl)-9-oxo-9H-xanthen-3-yl
(2,3-dichlorophenyl) carbamate (**5b**)

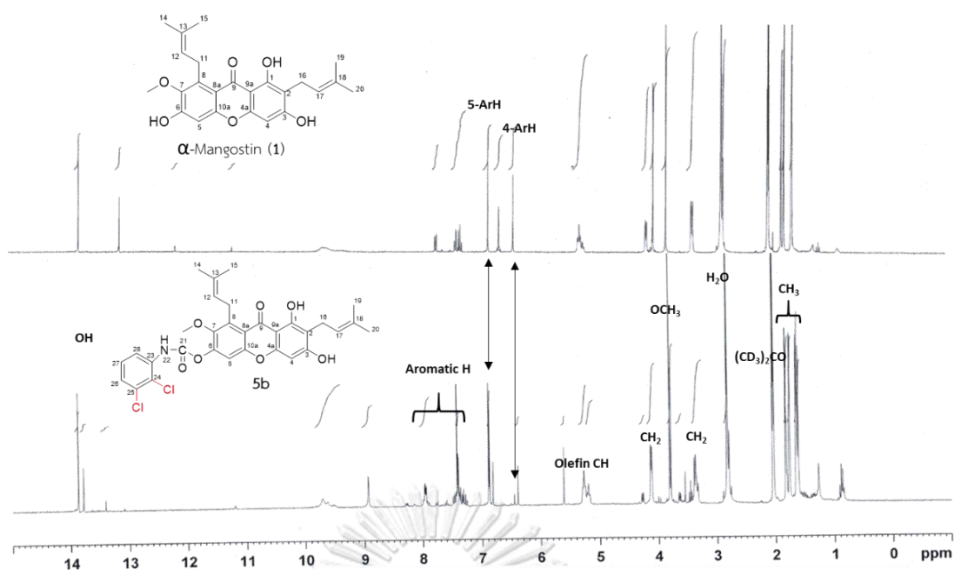
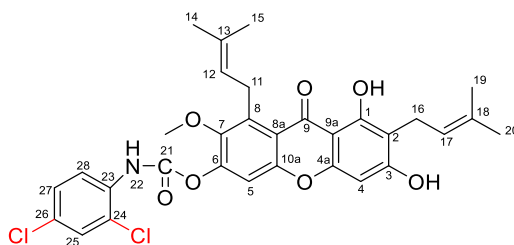


Figure 22 Comparison of ^1H NMR (300 MHz) spectrum of compounds **1** and **5b**

4.3.2.3 Structural determination of compound **5c**

The compound **5c** was obtained as the yellow amorphous solid. The ^1H NMR spectrum (**Figure 41** in Appendix and **Table 21**) revealed the signal of amide proton at δ 9.67 ppm, together with a signal of methoxy at δ 3.81 (3H, s, 7-OCH₃). The major differences of the signals of the carbamate aromatic protons from the compound **5a** were one *ortho*-coupled doublet at δ 7.98 (1H, d, J = 8.7 Hz), one meta-coupled doublet at δ 7.60 (1H, d, J = 2.4 Hz), and one double doublet with the coupling of *ortho* and *meta* position at δ 7.44 (1H, dd, J = 9, 2.4 Hz). The comparison of the ^1H NMR spectrum of compounds **5c** and α -mangostin have shown in **Figure 23**.



6,8-dihydroxy-2-methoxy-1,7-bis(3-methylbut-2-en-1-yl)-9-oxo-9H-xanthen-3-yl
(2,4-dichlorophenyl) carbamate (**5c**)

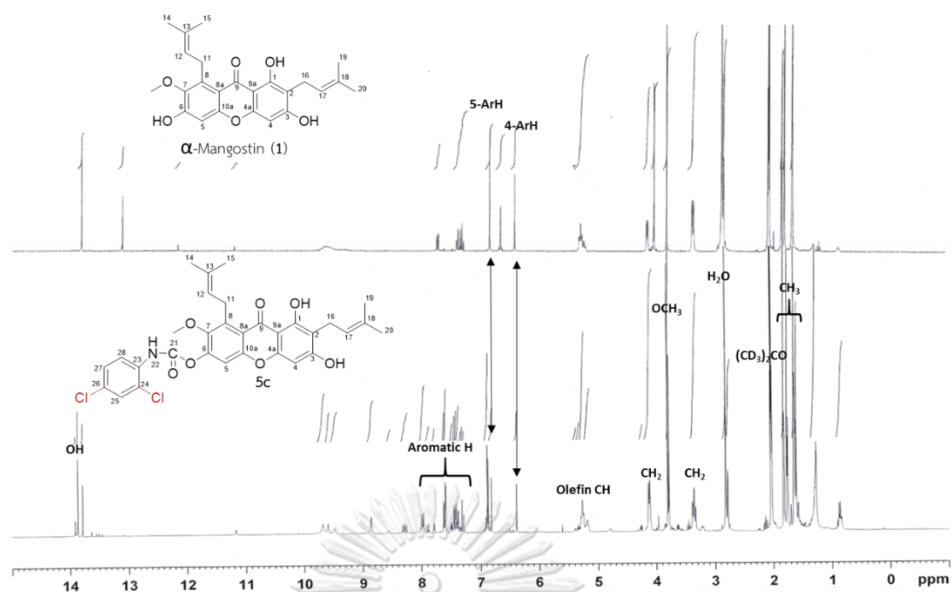
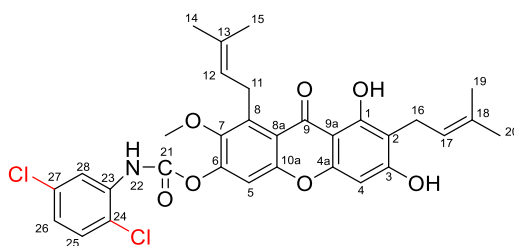


Figure 23 Comparison of ^1H NMR (300 MHz) spectrum of compounds **1** and **5c**

4.3.2.4 Structural determination of compound **5d**

The compound **5d** was obtained as the yellow amorphous solid. The proton NMR spectrum (**Figure 42** in Appendix and **Table 21**) indicated the presence of the signals of amide proton at δ 9.63 (1H, br s) and a methoxy proton at δ 3.79 (3H, s, 7-OCH₃). The signals of three aromatic protons of carbamate ring were proposed as one *meta*-coupled doublet at δ 8.41 (1H, d, $J = 2.4$), one *ortho*-coupled doublet at δ 7.56 (1H, d, $J = 8.7$), and one doublet of doublet at δ 7.11 (1H, dd, $J = 8.6, 2.7$). Based on the theory and reported data, the chemical shift of aromatic proton H-28 should be the most downfield in the aromatic region because of the electronegative atoms near H-28 and display as *meta*-coupled doublet. Besides, the chemical shifts should follow as H-26 with double doublet and later H-25 as *ortho*-coupled doublet [77]. Regarding the decomposition, the proton NMR of compound **5d** was mixed with three compounds such as **5d** together with α -mangostin, and 2,5-dichloroaniline. Thereupon the aromatic region was difficult to elucidate (**Figure 24**).



6,8-dihydroxy-2-methoxy-1,7-bis (3-methylbut-2-en-1-yl)-9-oxo-9H-xanthen-3-yl
(2,5-dichlorophenyl) carbamate (**5d**)

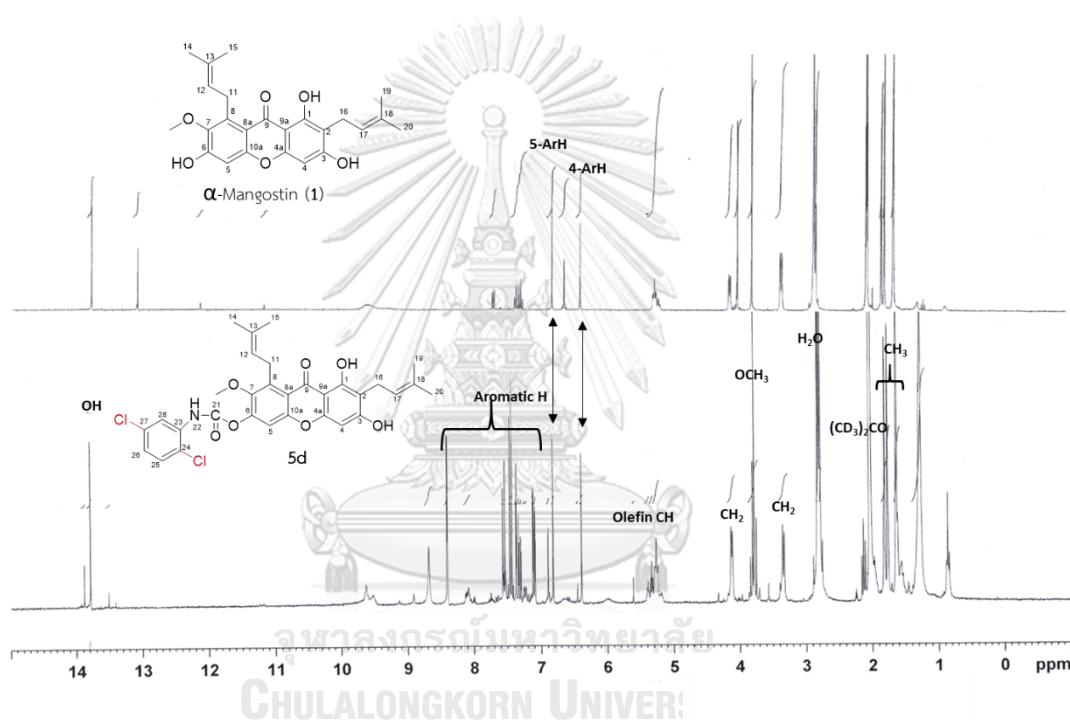
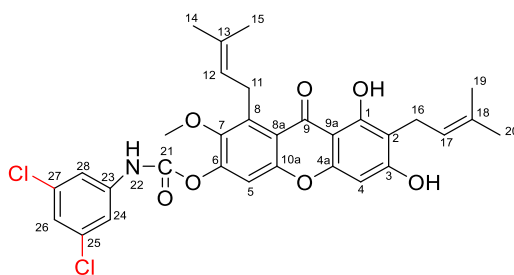


Figure 24 Comparison of ^1H NMR (300 MHz) spectrum of compounds **1** and **5d**

4.3.2.5 Structural determination of compound **5e**

The compound **5e** was obtained in yellow amorphous solid. The ^1H NMR spectrum (**Figure 43** in Appendix and **Table 21**) exhibited the signal of amide proton at δ 9.65 (1H, br s) and the protons of methoxy signal at δ 3.81 (3H, s, 7-OCH₃). The provable three aromatic protons from the carbamate ring displayed as *meta*-coupled triplets at δ 7.66 (1H, t, J = 1.8 Hz), and δ 7.20 (2H, overlapped).



6,8-dihydroxy-2-methoxy-1,7-bis(3-methylbut-2-en-1-yl)-9-oxo-9H-xanthen-3-yl
(3,5-dichlorophenyl) carbamate (**5e**)

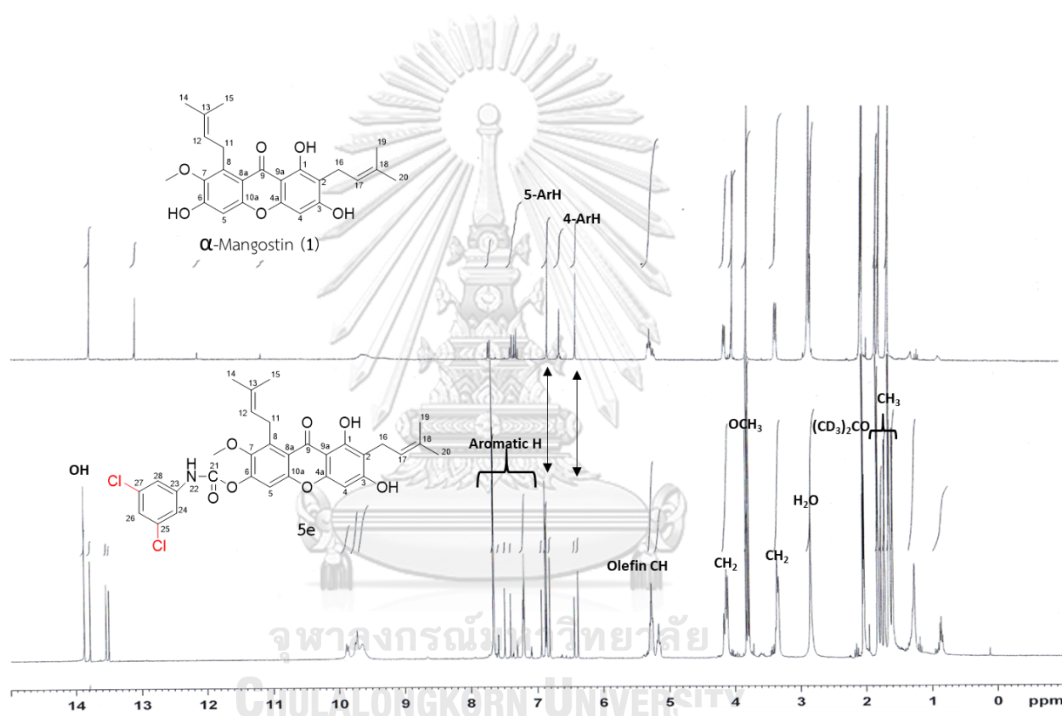


Figure 25 Comparison of ¹H NMR (300 MHz) spectrum of compounds **1** and **5e**

Table 21 ¹H NMR spectral data of compound **5b**, **5c**, **5d**, and **5e** in (CD₃)₂CO

Peak	δ_{H} (ppm, mult., <i>J</i> in Hz)				Functional group
	5b	5c	5d	5e	
1	13.78 (s)	13.87 (s)	13.79 (s)	13.87 (s)	OH
2	9.71 (br s)	9.67 (br s)	9.63 (br s)	9.65 (br s)	NH
3	8.93 (br s)	8.87 (br s)	8.68 (br s)	-	OH
4	7.96 (dd, 6.6, 3)	7.98 (d, 8.7)	8.41 (d, 2.4)	7.66 (t, 1.8)	Ar-H
5	7.42 (overlapped)	7.60 (d, 2.4)	7.56 (d, 8.7)	7.2 (overlapped)	Ar-H
6	7.41 (overlapped)	7.44 (dd, 9, 2.4)	7.11 (dd, 8.6, 2.7)	7.2 (overlapped)	Ar-H
7	6.89 (s)	6.89 (s)	6.82 (s)	6.88 (s)	Ar-H
8	6.39 (s)	6.39 (s)	6.39 (s)	6.38 (s)	Ar-H
9	5.27 (t, 6.0)	5.27 (t, 6.0)	5.34 (t, 4.5)	5.27 (t, 6.1)	=CH
10	5.20 (t, 6.9)	5.19 (t, 6.9)	5.27 (t, 6.8)	5.17 (t, 7.1)	=CH
11	4.13 (d, 6.6)	4.13 (d, 6.2)	4.12 (d, 6.3)	4.12 (d, 6.6)	CH ₂
12	3.81 (s)	3.81 (s)	3.79 (s)	3.81 (s)	OCH ₃
13	3.38 (d, 7.2)	3.37 (d, 7.8)	3.34 (d, 7.2)	3.35 (d, 6.6)	CH ₂

Table 21 ^1H NMR spectral data of compound **5b**, **5c**, **5d**, and **5e** in $(\text{CD}_3)_2\text{CO}$ (continued)

Peak	δ_{H} (ppm, mult., J in Hz)				Functional group
	5b	5c	5d	5e	
14	1.83 (s)	1.82 (s)	1.82 (s)	1.83 (s)	CH_3
15	1.76 (s)	1.77 (s)	1.77 (s)	1.72 (s)	CH_3
16	1.65 (s)	1.65 (s)	1.64 (s)	1.65 (s)	CH_3
17	1.62 (s)	1.62 (s)	1.28 (s)	1.60 (s)	CH_3

4.3.3 Aqueous solubility and drug-likeness of α -mangostin-carbamate derivatives

The general physicochemical properties and aqueous solubility of α -mangostin derivatives containing carbamate moiety were estimated (**Table 22**). In the previously reported data, having a carbamate functional group, increased the solubility and cytotoxicity activity [12]. The aqueous solubility of the compounds was evaluated by log *S* depended on three predictive parameters such as ESOL, Ali, and SILICOS-IT. The results showed the aqueous solubility of the derivatives was decreased when compared with starting material α -mangostin.

The estimation of the drug-likeness of α -mangostin derivatives containing carbamate moiety was shown in **Table 23**. All compounds proved to conform with rules of Lipinski filters, which was considered as the principal pattern of all drug-likeness means, accomplished from the drug discovery screens of Pfizer with one violation of molecular weight >500. Also, the compounds had no violations of the rules of Veber but had variable and acceptable rates in Ghose and Egan. The Abbot bioavailability score (ABS) showed 0.55 in all compounds mean the probability of the compounds had oral bioavailability in rat >10 % and measurable CaCO₂ permeability.

Table 22 General physicochemical properties and aqueous solubility of α -mangostin derivatives containing carbamate moiety

Properties	1	5a	5b	5c	5d	5e
Formula	$C_{24}H_{26}O_6$	$C_{31}H_{30}ClNO_7$	$C_{31}H_{29}Cl_2NO_7$	$C_{31}H_{29}Cl_2NO_7$	$C_{31}H_{29}Cl_2NO_7$	$C_{31}H_{29}Cl_2NO_7$
1. Molecular weight (MW)	410.46	564.03	598.47	598.47	598.47	598.47
2. Numbers of heavy atoms (HA)	30	40	41	41	41	41
3. Numbers of rotatable bonds (RB)	5	9	9	9	9	9
4. Numbers of H-bond acceptors (HBA)	6	7	7	7	7	7
5. Numbers of H-bond donors (HBD)	3	3	3	3	3	3
6. Log S (ESOL)	-6.35	-8.4	-9	-9	-9	-9
6.1 Solubility (mg/mL)	1.83×10^{-04}	2.25×10^{-06}	5.98×10^{-07}	5.98×10^{-07}	5.98×10^{-07}	5.98×10^{-07}
6.2 Solubility (mol/L)	4.46×10^{-07}	3.99×10^{-09}	1.00	1.00	1.00	1.00
6.3 Class (ESOL)	Poorly soluble	Poorly soluble	Poorly soluble	Poorly soluble	Poorly soluble	Poorly soluble
7. Log S (Ali)	-8.16	-10.74	-11.39	-11.39	-11.39	-11.39
7.1 Solubility (mg/mL)	2.84×10^{-06}	1.03×10^{-08}	2.42	2.42	2.42	2.42
			$\times 10^{-09}$	$\times 10^{-09}$	$\times 10^{-09}$	$\times 10^{-09}$

Table 23 Drug-likeness parameters of α -mangostin derivatives containing carbamate moiety

Properties	1	5a	5b	5c	5d	5e
Lipinski	Yes	Yes	Yes	Yes	Yes	Yes
	0 v	1 v	1 v	1 v	1 v	1 v
		MW>500	MW>500	MW>500	MW>500	MW>500
Ghose	Yes	No	No	No	No	No
		3 v	3 v	3 v	3 v	3 v
		MW>480	MW>480	MW>480	MW>480	MW>480
		WLOGP >5.6	WLOGP >5.6	WLOGP >5.6	WLOGP >5.6	WLOGP >5.6
		MR>130	MR>130	MR>130	MR>130	MR>130
Veber	Yes	Yes	Yes	Yes	Yes	Yes
Egan	Yes	No	No	No	No	No
		1 v	1 v	1 v	1 v	1 v
		WLOGP >5.88	WLOGP >5.88	WLOGP >5.88	WLOGP >5.88	WLOGP >5.88
Muegge	No	No	No	No	No	No
	1 v	1 v	1 v	1 v	1 v	1 v
	XLOGP3	XLOGP3	XLOGP3	XLOGP3	XLOGP3	XLOGP3
	>5	>5	>5	>5	>5	>5
ABS	0.55	0.55	0.55	0.55	0.55	0.55

ABS = Abbot Bioavailability Score, v = Violation (s), MR = Molar refractivity, WLOGP = Atomistic method accomplished from Wildman SA and Crippen GM, XLOGP3 = Atomistic and knowledge-based method calculated Log *P* by XLOGP program.

4.3.4 Stability of α -mangostin-carbamate derivatives evaluated by UV-vis spectroscopy

The α -mangostin derivatives containing carbamate moiety were unstable and decomposed during proton NMR measurement. The decomposition potentially related to the free hydroxyl group from solvent, trace of water and hydroxyl moiety in the molecule. Thus, the stability of α -mangostin derivatives was determined by using UV-vis spectrophotometer. In this experiment, analytical grade CHCl_3 and MeOH were chosen as the solvents. Due to the limitation of the quantity of products, only three α -mangostin derivatives including **5a**, **5b**, and **5e** were employed in the stability test. It was noted that **5a**, **5b**, and **5e** were not decomposed until 20 mins in both solvents. However, the hydrolysis of compound **5e** was observed after 24 h in MeOH (**Table 24**).

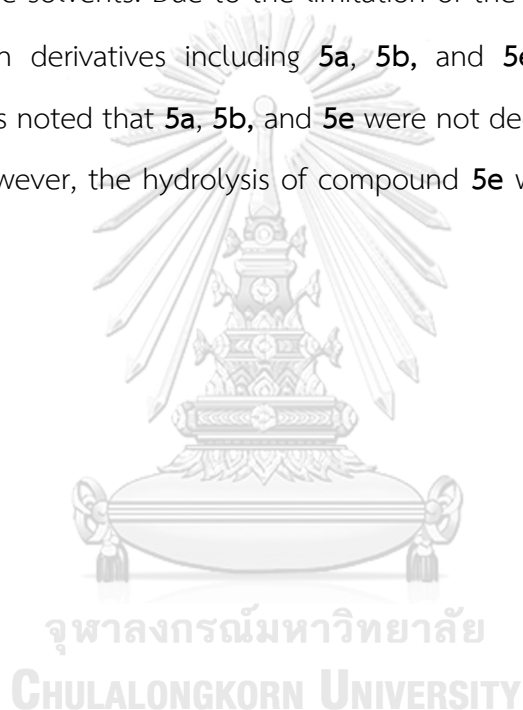


Table 24 Stability of α -mangostin-carbamate derivatives evaluated by UV-vis spectroscopy

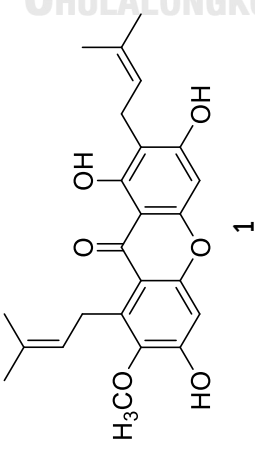
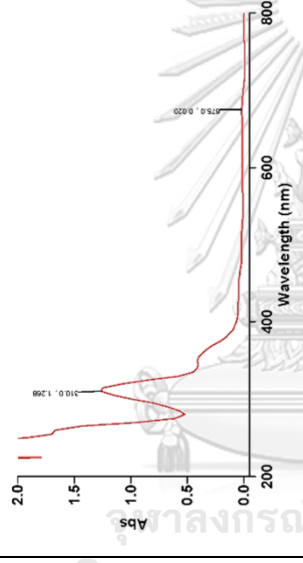
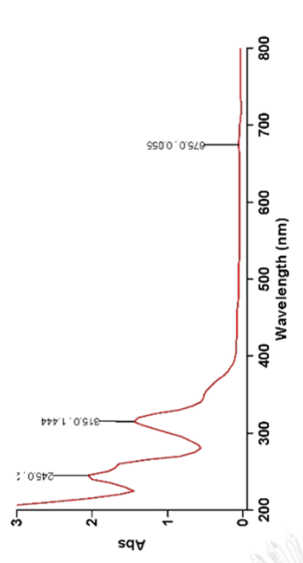
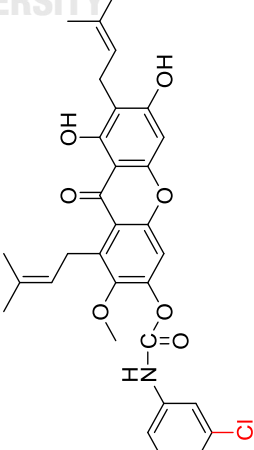
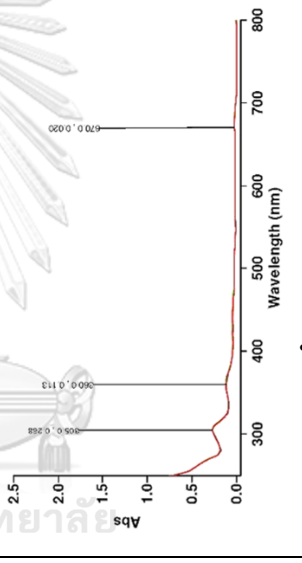
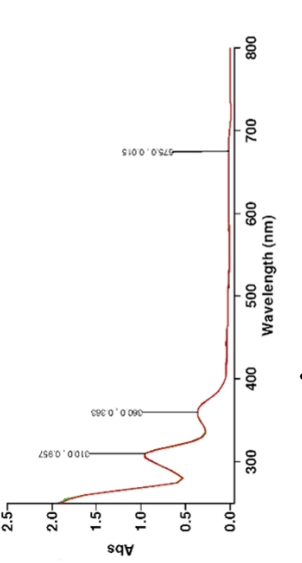
Compound	UV spectra	
	CHCl ₃	MeOH
 <p style="text-align: center;">1</p>	 <p>0 mins, $\lambda_{\text{max}} = 310 \text{ nm}$ 20 mins, $\lambda_{\text{max}} = 310 \text{ nm}$</p>	 <p>0 mins, $\lambda_{\text{max}} = 315 \text{ nm}$ 20 mins, $\lambda_{\text{max}} = 315 \text{ nm}$</p>
 <p style="text-align: center;">5a</p>	 <p>0 mins, $\lambda_{\text{max}} = 305, 360 \text{ nm}$ 20 mins, $\lambda_{\text{max}} = 305, 360 \text{ nm}$</p>	 <p>0 mins, $\lambda_{\text{max}} = 310, 360 \text{ nm}$ 20 mins, $\lambda_{\text{max}} = 310, 360 \text{ nm}$</p>

Table 28 Stability of α -mangostin-carbamate derivatives evaluated by UV-vis spectroscopy (continued)

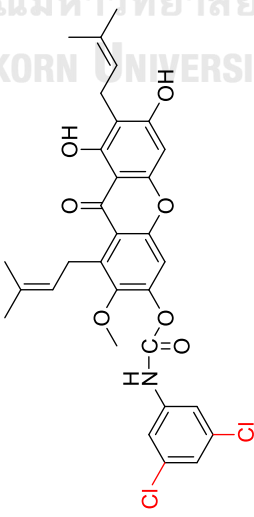
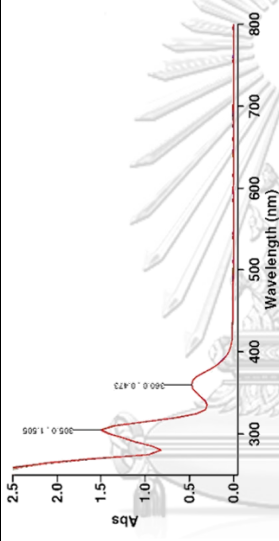
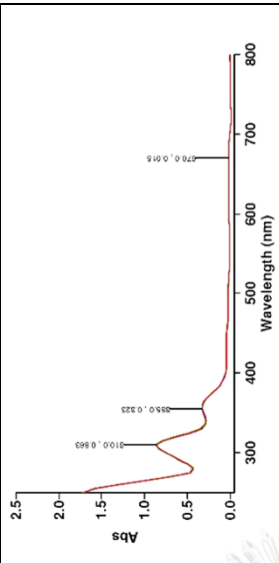
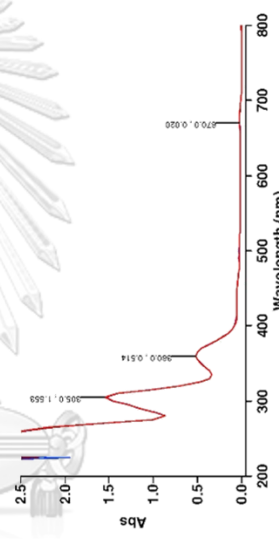
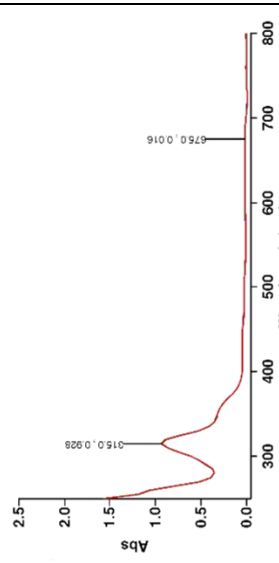
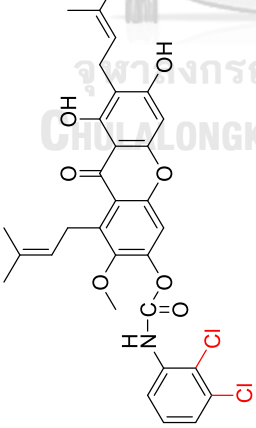
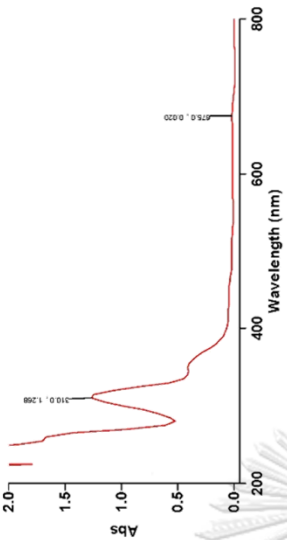
Compound	UV spectra	
	CHCl ₃	MeOH
 <p style="text-align: center;">5e</p>	 <p>0 mins, $\lambda_{\text{max}} = 305, 360$ nm</p>	 <p>0 mins, $\lambda_{\text{max}} = 310, 355$ nm</p>
	 <p>24 h, $\lambda_{\text{max}} = 305, 360$ nm</p>	 <p>24 h, $\lambda_{\text{max}} = 315, 355$ nm</p>

Table 28 Stability of α -mangostin-carbamate derivatives evaluated by UV-vis spectroscopy (continued)

Compound	UV spectra (CHCl ₃)
 <p>5b</p>	 <p>0 mins, $\lambda_{\text{max}} = 305, 360$ nm 20 mins, $\lambda_{\text{max}} = 305, 360$ nm</p>

4.3.5 Cytotoxic activity against H460 cell line

The cytotoxic effects of α -mangostin-carbamate derivatives were evaluated by *in vitro* MTT assay on human H460 cells. The results indicated that the compound **5b** showed approximately 3-fold more potent than **1** towards H460 cell line. It possessed the most potent cytotoxicity among the derivatives in this series. It was noteworthy that chlorinated substituent on the phenyl side chain of carbamate at the specific position such as C-13 and C-14 was important for the cytotoxic activity (Table 25).

Table 25 Cytotoxic activity of α -mangostin derivatives containing carbamate moiety

Compound	H460 IC ₅₀ ± S.D. (μM)
1	38.04 ± 2.44
5a	35.07 ± 2.89
5b	11.52 ± 1.32
5c	50.44 ± 1.17
5d	42.48 ± 1.34
5d	48.91 ± 2.64

Note: Data are expressed as mean ± standard deviation.

Although, compound **5b** exhibited improved cytotoxic activity greater than mother compound **1**, the stability of this compound seems to be the drawback and limits the development of this compound as an anti-lung cancer agent. Toward the future study, it could be applied as a prodrug to achieve the mother compound α -mangostin over its limitation.

CHAPTER V CONCLUSION

In this research, the multidisciplinary study of α -mangostin was described both chemistry and pharmacology aspects. Herein, α -mangostin was isolated and employed as the starting material for Smiles rearrangement and carbamate formation. The two series of α -mangostin derivatives were evaluated their cytotoxic activity against the H460 and H-290 non-small-cell lung cancer cell lines.

The three xanthenes were isolated from mangosteen pericarp in this study. Among them, the major xanthone, α -mangostin, was mainly isolated and obtained at 15.8 g as a yellow powder with 80-90% purity with 3.3% weight by dry weight. The structure of α -mangostin was confirmed by ^1H NMR. Then, the isolated α -mangostin was used as starting material for the chemical modification studies.

Besides, novel α -mangostin derivatives including **4a**, **4b**, and **4c** were semi-synthesized *via* Smiles rearrangement from α -mangostin. This starting material was modified at the hydroxy group to the amine motif involving the three-step-one-pot Smiles rearrangement, which mechanistically consists of nucleophilic substitution, rearrangement, and hydrolysis. Our findings provide the optimum method for semi-synthesis of the new α -mangostin derivatives **4a**, and **4c** by using Cs_2CO_3 as a base and KI as a catalyst and **4b** with K_2CO_3 and KI. The physicochemical properties of **4a**, **4b**, and **4c** were calculated by *in silico* technique. It was noteworthy that **4a** and **4c** potentially improved the water solubility and possible to maintain the bioavailability based on predicted data. The cytotoxicity of the derivatives emphasizing human non-small-cell lung cancer cell lines such as H460 and H292 was evaluated by *in vitro* MTT assay and the cell death mechanism was confirmed by nuclear staining assay (Hoechst33342/PI). Our findings confirmed that conversion α -mangostin structure by transforming the hydroxy at C-3 and C-6 to the amine group reduced the cytotoxicity toward the selected lung cancer cell lines and the mode of cell death was

confirmed to apoptosis mechanism. Thus, the hydroxy groups on α -mangostin are crucial for the cytotoxicity against human non-small cell lung cancer cell lines. Further studies of α -mangostin derivatives **4a**, **4b**, and **4c** would be the exploration of applications for anti-microbial to treat the respiratory tract infection.

In addition, this study provided a new method for the semi-synthesis of α -mangostin-carbamate derivatives. Under the optimum condition, compounds **5a** and **5e** were produced in high yield, **5b** and **5d** were obtained in moderate yield, and **5c** was afforded in low yield. Unfortunately, the hydrolysis of the α -mangostin-carbamate derivatives was observed. Therefore, the stability test was performed by using spectroscopic technique and confirmed that α -mangostin-carbamate derivatives have limit stability at a short time with no longer than 24 h, when the compounds were prepared in alcoholic solution. The physicochemical properties of the α -mangostin-carbamate derivatives were predicted by the *in silico* method to display improved water solubility but retained the optimum bioavailability. The cytotoxicity of the **5a-5e** was evaluated against H460 cell line by the MTT assay. The results showed that α -mangostin-carbamate derivative **5b** exhibited IC_{50} 11.52 ± 1.32 μ M, which was 3-fold more potent than α -mangostin (IC_{50} 38.04 ± 2.44 μ M). Hence, compound **5b** would be further studied to improve its stability and developed as anti-non-small-cell lung cancer agent.

REFERENCES



จุฬาลงกรณ์มหาวิทยาลัย
CHULALONGKORN UNIVERSITY

1. Bray, F., Ferlay, J., Soerjomataram, I., Siegel, R.L., Torre, L.A., and Jemal, A. Global cancer statistics 2018: GLOBOCAN estimates of incidence and mortality worldwide for 36 cancers in 185 countries. **CA: A Cancer Journal for Clinicians** 68 (2018): 394-424.
2. Malhotra, J., Malvezzi, M., Negri, E., La Vecchia, C., and Boffetta, P. Risk factors for lung cancer worldwide. **European Respiratory Journal** 48 (2016): 889-902.
3. Ye, M.-X., Li, Y., Yin, H., and Zhang, J. Curcumin: updated molecular mechanisms and intervention targets in human lung cancer. **International Journal of Molecular Sciences** 13 (2012): 3959-3978.
4. Jin, L., Li, C., Xu, Y., Wang, L., Liu, J., Wang, D., Hong, C., Jiang, Z., Ma, Y., Chen, Q., and Yu, F. Epigallocatechin gallate promotes p53 accumulation and activity via the inhibition of MDM2-mediated p53 ubiquitination in human lung cancer cells. **Oncology Reports** 29 (2013): 1983-1990.
5. Zhong, W.-l., Qin, Y., Chen, S., and Sun, T. Antitumor effect of natural product molecules against lung cancer. **A Global Scientific Vision - Prevention, Diagnosis, and Treatment of Lung Cancer**. IntechOpen 2017: 201-220
6. Shapiro, T.A., Fahey, J.W., Wade, K.L., Stephenson, K.K., and Talalay, P. Chemoprotective glucosinolates and isothiocyanates of broccoli sprouts: metabolism and excretion in humans. **Cancer Epidemiology, Biomarkers & Prevention** 10 (2001): 501-508.
7. Zhu, H., Cheng, H., Ren, Y., Liu, Z.G., Zhang, Y.F., and De Luo, B. Synergistic inhibitory effects by the combination of gefitinib and genistein on NSCLC with acquired drug-resistance in vitro and in vivo. **Molecular Biology Reports** 39 (2012): 4971-4979.
8. Chen, G., Li, Y., Wang, W., and Deng, L. Bioactivity and pharmacological properties of α -mangostin from the mangosteen fruit: a review. **Expert Opinion on Therapeutic Patents** 28 (2018): 415-427.
9. Chi, X.-Q., Zi, C.-T., Li, H.-M., Yang, L., Lv, Y.-F., Li, J.-Y., Hou, B., Ren, F.-C., Hu, J.M., and Zhou, J. Design, synthesis and structure-activity relationships of mangostin analogs as cytotoxic agents. **The Royal Society of Chemistry. RSC Advances** 8 (2018): 41377-41388.

10. Fei, X., Jo, M., Lee, B., Han, S.-B., Lee, K., Jung, J.-K., Seo, S.-Y., and Kwak, Y.-S. Synthesis of xanthone derivatives based on α -mangostin and their biological evaluation for anti-cancer agents. **Bioorganic & Medicinal Chemistry Letters** 24 (2014): 2062-2065.
11. Xie, Y.-S., Vijaykumar, B.V.D., Jang, K., Shin, H.-H., Zou, H., and Shin, D.-S. One-pot conversion of phenols to anilines via Smiles rearrangement. **Tetrahedron Letters** 54 (2013): 5151-5154.
12. Ghosh, A.K., and Brindisi, M. Organic carbamates in drug design and medicinal chemistry. **Journal of Medicinal Chemistry** 58 (2015): 2895-2940.
13. Akao, Y., Nakagawa, Y., Inuma, M., and Nozawa, Y. Anti-cancer effects of xanthenes from pericarps of mangosteen. **International Journal of Molecular Sciences** 9 (2008): 355-370.
14. Ketsa S., and Paull, R.E. 1-Mangosteen (*Garcinia mangostana* L.). **Postharvest Biology and Technology of Tropical and Subtropical Fruits**. Woodhead Publishing Series in Food Science, Technology and Nutrition 2011: 1-30.
15. Pedraza-Chaverri, J., Cardenas-Rodriguez, N., Orozco-Ibarra, M., and Perez-Rojas, J.M. Medicinal properties of mangosteen (*Garcinia mangostana*). **Food and Chemical Toxicology** 46 (2008): 3227-3239.
16. Zhou, H.-C., Lin, Y.-M., Wei, S.-D., and Tam, N.F.-y. Structural diversity and antioxidant activity of condensed tannins fractionated from mangosteen pericarp. **Food Chemistry** 129 (2011): 1710-1720.
17. Pratiwi, L., Fudholi, A., Martien, R., and Pramono, S. Development of TLC and HPTLC method for determination α -mangostin in mangosteen peels (*Garcinia Mangostana* L.). **International Journal of Pharmacognosy and Phytochemical Research** 9 (2017): 297-302.
18. Suksamrarn, S., Suwannapoch, N., Ratananukul, P., Aroonlerk, N., and Suksamrarn, A. Xanthenes from the green fruit hulls of *Garcinia mangostana*. **Journal of Natural Products** 65 (2002): 761-763.

19. Yang, R., Li, P., Li, N., Zhang, Q., Bai, X., Wang, L., Xiao, Y., Sun, L., Yang, Q., and Yan, J. Xanthones from the pericarp of *Garcinia mangostana*. **Molecules** 22 (2017): 1-10.
20. Chaivisuthangkura, A., Malaikaew, Y., Chaovanalikit, A., Jaratrungtawee, A., Panseeta, P., Ratananukul, P., and Suksamran, S. Prenylated xanthone composition of *Garcinia mangostana* (Mangosteen) fruit hull. **Chromatographia** 69 (2008): 315-318.
21. Mahabusarakam, W., Wiriyachitra, P., and Taylor, W.C. Chemical constituents of *Garcinia mangostana*. **Journal of Natural Products** 50 (1987): 474-478.
22. Gopalakrishnan, G., Banumathi, B., and Suresh, G. Evaluation of the antifungal activity of natural xanthones from *Garcinia mangostana* and their synthetic derivatives. **Journal of Natural Products** 60 (1997): 519-524.
23. Ovalle-Magallanes, B., Eugenio-Perez, D., and Pedraza-Chaverri, J. Medicinal properties of mangosteen (*Garcinia mangostana* L.): A comprehensive update. **Food and Chemical Toxicology** 109 (2017): 102-122.
24. Ghasemzadeh, A., Jaafar, H. Z. E., Baghdadi, A., and Tayebi-Meigooni, A. Alpha-mangostin-rich extracts from mangosteen pericarp: Optimization of green extraction protocol and evaluation of biological activity. **Molecules** 23 (2018): 1-16.
25. Yates, P., and Stout, G.H. The structure of mangostin. **Journal of the American Chemical Society** 80 (1958): 1691-1700.
26. Sakagami, Y., Iinuma, M., Piyasena, K.G.N.P., and Dharmaratne, H.R.W. Antibacterial activity of α -mangostin against vancomycin resistant *Enterococci* (VRE) and synergism with antibiotics. **Phytomedicine** 12 (2005): 203-208.
27. Yates, P., and Bhat, H.B. Structure of β -mangostin. **Canadian Journal of Chemistry** 46 (1968): 3770-3772.
28. Govindachari, T.R., Kalyanaraman, P.S., Muthukumaraswamy, N., and Pai, B.R. Xanthones of *Garcinia mangostana* Linn. **Tetrahedron** 27 (1971): 3919-3926.
29. Han, A.-R., Kim, J.-A., Lantvit, D.D., Kardono, L.B.S., Riswan, S., Chai, H. Carcacha de Blanco, E.J. Farnsworth, N.R., Swanson, S.M., and Kinghorn, A.D. Cytotoxic

- xanthone constituents of the stem bark of *Garcinia mangostana* (Mangosteen). **Journal of Natural Products** 72 (2009): 2028-2031.
30. Nilar, and Harrison L.J. Xanthenes from the heartwood of *Garcinia mangostana*. **Phytochemistry** 60 (2002): 541-548.
31. Dharmaratne, H.R.W, Piyasena, K.G.N.P., and Tennakoon, S.B. A geranylated biphenyl derivative from *Garcinia mangostana*. **Natural Product Research** 19 (2005): 239-243.
32. Jung, H.-A., Su, B.-N., Keller, W.J., Mehta, R.G., and Kinghorn D. Antioxidant xanthenes from the pericarp of *Garcinia mangostana* (Mangosteen). **Journal of Agricultural and Food Chemistry** 54 (2006): 2077-2082.
33. Parveen, M., and Khan, N.U-d. Two xanthenes from *Garcinia mangostana*. **Phytochemistry** 27 (1988): 3694-3696.
34. Sen, A.K., Sarkar, K.K., Mazumder, P.C., Banerji, N., Uusvuori, R., and Hase, T.A. The structures of garcinones A, B and C: Three new xanthenes from *Garcinia mangostana*. **Phytochemistry** 21 (1982): 1747-1750.
35. Suksamran, S., Komutiban, O., Ratananukul, P., Chimnoi, N., Lartpornmatulee, N., and Suksamran, A. Cytotoxic prenylated xanthenes from the young fruit of *Garcinia mangostana*. **Chemical and Pharmaceutical Bulletin** 54 (2006): 301-305.
36. Ee, G.C.L., Daud, S., Taufiq-Yap, Y.H., Ismail, N.H., and Rahmani, M. Xanthenes from *Garcinia mangostana* (Guttiferae). **Natural Product Research** 20 (2006): 1067-1073.
37. Suksamran, S., Suwannapoch, N., Phakhodee, W., Thanuhiranlert, J., Ratananukul, P., Chimnoi, N., and Suksamran, A. Antimycobacterial activity of prenylated xanthenes from the fruits of *Garcinia mangostana*. **Chemical and Pharmaceutical Bulletin** 51 (2003): 857-859.
38. Balasubramanian, K., and Rajagopalan, K. Novel xanthenes from *Garcinia mangostana*, Structures of BR-Xanthone-A and BR-Xanthone-B. **Phytochemistry** 27 (1988): 1552-1554.

39. Nilar, Nguyen, L.-H.D., Venkatraman, G., Sim, K.-Y., and Harrison, L.J. Xanthonones and benzophenones from *Garcinia griffithii* and *Garcinia mangostana*. **Phytochemistry** 66 (2005): 1718-1723.
40. Holloway, D.M., and Scheinmann, F. Phenolic compounds from the heartwood of *Garcinia mangostana*. **Phytochemistry** 14 (1975): 2517-2518.
41. Iinuma, M., Tosa, H., Tanaka, T., Asai, F., Kobayashi, Y., Shimano, R., and Miyauchi, K.-I. Antibacterial activity of xanthonones from guttiferaceous plants against methicillin-resistant *Staphylococcus aureus*. **Journal of Pharmacy and Pharmacology** 48 (1996): 861-865.
42. Chin, Y.W., Jung, H.A., Chai, H., Keller, W.J., and Kinghorn, A.D. Xanthonones with quinone reductase-inducing activity from the fruits of *Garcinia mangostana* (Mangosteen). **Phytochemistry** 69 (2008): 754-758.
43. Abdallah, H.M., El-Bassossy, H.M., Mohamed, G.A., El-Halawany, A.M., Alshali, K.Z., and Banjar, Z.M. Mangostanaxanthonones III and IV: advanced glycation end-product inhibitors from the pericarp of *Garcinia mangostana*. **Journal of Natural Medicines** 71 (2017): 216-226.
44. Huang, Y.-L., Chen, C.-C., Chen, Y.-J., Huang, R.-L., and Shieh, B.-J. Three xanthonones and a benzophenone from *Garcinia mangostana*. **Journal of Natural Products** 64 (2001): 903-906.
45. Ho, C.K., Huang, Y.L., and Chen, C.C. Garcinone E, a xanthone derivative, has potent cytotoxic effect against hepatocellular carcinoma cell lines. **Planta Medica** 68 (2002): 975-979.
46. Ryu, H.W., Jeong, S.H., Curtis-Long, M.J., Jung, S., Lee, J.W., Woo, H.S., Cho, J.K., and Park, K.H. Inhibition effects of mangosenone F from *Garcinia mangostana* on melanin formation in B16F10 cells. **Journal of Agricultural and Food Chemistry** 60 (2012): 8372-8378.
47. Mohamed, G.A., Ibrahim, S.R., Shaaban, M.I., and Ross, S.A. Mangostanaxanthonones I and II, new xanthonones from the pericarp of *Garcinia mangostana*. **Fitoterapia** 98 (2014): 215-221.
48. Matsumoto, K., Akao, Y., Kobayashi, E., Ohguchi, K., Ito, T., Tanaka, T., Iinuma, M., and Nozawa, Y. Induction of apoptosis by xanthonones from mangosteen in

- human leukemia cell lines. **Journal of Natural Products** 66 (2003): 1124-1127.
49. Shih, Y.-W., Chien, S.-T., Chen, P.-S., Lee, J.-H., Wu, S.-H., and Yin, L.-T. α -Mangostin suppresses phorbol 12-myristate 13-acetate-induced MMP-2/MMP-9 expressions via $\alpha_v\beta_3$ integrin/FAK/ERK and NF- κ B signaling pathway in human lung adenocarcinoma A549 cells. **Cell Biochemistry and Biophysics** 58 (2010): 31-44.
50. Shibata, M.-A., Iinuma, M., Morimoto, J., Kurose, H., Akamatsu, K., Okuno, Y., Akao, Y., and Otsuki, Y. α -Mangostin extracted from the pericarp of the mangosteen (*Garcinia mangostana* Linn) reduces tumor growth and lymph node metastasis in an immunocompetent xenograft model of metastatic mammary cancer carrying a p53 mutation. **BioMed Central Medicine**. 9 (2011): 69.
51. Andayani, R., Wahyuni, F.S., Wirasti, Y., and Hamidi, D. Development and validation of RP-HPLC method for quantitative estimation of α -mangostin in the rind extract and fractions of *Garcinia mangostana* L. and their cytotoxic activity on T47D breast cancer cell line. **International Journal of Pharmacy and Pharmaceutical Sciences** 7 (2015): 174-178.
52. Ittiudomrak, T., Puthong, S., Roytrakul, S., and Chanchao, C. α -Mangostin and apigenin induced cell cycle arrest and programmed cell death in SKOV-3 ovarian cancer cells. **Toxicological Research** 35 (2019): 167-179.
53. Wudtiwai, B., Pitchakarn, P., and Banjerdpongchai, R. Alpha-mangostin, an active compound in *Garcinia mangostana*, abrogates anoikis-resistance in human hepatocellular carcinoma cells. **Toxicology in Vitro** 53 (2018): 222-232.
54. Wang, J.J., Sanderson, B.J.S., and Zhang, W. Cytotoxic effect of xanthenes from pericarp of the tropical fruit mangosteen (*Garcinia mangostana* Linn.) on human melanoma cells. **Food and Chemical Toxicology** 49 (2011): 2385-2391.

55. Chao, A.-C., Hsu, Y.-L., Liu, C.-K., and Kuo, P.-L. α -Mangostin, a dietary xanthone, induces autophagic cell death by activating the AMP-activated protein kinase pathway in glioblastoma cells. **Journal of Agricultural and Food Chemistry** 59 (2011): 2086-2096.
56. Johnson, J.J., Petiwala, S.M., Syed, D.N., Rasmussen, J.T., Adhami, V.M., Siddiqui, I.A., Kohl, A.M., and Mukhtar, H. α -Mangostin, a xanthone from mangosteen fruit, promotes cell cycle arrest in prostate cancer and decreases xenograft tumor growth. **Carcinogenesis** 33 (2012): 413-419.
57. Nakagawa, Y., Iinuma, M., Naoe, T., Nozawa, Y., and Akao, Y. Characterized mechanism of α -mangostin-induced cell death: Caspase-independent apoptosis with release of endonuclease-G from mitochondria and increased miR-143 expression in human colorectal cancer DLD-1 cells. **Bioorganic & Medicinal Chemistry** 15 (2007): 5620-5628.
58. Lee, C.-H., Ying, T.-H., Chiou, H.-L., Hsieh, S.-C., Wen, S.-H., Chou, R.-H., and Hsieh, Y.-H. Alpha-mangostin induces apoptosis through activation of reactive oxygen species and ASK1/p38 signaling pathway in cervical cancer cells. **Oncotarget** 8 (2017): 47425-47439.
59. Phan, T.K.T., Shahbazzadeh, F. and Kihara, T. Alpha-mangostin reduces mechanical stiffness of various cells. **Human Cell** 33 (2020): 347-355.
60. Shan, T., Ma, Q., Guo, K., Liu, J., Li, W., Wang, F., and Wu, E. Xanthones from mangosteen extracts as natural chemopreventive agents: Potential anticancer drugs. **Current Molecular Medicine** 11 (2011): 666-677.
61. Verma, R.K., Yu, W., Shrivastava, A., Shankar, S., and Srivastava, R.K. α -Mangostin-encapsulated PLGA nanoparticles inhibit pancreatic carcinogenesis by targeting cancer stem cells in human, and transgenic (KrasG12D, and KrasG12D/tp53R270H) mice. **Scientific Reports** 6 (2016): 32743.
62. Li, L., Brunner, I., Han, A.-R., Hamburger, M., Kinghorn, A.D., Frye, R., and Butterweck, V. Pharmacokinetics of α -mangostin in rats after intravenous and oral application. **Molecular Nutrition & Food Research** 55 (2011): 67-74.

63. Lin, S., Sin, W. L. W., K, J-J., Lim, F., Wang, L., Cao, D. Beuerman, R.W., Ren, L., and Liu, D. Semisynthesis and biological evaluation of xanthone amphiphilics as selective, highly potent antifungal agents to combat fungal resistance. **Journal of Medicinal Chemistry** 60 (2017): 10135-10150.
64. Chen, Y., Bian, Y., Wang, J-W., Gong, T-T., Ying, Y-M., Ma, L-F., Shan, W-G., Xie, X-Q., and Zhan, Z-J. Effects of α -mangostin derivatives on the Alzheimer's disease model of rats and their mechanism: A combination of experimental study and computational systems pharmacology analysis. **American Chemical Society Omega** 5 (2020): 9846-9863.
65. Morelli, C.F., Biagiotti, M., Pappalardo, V. M., Rabuffetti, M., and Speranza, G. Chemistry of α -mangostin. Studies on the semisynthesis of minor xanthenes from *Garcinia mangostana*. **Natural Product Research** 29 (2015): 750-755.
66. Liang, J., Huang, Y-Y., Zhou, Q., Gao, Y., Li, Z., Wu, D., Yu, S., Guo, L., Chen, Z., Huang, L., Liang, S. H., Wu, R., and Luo, H-B. Discovery and optimization of α -mangostin derivatives as novel PDE4 inhibitors for the treatment of vascular dementia. **Journal of Medicinal Chemistry** 63 (2020): 3370-3380.
67. Buravlev, E.V. Synthesis of new derivatives of α -mangostin (microreview). **Chemistry of Heterocyclic Compounds** 55 (2019): 1038-1040.
68. Buravlev, E.V., Shevchenko, O. G., Anisimov, A. A., and Suponitsky, K. Y. Novel Mannich bases of α - and γ -mangostins: Synthesis and evaluation of antioxidant and membrane-protective activity. **European Journal of Medicinal Chemistry** 152 (2018): 10-20.
69. Daina, A., O. Michielin, and V. Zoete, *SwissADME*: A Free Web Tool to Evaluate Pharmacokinetics, Drug-likeness and Medicinal Chemistry Friendliness of Small Molecules. **Scientific Reports** 7 (2017): 42717.
70. Phitaktim, S., Chomnawang, M., Sirichaiwetchakoon, K., Dunkhunthod, B., Hobbs, G., Eumkeb, G. Synergism and the mechanism of action of the combination of α -mangostin isolated from *Garcinia mangostana* L. and oxacillin against an oxacillin-resistant *Staphylococcus saprophyticus*. **BioMed Central Microbiology** 16 (2016): 195.

71. Huber, V.J., Bartsch, R.A. Preparation of nitriles from carboxylic acids: a new synthetically useful example of the Smiles rearrangement. **Tetrahedron** 54 (1998): 9281-9288.
72. Kozaki, K-i., Miyaiishi, O., Tsukamoto, T., Tatematsu, Y., Hida, T., Takahashi, T., and Takahashi, T. Establishment and characterization of a human lung cancer cell line NCI-H460-LNM35 with consistent lymphogenous metastasis via both subcutaneous and orthotopic propagation. **Cancer Research** 60 (2000): 2535-2540.
73. Tang, D., Yue, L., Yao, R., Zhou, L., Yang, Y., Lu, L., and Gao, W. P53 prevent tumor invasion and metastasis by down-regulating IDO in lung cancer. **Oncotarget** 8 (2017): 54548-54557.
74. Syed Abdul Rahman, S.N., Abdul Wahab, N., Abd Malek, S.N. *In vitro* morphological assessment of apoptosis induced by antiproliferative constituents from the rhizomes of *Curcuma zedoaria*. **Evidence-Based Complementary and Alternative Medicine** 2013 (2013): 257108.
75. Leppänen, J., Huuskonen, J., Nevalainen, T., Gynther, J., Taipale, H., and Järvinen, T. Design and synthesis of a novel L-Dopa–Entacapone codrug. **Journal of Medicinal Chemistry** 45 (2002): 1379-1382.
76. Mattarei, A., Azzolini, M., Spina, M. L., Zoratti, M., Paradisi, C., and Biasutto, L. Amino acid carbamates as prodrugs of resveratrol. **Scientific Reports** 5 (2015): 15216.
77. Kazemnejadi, M., Dehno Khalaji, A., and Mighani, H. Synthesis and characterization of Schiff-base polymer derived from 2,5-dichloroaniline and 2-hydroxybenzaldehyde. **Quarterly Journal of Iranian Chemical Communication** 5 (2017): 237-241.

APPENDIX

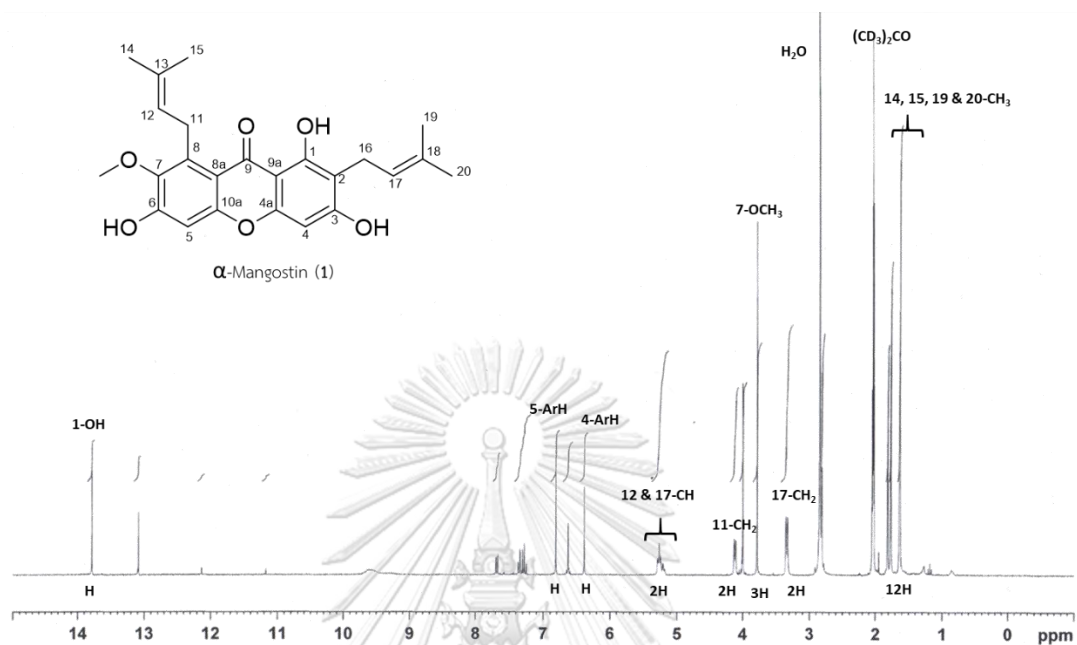


Figure 26 ^1H NMR (300 MHz) spectrum of compound 1 in $(\text{CD}_3)_2\text{CO}$

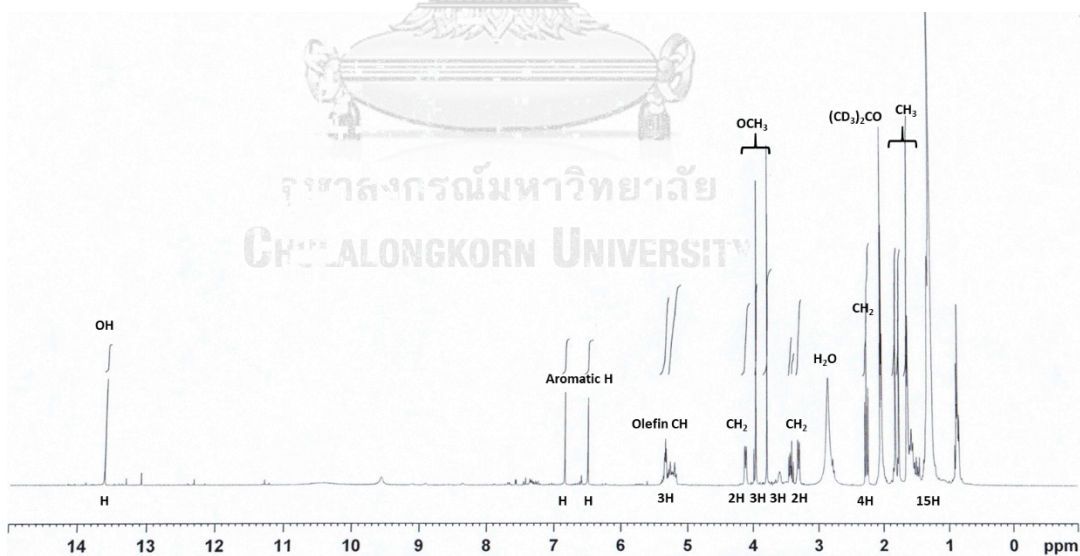


Figure 27 ^1H NMR (300 MHz) spectrum of compound from fraction X-1 in $(\text{CD}_3)_2\text{CO}$

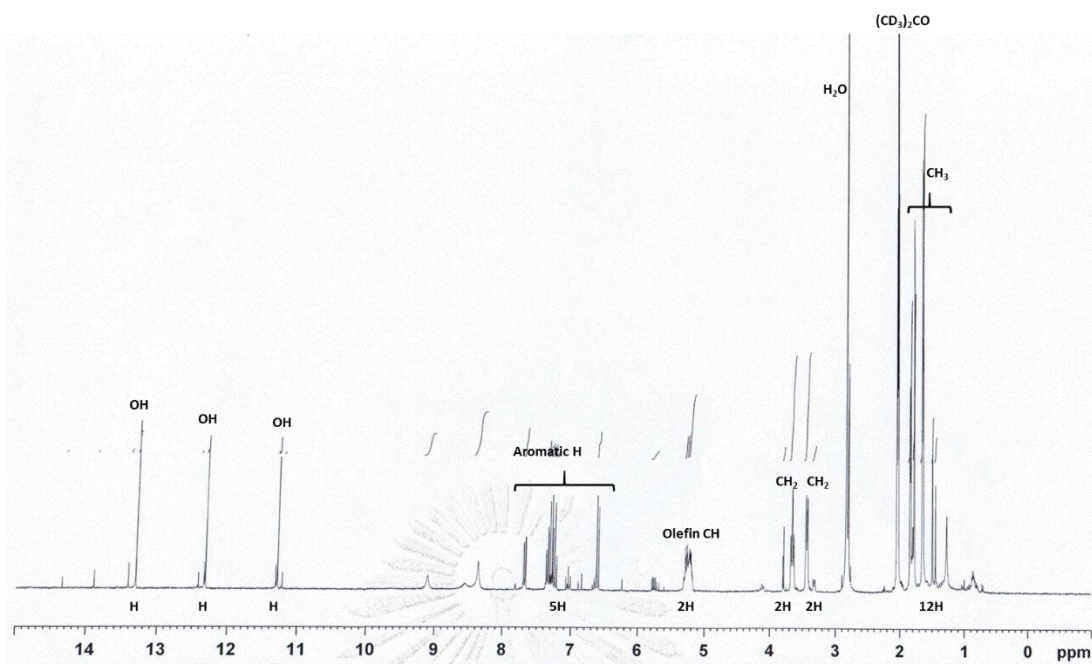


Figure 28 ^1H NMR (300 MHz) spectrum of compound from fraction X-2 in $(\text{CD}_3)_2\text{CO}$

Mass Spectrum List Report

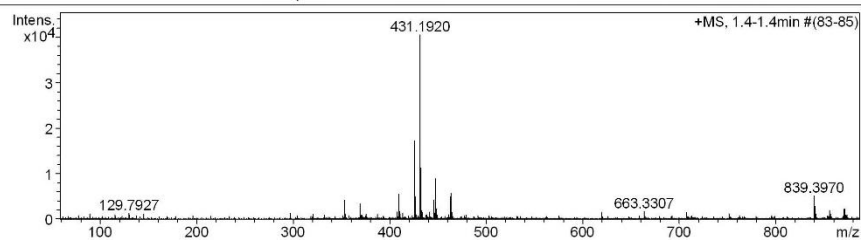
Analysis Info

Analysis Name OSNP03062019001.d
 Method Tune_low_02092017.m
 Sample Name 4a
 4a

Acquisition Date 6/3/2019 3:26:09 PM
 Operator Administrator
 Instrument micrOTOF 72

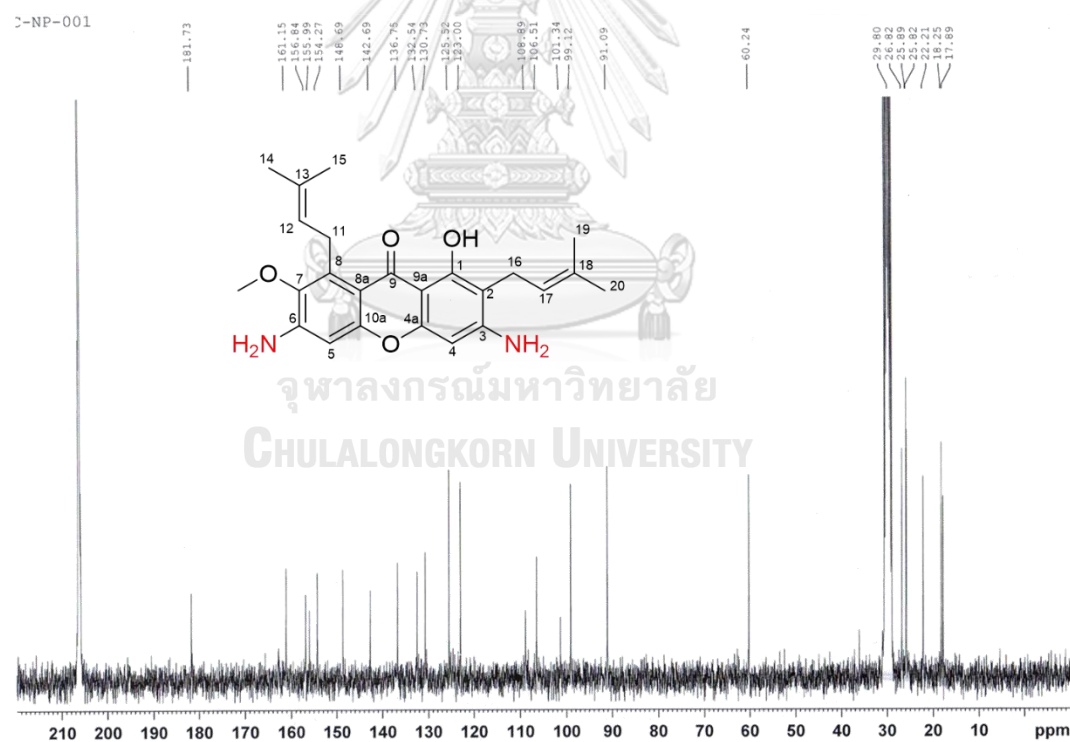
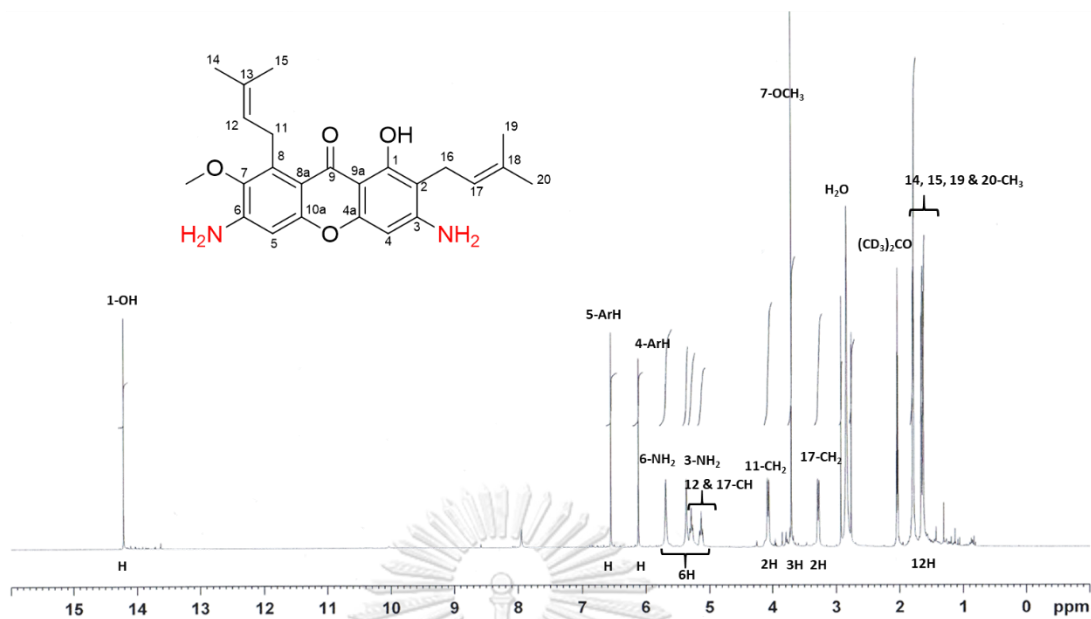
Acquisition Parameter

Source Type	ESI	Ion Polarity	Positive	Set Corrector Fill	50 V
Scan Range	n/a	Capillary Exit	180.0 V	Set Pulsar Pull	337 V
Scan Begin	50 m/z	Hexapole RF	400.0 V	Set Pulsar Push	337 V
Scan End	3000 m/z	Skimmer 1	70.0 V	Set Reflector	1300 V
		Hexapole 1	25.0 V	Set Flight Tube	9000 V
				Set Detector TOF	2295 V



#	m/z	I	I %	S/N	Res.
1	353.1478	4195	10.3	71.1	4289
2	369.1383	3351	8.3	56.7	4471
3	407.1950	1647	4.1	27.4	4636
4	409.2033	5526	13.6	94.0	4193
5	410.2069	1793	4.4	29.9	4357
6	425.2038	17353	42.8	297.0	4591
7	426.2062	5009	12.4	85.1	4746
8	431.1920	40548	100.0	695.2	4632
9	432.1934	11329	27.9	193.6	4777
10	433.1962	2013	5.0	33.7	4445
11	441.2013	1632	4.0	27.1	4597
12	445.1691	4247	10.5	72.0	4909
13	446.1734	1320	3.3	21.8	3775
14	447.1802	8896	21.9	151.9	4363
15	448.1806	2343	5.8	39.3	4314
16	463.1791	5659	14.0	96.3	4514
17	464.1830	1489	3.7	24.6	4130
18	619.3071	1544	3.8	26.0	4933
19	663.3307	1697	4.2	29.0	4899
20	707.3593	1505	3.7	25.9	4786
21	839.3970	5109	12.6	93.5	4873
22	840.3992	2672	7.1	52.1	4422
23	855.3693	1977	4.9	35.6	4981
24	870.3272	2242	5.5	40.7	4727
25	871.3434	2367	5.8	43.0	5083
26	1442.9715	1329	3.3	30.0	45638
27	1443.1233	1612	4.0	36.6	52693
28	1864.1578	1398	3.4	33.8	62983
29	2339.1430	1326	3.3	32.1	58196
30	2339.3592	1674	4.1	40.7	74297

CHULALONGKORN UNIVERSITY
 Figure 29 Mass spectrum of 4a



Mass Spectrum List Report

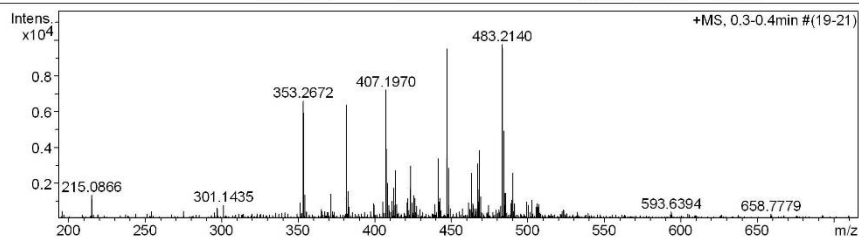
Analysis Info

Analysis Name OSCU19072019001_1.d
 Method Tune_low_1_POS_2019.m
 Sample Name 4b

Acquisition Date 7/19/2019 9:58:27 AM
 Operator Administrator
 Instrument micrOTOF 72

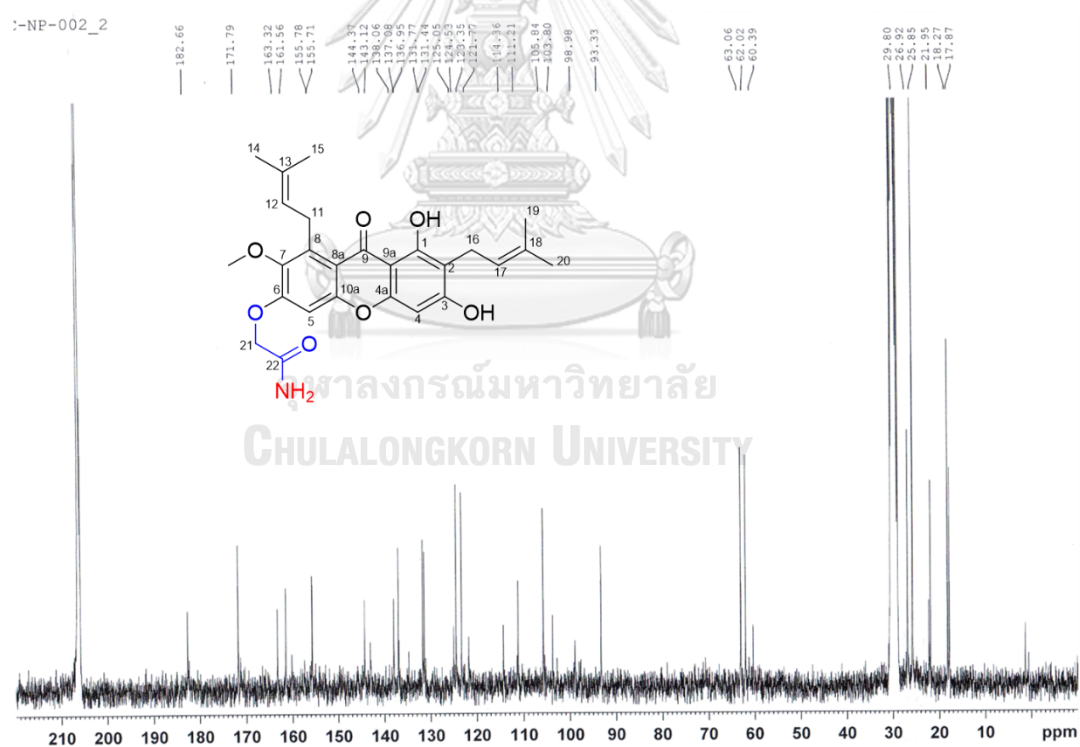
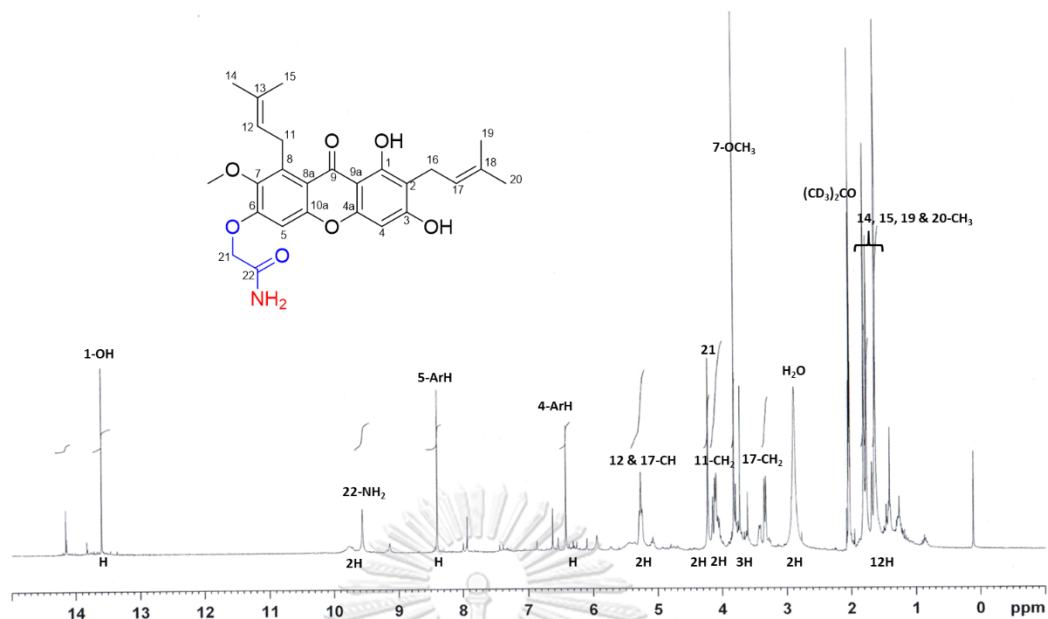
Acquisition Parameter

Source Type	ESI	Ion Polarity	Positive	Set Corrector Fill	50 V
Scan Range	n/a	Capillary Exit	150.0 V	Set Pulsar Pull	337 V
Scan Begin	50 m/z	Hexapole RF	150.0 V	Set Pulsar Push	337 V
Scan End	3000 m/z	Skimmer 1	45.0 V	Set Reflector	1300 V
		Hexapole 1	24.3 V	Set Flight Tube	9000 V
				Set Detector TOF	2295 V



#	m/z	I	I%	S/N	Res.
1	145.0118	1045	10.7	46.5	14365
2	215.0866	1342	13.8	52.3	4438
3	353.2672	6601	67.7	210.6	4473
4	354.2700	1369	14.0	42.8	4315
5	371.2568	1401	14.4	43.3	4438
6	381.2978	6389	65.5	200.2	4616
7	382.3027	1539	15.8	47.3	4592
8	407.1970	7218	74.0	222.7	4634
9	408.2024	2000	20.5	60.8	4469
10	411.1627	1002	10.3	29.8	3692
11	412.1418	1710	17.5	51.6	4209
12	413.2659	2708	27.8	82.5	4143
13	421.1988	1155	11.8	34.2	3367
14	423.1908	2984	30.6	90.4	4944
15	425.2063	1337	13.7	39.7	3767
16	426.1926	1163	11.9	34.4	4368
17	441.2059	3388	34.8	101.7	4221
18	442.2045	1192	12.2	34.9	4556
19	447.1880	9494	97.4	286.3	4852
20	448.1922	2848	29.2	84.9	4790
21	463.1781	2584	26.5	76.2	4464
22	467.2175	3111	31.9	91.7	4625
23	468.2046	3829	39.3	113.2	4728
24	469.2098	1271	13.0	36.6	4348
25	483.2140	9748	100.0	287.8	4750
26	484.2118	4926	50.5	144.6	4463
27	485.2151	1462	15.0	41.9	4663
28	489.2060	1088	11.2	30.7	4472
29	490.1883	2604	26.7	75.5	4067
30	502.6583	1083	11.1	30.3	34138

CHULALONGKORN UNIVERSITY
 Figure 32 Mass spectrum of 4b



Mass Spectrum List Report

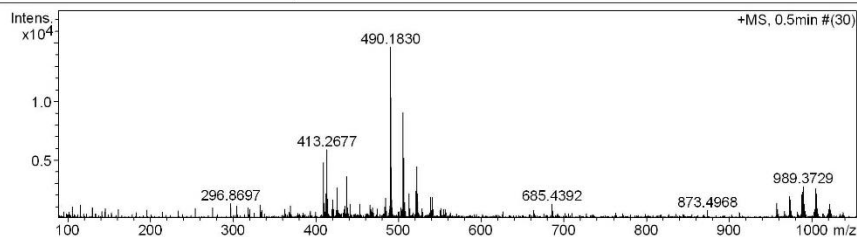
Analysis Info

Analysis Name OSNP03062019002.d
 Method Tune_low_02092017.m
 Sample Name 4c
 4c

Acquisition Date 6/3/2019 3:29:29 PM
 Operator Administrator
 Instrument micrOTOF 72

Acquisition Parameter

Source Type	ESI	Ion Polarity	Positive	Set Corrector Fill	50 V
Scan Range	n/a	Capillary Exit	180.0 V	Set Pulsar Pull	337 V
Scan Begin	50 m/z	Hexapole RF	400.0 V	Set Pulsar Push	337 V
Scan End	3000 m/z	Skimmer 1	70.0 V	Set Reflector	1300 V
		Hexapole 1	25.0 V	Set Flight Tube	9000 V
				Set Detector TOF	2295 V



#	m/z	I	I%	S/N	Res.
1	296.8697	1297	8.8	22.7	20584
2	409.1599	4818	32.9	78.9	4783
3	410.1590	1382	9.4	21.9	4616
4	412.1429	2099	14.3	33.7	4359
5	413.2677	5881	40.1	96.2	4520
6	414.2710	1671	11.4	26.6	4273
7	420.2145	1653	11.3	26.1	4395
8	425.2071	2672	18.2	42.6	4288
9	437.1927	3601	24.6	57.1	5218
10	484.1979	1794	12.2	26.5	4785
11	490.1830	14860	100.0	224.3	4879
12	491.1886	4392	30.0	66.3	4783
13	505.1956	9054	61.8	136.2	4571
14	506.1838	5183	35.4	77.3	4352
15	507.1888	1396	9.5	19.9	4431
16	512.5064	2164	14.8	31.3	5559
17	521.1785	2379	16.2	34.3	4370
18	522.1721	4463	30.4	65.4	4564
19	523.1764	1420	9.7	19.9	4334
20	538.1535	1847	12.6	25.9	4091
21	540.5399	1848	12.6	26.0	5088
22	957.3807	1343	9.2	21.0	5222
23	972.3939	1906	13.0	30.9	5087
24	973.3892	1639	11.2	26.4	4842
25	987.3943	1974	13.5	32.6	4980
26	988.3876	2286	15.5	37.6	4714
27	989.3729	2742	18.7	45.9	4922
28	1004.3798	2549	17.4	43.3	4978
29	1005.3674	2105	14.4	35.5	5517
30	2339.3685	1300	8.9	27.3	76495

CHULALONGKORN UNIVERSITY
 Figure 35 Mass spectrum of 4c

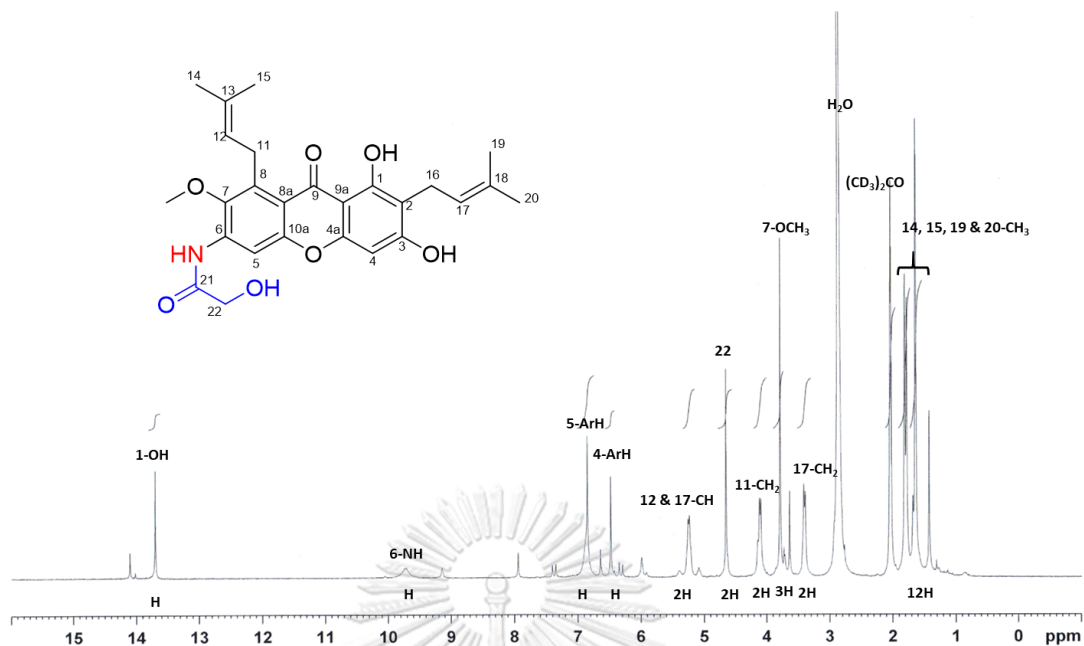


Figure 36 ^1H NMR (300 MHz) spectrum of compound **4c** in $(\text{CD}_3)_2\text{CO}$

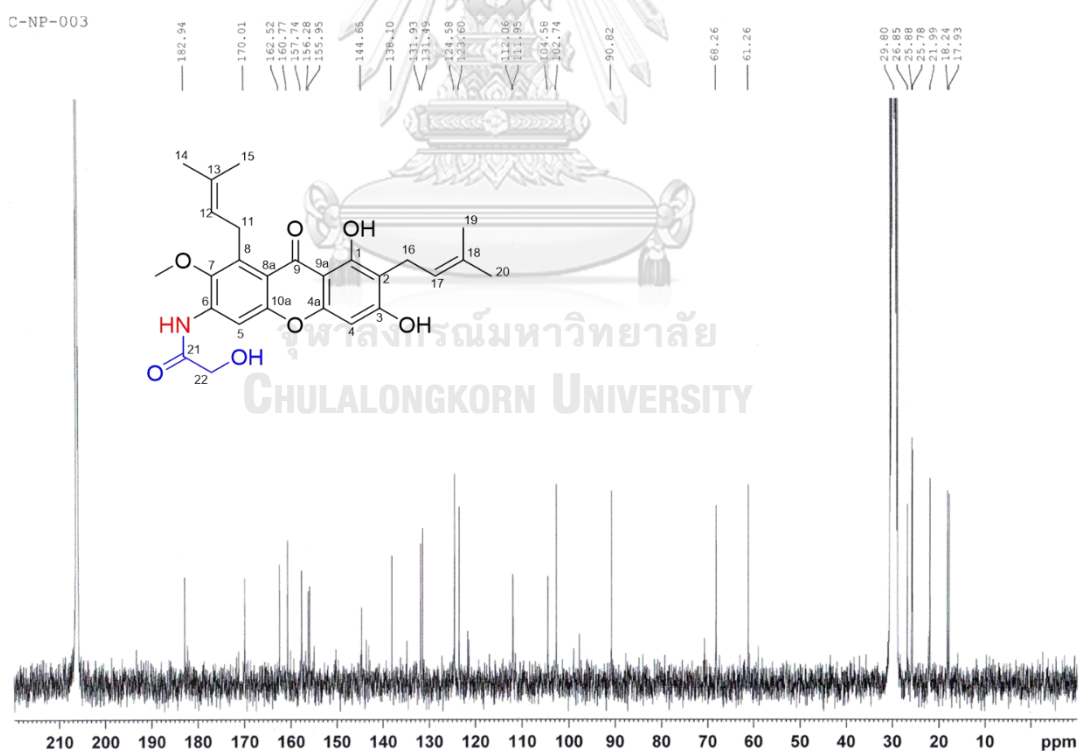


Figure 37 ^{13}C NMR (300 MHz) spectrum of compound **4c** in $(\text{CD}_3)_2\text{CO}$

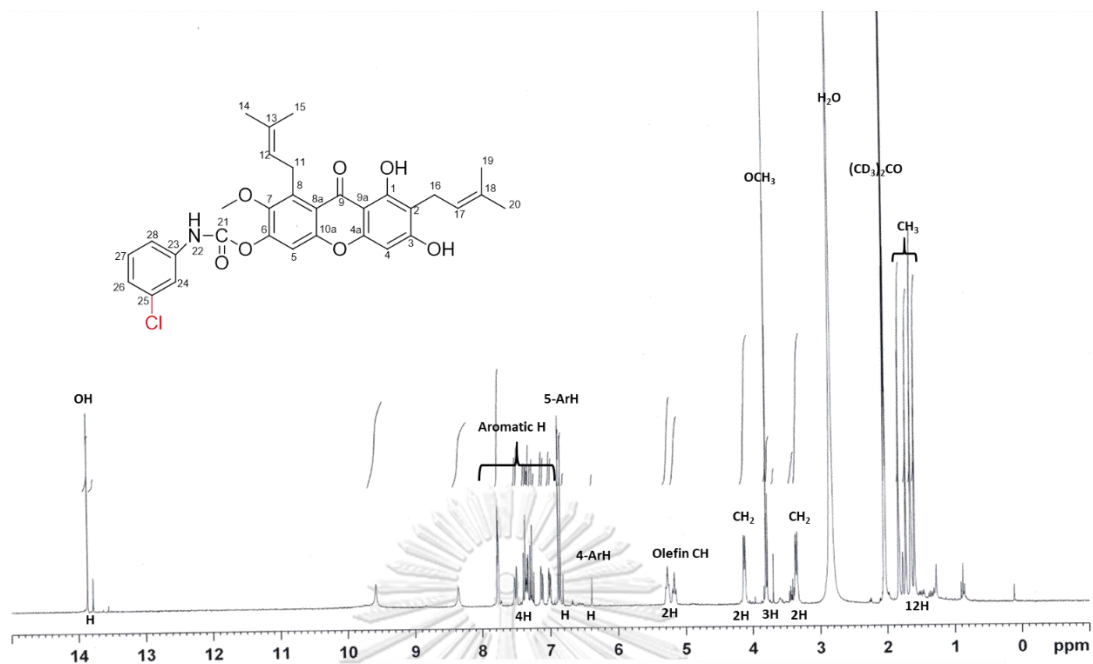


Figure 38 ^1H NMR (300 MHz) spectrum of compound **5a** in $(\text{CD}_3)_2\text{CO}$

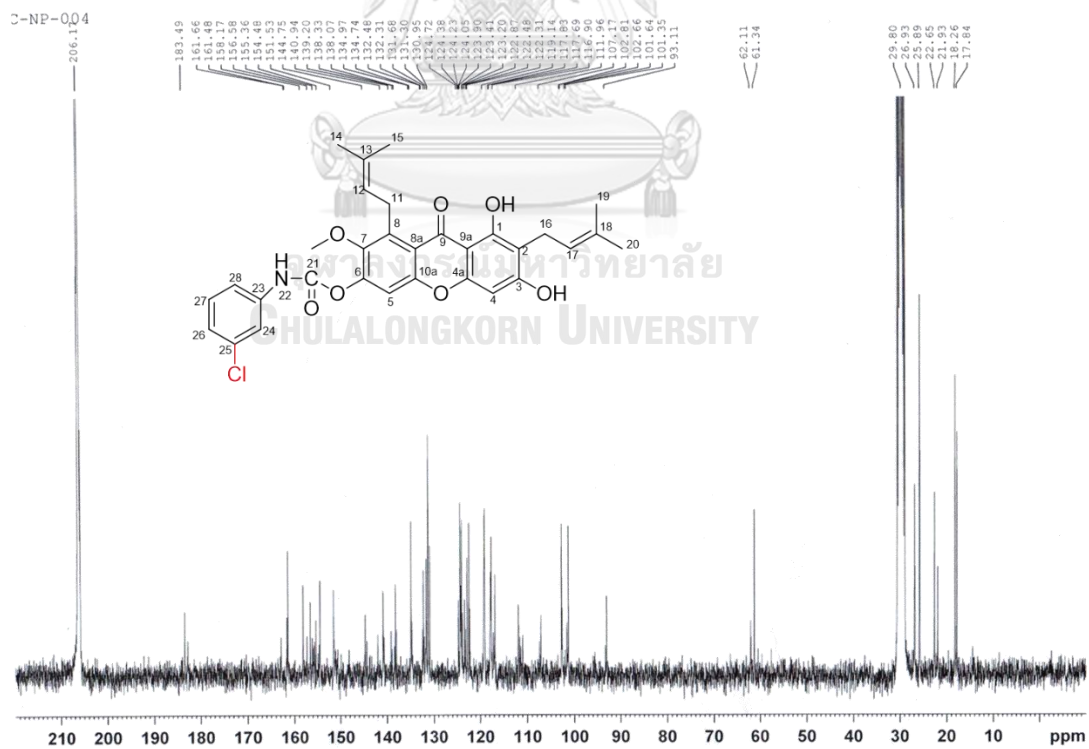


Figure 39 ^{13}C NMR (300 MHz) spectrum of compound **5a** in $(\text{CD}_3)_2\text{CO}$

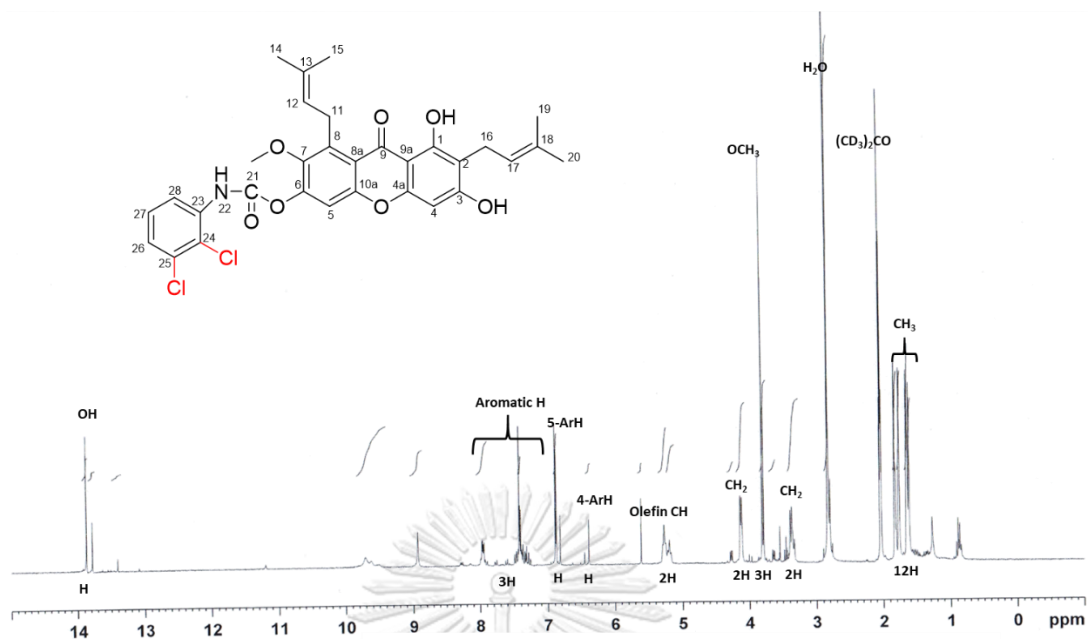


Figure 40 ^1H NMR (300 MHz) spectrum of compound **5b** in $(\text{CD}_3)_2\text{CO}$

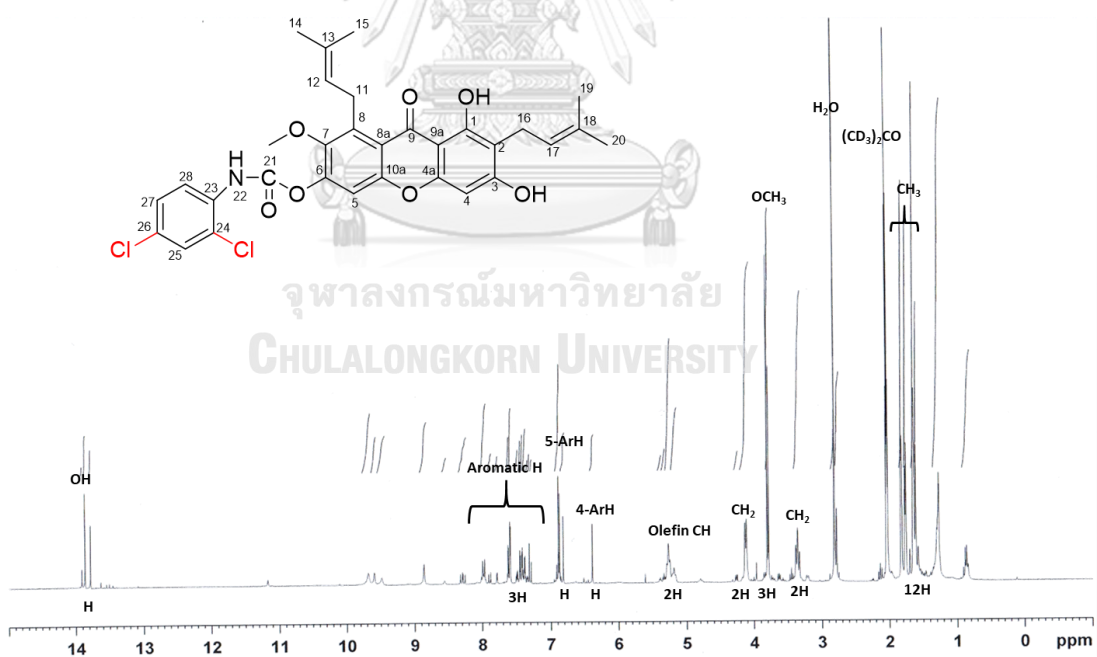


Figure 41 ^1H NMR (300 MHz) spectrum of compound **5c** in $(\text{CD}_3)_2\text{CO}$

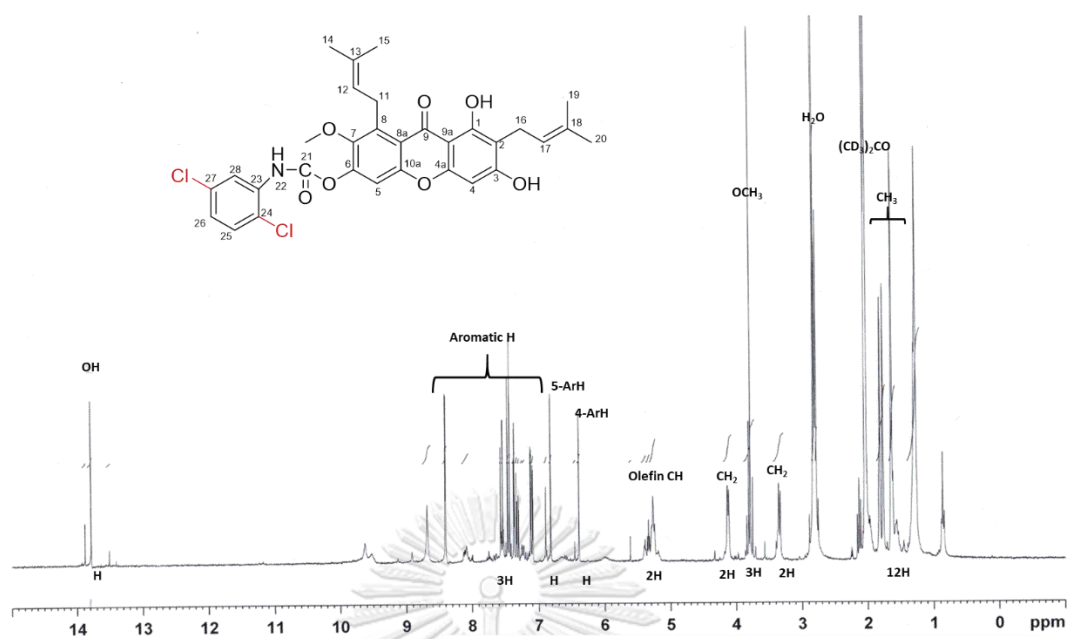


Figure 42 ^1H NMR (300 MHz) spectrum of compound **5d** in $(\text{CD}_3)_2\text{CO}$

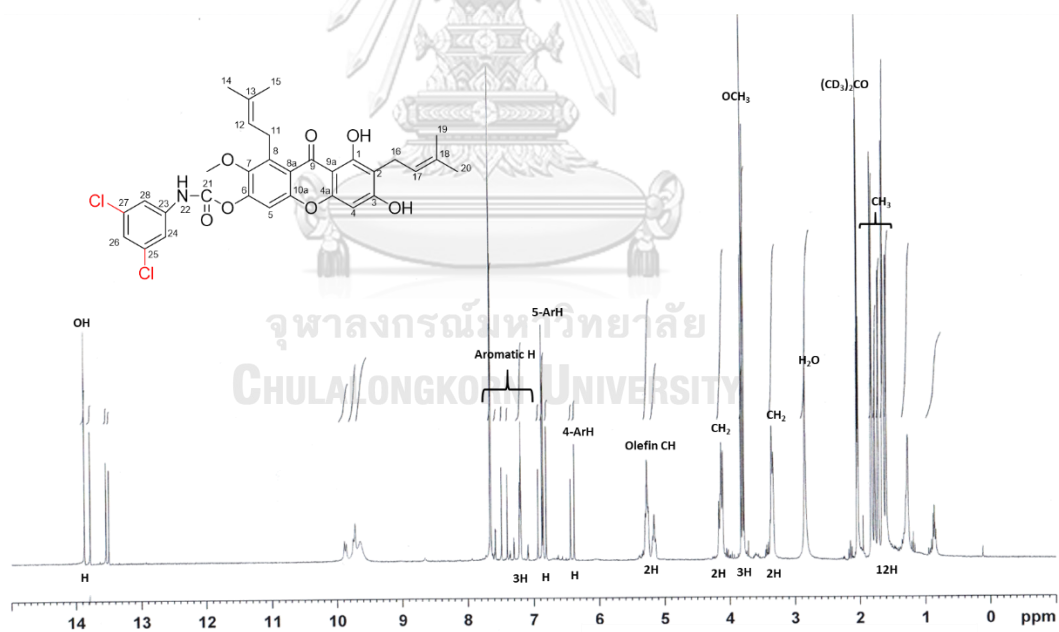


Figure 43 ^1H NMR (300 MHz) spectrum of compound **5e** in $(\text{CD}_3)_2\text{CO}$

VITA

NAME Nan Yadanar Lin Pyae

DATE OF BIRTH 04 January 1995

PLACE OF BIRTH Myanmar

INSTITUTIONS ATTENDED University of Pharmacy, Yangon

HOME ADDRESS No.69, Bokyoke Road, Quarter (1), Kyondoe, Kayin State,
Myanmar

